

The author(s) shown below used Federal funds provided by the U.S. Department of Justice and prepared the following final report:

Document Title: Improving Facial Reproduction Using Empirical Modeling, Final Technical Report

Author: J. Wesley Hines, Dr. Chester Ramsey, Dr. Lee Meadows Jantz, Dr. Richard L. Jantz, Ms. Joanna Hughes, Brian Wood

Document No.: 231669

Date Received: September 2010

Award Number: 2008-DN-BX-K183

This report has not been published by the U.S. Department of Justice. To provide better customer service, NCJRS has made this Federally-funded grant final report available electronically in addition to traditional paper copies.

Opinions or points of view expressed are those of the author(s) and do not necessarily reflect the official position or policies of the U.S. Department of Justice.

Improving Facial Reproduction Using Empirical Modeling

Final Technical Report

Report No. 2008-DN-BX-K183 /UTNE/2009-1

DOJ Grant Number: 2008-DN-BX-K183

Graduate Research Assistant: Brian Wood

J. Wesley Hines
(Principal Investigator)

Dr. Chester Ramsey,

Dr. Lee Meadows Jantz

Dr. Richard L. Jantz

Ms. Joanna Hughes

The University of Tennessee
212 Pasqua Engineering Building
Knoxville, TN 37996-2300
E-mail: jhines2@utk.edu

May 31, 2010



Abstract

Forensic facial reconstruction has been used for many years to identify skeletal remains. The face of the unknown person can be reproduced based upon the soft facial tissue thickness, which overlays the bony structure of the skull. Currently, forensic artists place average facial tissue markers at 21 specific anatomical locations on the skull and use clay to model the face based on the length of the markers. The purpose of this study was to develop a new technique for estimating the facial soft tissue thickness at the 21 traditional craniometrical landmarks used in forensic facial reconstruction. The soft tissue thicknesses or marker lengths used in the forensic facial reconstruction are currently the average tissue depths of various examined cadavers of different ethnicity, sex, and body type; whereas this new technique uses a non-parametric modeling technique to predict the facial tissue depths based on a unique skull input.

The development of the methodology for this pilot study has been completed. The 100 live male subjects' Computed Tomography (CT) images have been identified. Extended amounts of time were spent researching feasible ways of accurately measuring the tissue thicknesses at the desired craniometrical locations. Problems occurred in trying to align and orient, called registering, the database of male skulls with a base skull that has markers at the 21 locations where the tissue thickness must be measured. A viable option to automatically register CT images and consistently take accurate measurements for the entire database was found in a software package, IDAS. It is being developed by Dr. Mohamed Mahfouz at the Center for Musculoskeletal Research (CMR) at The University of Tennessee.

Computed Tomography (CT) images of 100 Caucasian male subjects' skulls were used to build a database of facial tissue thicknesses and input predictors for the non-parametric model. The inputs to the model are various cranial bone thicknesses and measurements along specific anatomical lines, which then are used to predict the facial tissue thicknesses at the traditional landmarks using a Non-Parametric Kernel Regression model. The tissue and bone measurements were performed using the software package IDAS. Hetero-Associative Kernel Regression (HAKR) and Inferential Kernel Regression models were built using the measurements from the 100 male subjects. The performance of the empirical model was initially judged by comparing the predicted facial tissue depths to the actual known tissue depths for each skull in the database using a Leave One out Cross Validation (LOOCV) technique. Two results were computed for each model; one including the query's demographics as a predictor and the other with demographics removed from the model. The Root Mean Squared Error (RMSE) when not using the demographics as an input to the model was 2.21mm for the HAKR architecture and 2.19 mm for the Inferential. When including the demographics, the RMSE for the HAKR architecture was 2.04mm and 1.89mm for the inferential architecture. The HAKR and Inferential model's RMSE were both less than the currently used tabled tissue thickness RMSE from the actual measured tissue thicknesses of 3.07 mm. The newly developed inferential model provided forensic facial tissue thickness approximations with an average of 38% less error when using demographics or 29% less error

when not using demographics. The error reduction is based on the tabled tissue thicknesses that are used in facial reconstructions today. The similarity metric for the models' predictions, after a LOOCV, was computed to be 0.19 and 0.81 for the HAKR and inferential models, respectively. This metric displays how close the query input skull is to one of the memory skulls based on their input parameters and can be used to give an estimate of the model's prediction confidence. The average prediction uncertainty from the LOOCV was computed to be 19.7% for the HAKR model and 20.5% for the inferential model.

The above quantitative results supporting the empirical model's ability to accurately predict facial tissue thickness were put to the test on 3 male skulls from the William Bass Donated Collection at The University of Tennessee. A certified forensic artist was used to construct the facial reconstructions. The facial reconstructions using tabled tissue thicknesses were compared to the reconstructions of the same subject using the inferential models' predicted tissue thicknesses. Certain landmarks, particularly the zygomatics, were estimated too large, but overall the model seemed to do a better job of estimating the face in each case.

Table of Contents

Table of Contents	4
I. Introduction	28
Statement of the Problem.....	28
Literature Review	28
Forensic Facial Reproduction	28
Background into Empirical Modeling	30
Statement of hypothesis	34
II. Methods	35
CT Image Collection.....	35
Surface Model Morphing and Registration.....	42
Additional Predictor Variables	48
Forensic Facial Soft Tissue Kernel Regression Model	54
III. Results	56
Tissue and Bone Thickness Measurement Results	56
Initial Kernel Regression Model Results.....	61
3D Clay Facial Reproductions	67
IV. Conclusions	71
Discussion of Findings	71
Implications for Policy and Practice	72
Implications for Further Research.....	72
V. References	74
VI. Dissemination	75
Appendix A.....	76
Appendix B	78
MATLAB Code used to build memory matrices	78
Bandwidth optimization used for Inferential Model	90
Bandwidth Optimization for HAKR model	91
LOOCV for Inferential Model.....	92
Inferential Prediction Model	94

LOOCV for HAKR Modeling.....	95
HAKR Model used in LOOCV	97
Inferential Model function used for 5 unknown skulls	98
Appendix C	101
Model’s Predicted Facial Tissue Thicknesses for 3 Unknown Skulls.....	101
Appendix D.....	102
Full Correlation Matrix of Collected Data	102

List of Figures

Figure 1: Traditional locations of the fiducial landmarks used in this study (Taylor, 2001).....	28
Figure 2: Different Kernel Regression (KR) Architectures.....	31
Figure 3: Affect of changing the Kernel bandwidth (h).....	33
Figure 4: Hounsfield Unit (HU) values for human body tissue along with water and air (Poulsen & Simonsen, 2007)	36
Figure 5: Segmented base skull with the 32 fiducial markers.....	38
Figure 6: Effect of data window setting on bone thickness measurement. Thickness measured in cm.....	39
Figure 7: DICOM slice to 3D surface model.....	40
Figure 8: Flowchart for the Data Collection and Analysis Process	40
Figure 9: Surface model with holes due to poor segmentation	41
Figure 10: IDAS software home screen with subject volume and model loaded	43
Figure 11: ICP algorithm in IDAS.....	44
Figure 12: Registered base model and new model in IDAS.....	45
Figure 13: Picking points in IDAS for tissue and bone thickness measurement	46
Figure 14: Cranial bone measurements in IDAS.....	47
Figure 15: Basion-Prosthion Distance Measurement in IDAS	49
Figure 16: Frontal cranial landmarks.....	50
Figure 17: Basion-Nasion distance measurement in IDAS	51
Figure 18: Orbit Height measurement in IDAS.....	51
Figure 19: Nasal Breadth measurement in IDAS.....	52
Figure 20: Biauricular Breadth measurement in IDAS	53
Figure 21: Kernel Regression Process.....	54
Figure 22: Hetero-Associative Kernel Regression Model flowchart	55
Figure 23: Body Mass Index of the 100 subjects.....	57
Figure 24: Craniometrical Locations that will be predicted using the KR model.....	58
Figure 25: Correlation matrix of model predictors and responses from 100 skulls.....	59
Figure 26: Model's MSE distribution	60
Figure 27: Bandwidth Optimization for HAKR using demographics	61
Figure 28: Bandwidth Optimization for HAKR without using demographics.....	62
Figure 29: Predictions and Actual tissue thicknesses for HAKR model.....	63
Figure 30: Optimal Bandwidth for the Inferential Model using demographics	65
Figure 31: Optimal Bandwidth for the Inferential Model without using demographics	65
Figure 32: Predictions and Actual tissue thicknesses for inferential model	66
Figure 33: Old (left) and New (right) reconstruction methods compared to actual living photo (middle) of the subject A	69
Figure 34: Old (left) and new (right) reconstructions compared to the actual living photo (middle) of the subject B70	
Figure 35: Old (left) and new (right) reconstructions compared to the actual living photo (middle) of the subject C71	

List of Tables

<i>Table 1: Traditional landmarks for location of tissue depth markers on the skull (Taylor, 2001)</i>	29
<i>Table 2: Bone Measurements</i>	48
<i>Table 3: Craniometrical Landmarks where tissue thickness measurements were made to build kernel regression model</i>	57
<i>Table 4: Average Performance Metrics for all HAKR models using demographic predictors</i>	64
<i>Table 5: Average Performance Metrics for all HAKR models without using demographic predictors</i>	64
<i>Table 6: Average Performance Metrics for Inferential modeling using demographic predictors</i>	67
<i>Table 7: Average Performance Metrics for Inferential modeling without using demographic predictors</i>	67
<i>Table 8: Performance Metrics for Inferential modeling using only 30 observations</i>	67

List of Equations

<i>Equation 1: Euclidean distance measure</i>	32
<i>Equation 2: Gaussian Kernel</i>	32
<i>Equation 3: Weighted sum prediction</i>	33
<i>Equation 5: Prediction Variance</i>	34
<i>Equation 4: Prediction Uncertainty Interval</i>	34
<i>Equation 6: Analytical Prediction Bias</i>	34
<i>Equation 7: Root Mean Squared Error (RMSE)</i>	56

Executive Summary

The purpose of this work is to develop a new technique for predicting facial tissue depths at the 21 traditional craniometrical landmarks used in forensic facial reconstruction based on underlying bone thicknesses and bone separations along specific anatomical lines. Unlike current forensic facial reconstruction techniques that use average facial tissue depths from a population sample of individuals, this technique uses a non-parametric empirical model to predict facial tissue depths that are unique to each skull query. The use of this technique could make possible more accurate facial reconstructions.

Forensic facial reconstruction has been used for many years to identify skeletal remains. The face of the unknown person can be reproduced based upon the soft facial tissue thickness, which overlays the bony structure of the skull. Currently, forensic artists place average facial tissue markers at 21 specific anatomical locations, shown in Figure 1, on the skull and use clay to model the face based on the length of the markers.

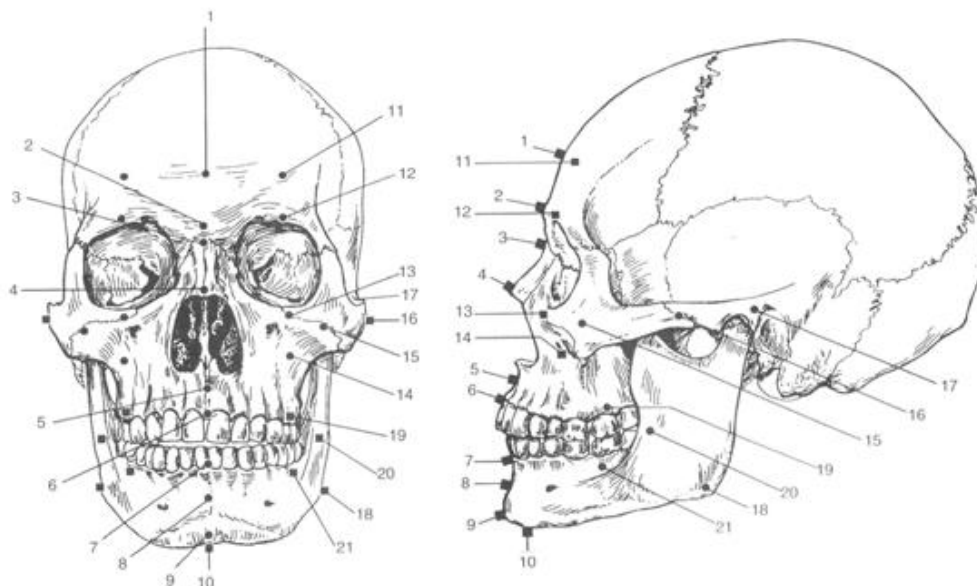


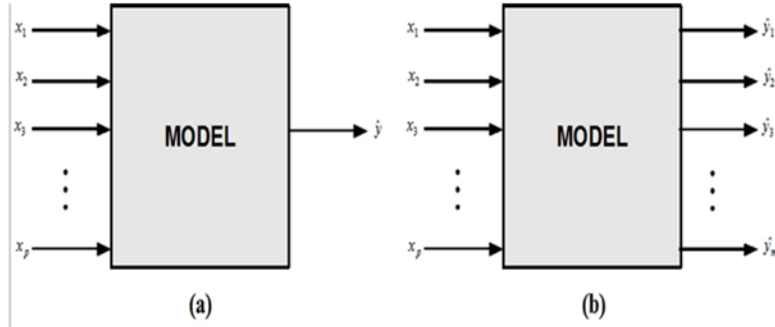
Figure 1: Craniometrical landmarks used in forensic facial reproductions

There are two major categories of empirical modeling methods used for prediction: parametric and non-parametric. The parametric methods include linear regression, neural networks and other techniques that map relationships in data by optimizing different parameter values using a data set similar but not exact to future data sets, which is called a training data set. However, once the parameters for the model are identified the training data are no longer used and the model's prediction equation is set. In order improve the facial tissue depths used in a forensic facial reconstruction and provide unique tissue thicknesses for

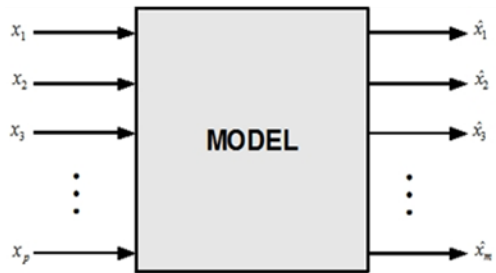
every unknown skull input, the model must be able to change its parameters based on the input to the model. This requires the use of a non-parametric modeling technique.

A non-parametric empirical technique does not use set parameters to define the model like the parametric modeling technique mentioned above. The non-parametric techniques use the actual training data to understand future predictions and store the training data in a "memory matrix". Non-parametric empirical modeling used for forensic facial reconstruction can provide advantages over parametric methods. Non-parametric methods are easily updated as additional data becomes available by simply appending the new data to the historical database or memory matrix. As new facial tissue measurements are made from additional CT images, the data can be added to the historical database and the model predictions become more accurate. There are no training times and no need to optimize the parameter value in the model. This means that new facial tissue measurements can be inserted into an existing model without additional software programming or optimization. As with any prediction method, there is a certain amount of uncertainty involved. Therefore, methods have been developed to produce uncertainty values on non-parametric predictions (Rasmussen & Hines, 2005). This allows the future users of the prediction software to have an estimate of the accuracy of the facial soft tissue thicknesses being used in the reconstruction. The ability to accompany a facial reconstruction with an uncertainty should help forensic investigators decide if the reconstruction should be used in an investigation.

Kernel regression (*KR*) is a technique used in statistics and empirical modeling to estimate a parameter's value by calculating a weighted average of historical observations, also known as exemplars (Atkeson, Moore, & Schaal, 1997b). There are three different *KR* architectures, which are characterized by the number and type of inputs and outputs, shown in Figure 2. These model architectures are inferential, hetero-associative, and auto-associative *KR*. This study uses a hetero-associative model architecture that uses multiple inputs to predict multiple outputs. The multiple inputs in this application consist of demographic information (*sex, age, race, etc...*) facial tissue depths, underlying bone thicknesses, and bone separations along specific anatomical lines collected from the CT images. The number of features collected from a particular subject may be a subset of the features that are considered to be important and that are stored in the historical database. For example, the race may not be known for the test subject. The conventional hetero-associative algorithm will be augmented to work under these cases of missing input variables.



Schematic diagram of (a) inferential and (b) heteroassociative models



Schematic diagram for autoassociative model

Figure 2: Different Kernel Regression (KR) Architectures

The empirical modeling architectures used in this project was Hetero-Associative Kernel Regression (HAKR) and Inferential. The HAKR type of modeling architecture is a non-linear, non-parametric, kernel regression model in which the number of inputs does not equal the number of outputs in the model. The only difference in the inferential type of modeling architecture is the number of outputs from the model is one. Therefore, a separate KR model is constructed for each output exemplar.

The first step in making a prediction using a KR model, regardless of architecture, is to compute how far the query inputs are from the memory matrix, which is built from the known skull data sets. A Euclidean distance operator, Equation 1, is used to determine the distance the query data, q , is from the training data, x . This is used iteratively through each observation in memory, i , through the total number of observations, n .

$$d(x_i, q) = \sqrt{\sum_{i=1}^n (x^i - q)^2}$$

Equation 1: Euclidean Distance Measure

These distances are then converted to a weight for each training vector. Equation 2 is the Gaussian kernel function used in the modeling architecture. The purpose of the kernel

bandwidth, h , is to help optimize which memory vectors are considered similar to the query input and therefore greatly used in the prediction.

$$w = K(d, h) = \frac{1}{\sqrt{2\pi \cdot h^2}} e^{-d^2/2h^2}$$

Equation 2: Gaussian Kernel

The kernel bandwidth must be optimized to reduce the model's error and predictive uncertainty. As the bandwidth increases the Gaussian kernel widens and incorporates more distant query vectors. This gives a greater weight to more query points. The optimal bandwidth is chosen by iteratively changing the bandwidth and computing the model's prediction error for each bandwidth. The bandwidth that produces a model with the least error is set as the permanent bandwidth.

The predictions are then computed using Equation 3, which is a weighted sum of the training output vectors. In the case of the HAKR model used in this study the number of outputs is different than the number of inputs. This requires the prediction to be a weighted sum of the output memory vectors, which are known facial tissue depths measured from the database of 100 male skulls.

$$\hat{y}(q) = \frac{\sum_{i=1:n} y_i w_i}{\sum_{i=1:n} w_i} = \frac{\sum_{i=1:n} y_i K(d(x_i, q))}{\sum_{i=1:n} K(d(x_i, q))}$$

Equation 3: Weighted Prediction

The weighted prediction outputs are the facial tissue depths for the unknown skull's input parameters. A flowchart of the step-by-step process of kernel regression is shown below in Figure 3.

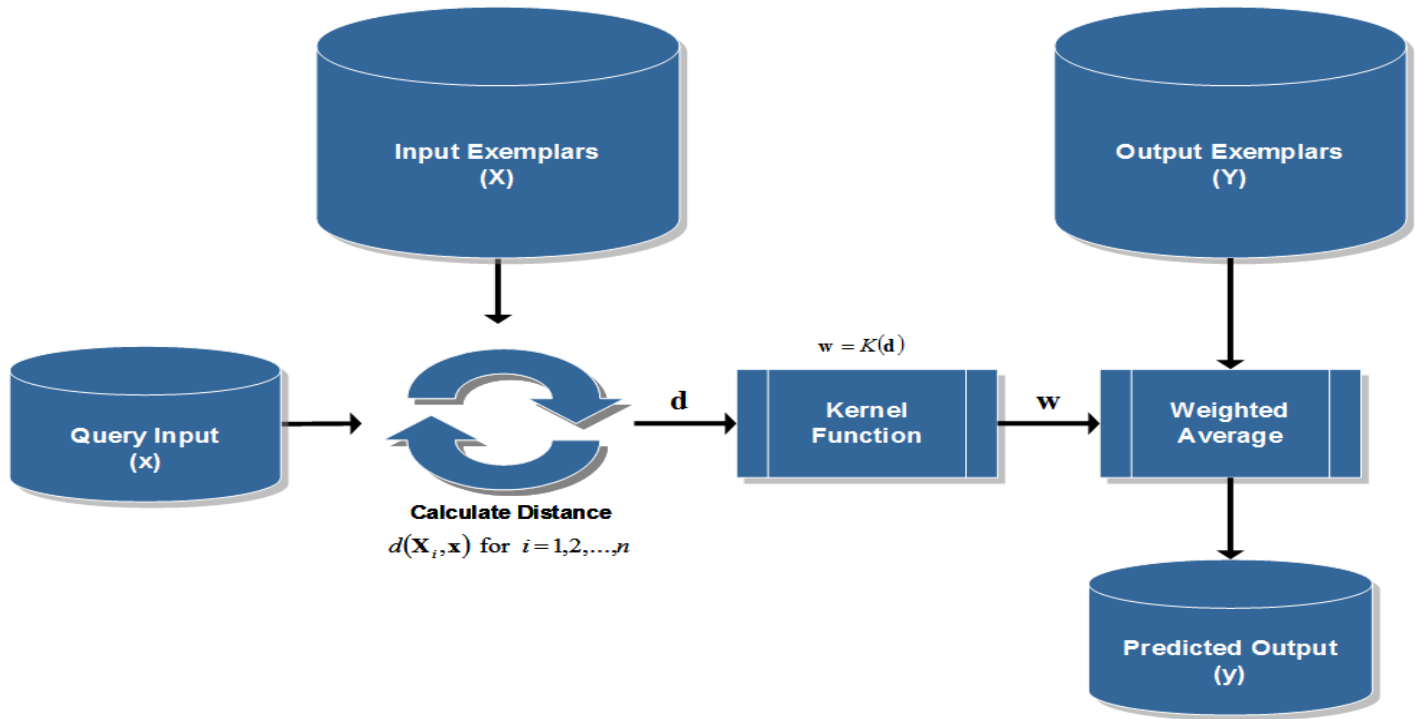


Figure 3: Kernel Regression Process

The final step in the tissue prediction model was to compute an uncertainty interval for each prediction. A 95% prediction uncertainty interval was calculated for the empirical model predictions, which means the measured tissue thickness value is covered 95% of the time. Noise in the output memory matrix, variance of the model's predictions, and the model's prediction bias all contribute to the size of the prediction interval. This metric along with the similarity metric would be used to help investigators determine if the predictions should be used in an investigation.

CT Data Collection and Processing

Data collection for this project required Computed Tomography (CT) scans that would be used to compute the facial tissue thicknesses and possible bony structure predictors for the non-parametric kernel regression model. 100 known male subjects' CT scans of the cranium were collected in the PET/CT Imaging Department of Thompson Cancer Survival Center West in Knoxville, Tennessee. Only the PET/CT scans labeled as melanoma, bone, and brain were examined as possible subjects to use in the study because their scan procedures should include the complete cranium and mandible. The scans were selected based on the advice from the PET/CT personnel. Also, if any noticeable skull deformations or lesions were found in the scan or if the patient was currently undergoing radiation therapy its data was not used in the study. The patient CT scans were verified to entail the entire cranium and mandible in the Picture

Archiving and Communication System (PACS) and then the Digital Image and Communication in Medicine (DICOM) image files were copied onto CDs. All male subjects on the PACS system that fit the criteria mentioned above were selected for this study. Along with the 100 CT image sets collected, if the patient's age, weight, and height were available they were recorded to be used as possible predictors. No African American subjects could be positively identified among the 100 subjects used; therefore potentially only Caucasian males were used in this study.

The problem of finding repeatable ways to identify the cranial features that could predict the facial soft tissue took considerable time. However, it was essential to being able to consistently take measurements at the 21 locations on each skull. A viable option to collect the measurements for the entire database of live tissue skulls was found in a software package called IDAS, which is being developed by Dr. Mohamed Mahfouz at the Center for Musculoskeletal Research (CMR) at The University of Tennessee. His current research involves trying to implement the cranium bone structure into the software. This software allowed the measurement of the tissue thicknesses and other features to be made automatically, which helps remove the variance of manually performing the measurements.

Prior to the cranial measurements being collected from the CT images in IDAS, the bone structure had to be separated or segmented from the rest of the facial tissue in separate image analysis software called *Amira*. Segmentation is the process of separating the cranium and mandible bone from the surrounding facial soft tissue. The segmentation process creates a surface model of the cranium and mandible. The 100 CT scans had different resolutions from one subject to another, which made registering difficult. Also, the slice thickness of the image sets, which is the distance between axial image slices, was far too large for accurate surface models to be created. In order to produce useable surface models of each subject, the data had to be interpolated to consistent resolutions of 0.6mm³. A detailed procedure was laid out to enable consistent surface models for each skull in the database to be produced. This allowed for the correct measurement of the tissue and bone thicknesses, as well as various bone features, for each of the 100 male skulls in our database. The measurement process is discussed in the following section. A simple flowchart of the procedure used to analyze the CT image sets in this project is shown below in Figure 4. Because of the difficulties in getting the data registered and analyzed correctly, we fell probably 4-5 months behind schedule. Therefore, we asked for and were granted a no-cost extension through the end of May 2010.

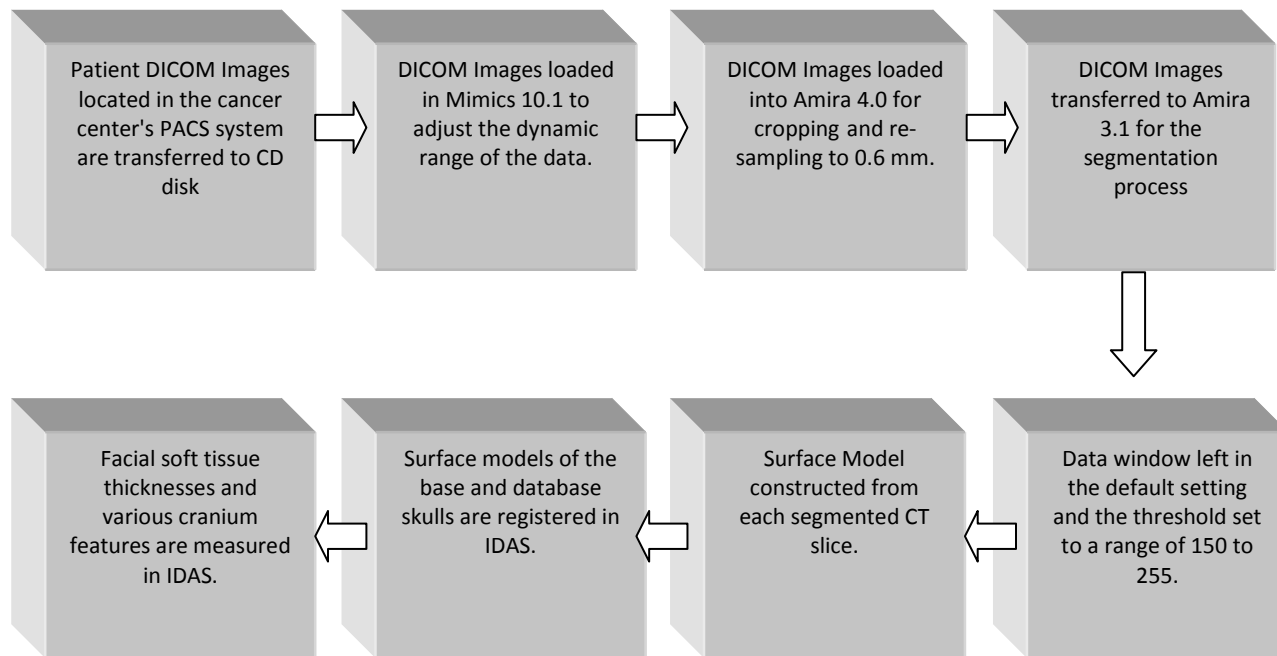


Figure 4: Flowchart of DICOM image processing to measurements made in IDAS

Tissue and Bone Measurements

The segmented skulls are analyzed in *IDAS* where they are aligned with their respective CT image sets to give the user the ability to pick points on the segmented skull where tissue and bone thickness measurements desired. Bone thicknesses were selected due to their ability to be easily measured in the *IDAS* software. The lack of previous studies in the potential of skull bone features being predictors of overlaying soft facial tissue prevented a more guided search. Therefore, bone thicknesses and bone measurements were chosen.

An important change to the study's methodology was to only take measurements of 13 of the 21 locations. This was done because of the high number of older and overweight subjects. The elderly and overweight tend to have more elasticity in their facial soft tissue, which can cause errors in the skin thickness measurements around the neck and side of the face due to their supine setup during CT imaging. This caused the tissue to pool on the sides of the face. Therefore, only locations along the forehead and midline of the skull were chosen with exception to the single lateral location of the zygomatic arch being used. Figure 5 shows the craniometrical locations where measurements were made.

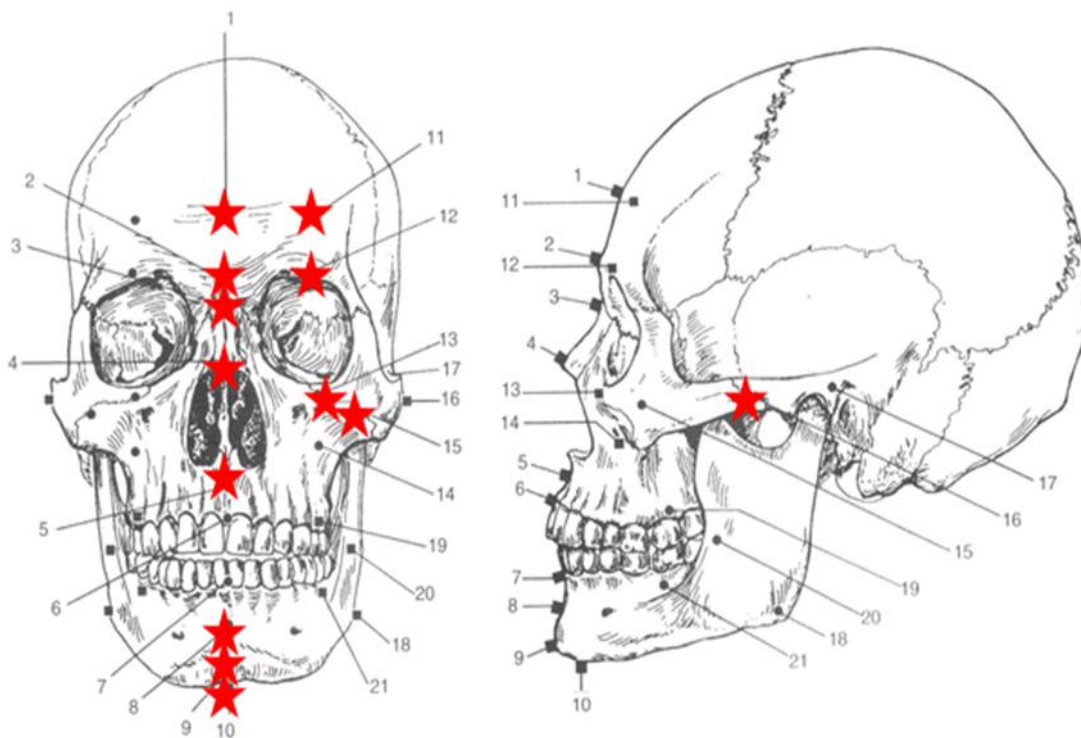


Figure 5: Craniometrical Locations that will be predicted using the KR model

The current version of IDAS only allows for user to manually pick the location on the segmented skull where the tissue and bone measurements are to be made. A group of 30-40 points are selected for each craniometrical location. IDAS then makes a profile line from the selected points on the surface model through the DICOM image set until the pixel value in the DICOM image falls to zero. A value of zero represents air in our image sets. The distance of the profile line is the skin thickness at that location. The bone thickness measurement is performed the same way. A trimmed mean is computed for each location's 30-40 distances in order to give a single tissue and bone thickness measurement for the 13 craniometrical locations. The 13 tissue thicknesses for each observation, or skull, are compiled into the model's output memory matrix. Likewise, the 13 bone thicknesses for each skull are used to build the model's input memory matrix. To try and discover other possible tissue thickness predictors from the skull, 5 landmark distance measurements were made for each skull.

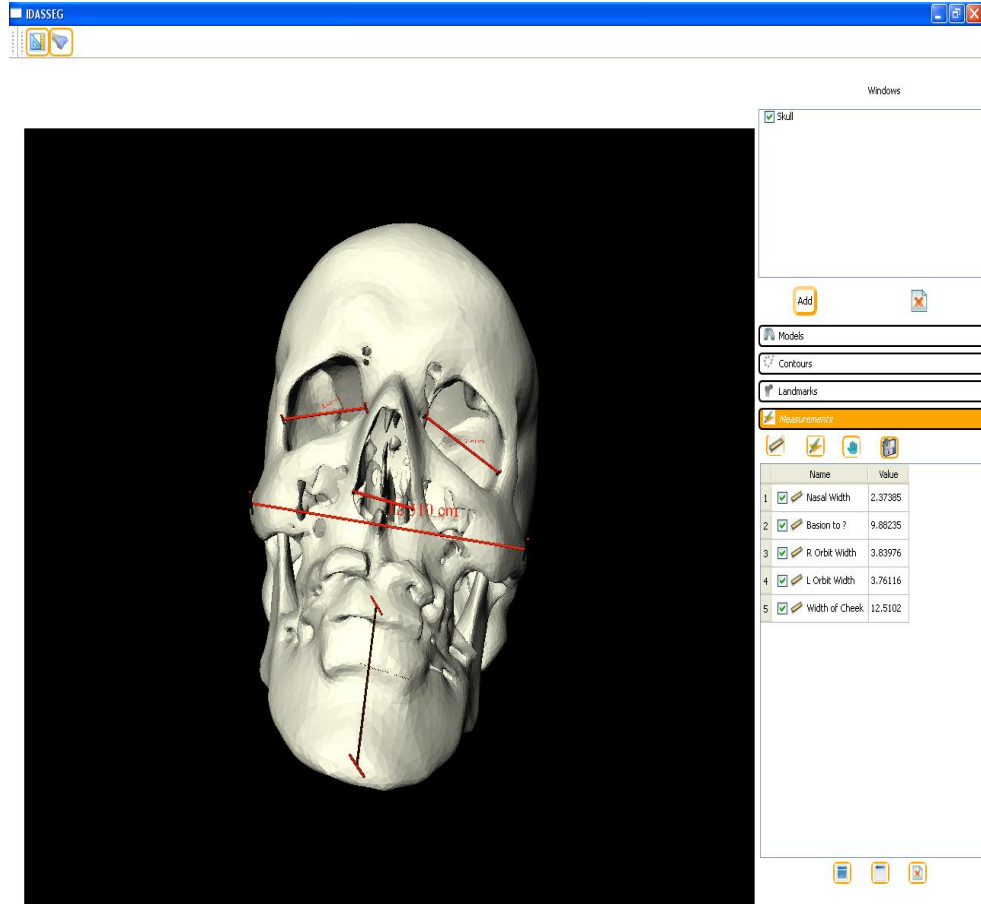


Figure 6: Landmark distance measurements made with IDAS

Dr. Richard Jantz from the Anthropology Department at The University of Tennessee provided the 5 distance measurements based on known cranial landmarks: basion to prosthion, basion to nasion, orbital height, nasal width, and biauricular breadth, shown being measured with IDAS in Figure 6. These measurements were chosen based on their ability to also be measured without the use of CT scanning. The 13 bone thickness measurements along with the 5 distance measurements and the subjects' age, height, weight, and Body Mass Index (BMI) make a total of 22 predictor variables for the non-parametric kernel regression model. The matrix layout of the modeling process is displayed in Figure 7.

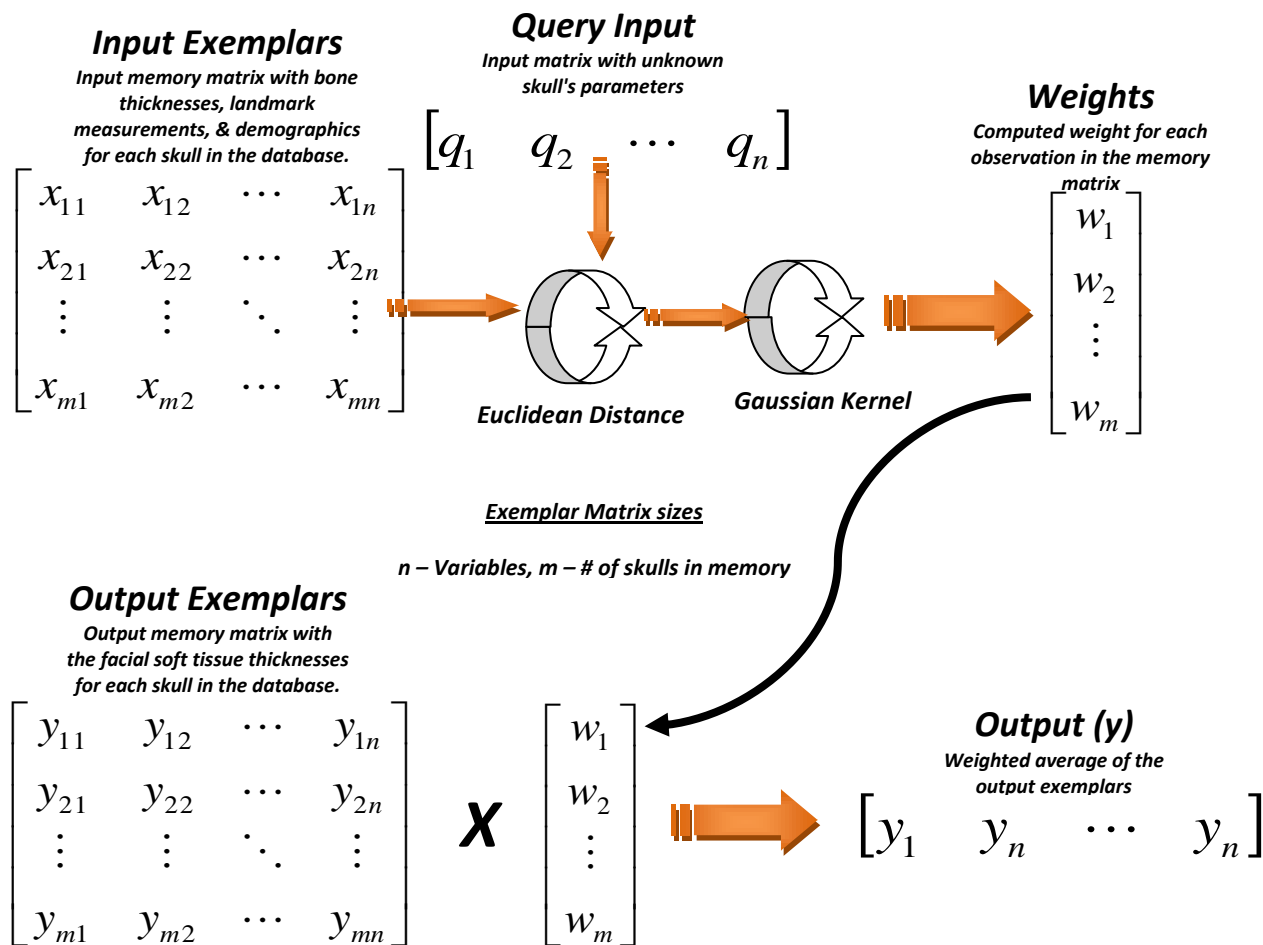


Figure 7: Hetero-Associative Model for Predicting Facial Soft Tissue Thickness

Using IDAS to collect the tissue and bone data allows for discovering the possible correlations between the bony structure features of the skull and the overlaying soft facial tissue. The correlations will enable one to accurately predict an unknown skull from only the cranial bone parameters. A linear correlation analysis of the collected tissue thickness measurements (columns) and the 22 predictor variable measurements (rows) for the 100 subjects is shown in Figure 8. If the absolute value of the correlation coefficient is computed to be 0.3 or greater that predictor was considered useful. The 13 bone thickness measurements for the locations shown in Figure 5, the 5 cranial landmark distance measurements discussed previously, and 4 demographics (age, weight, height, and BMI) make up the 22 predictor variables used in this study.

	Supraglabella	Glabella	Nasion	End of Nasals	Mid-Philtrum	Chin-Lip Fold	Mental Eminence	Beneath Chin	Frontal Eminence	Supraorbital	Suborbital	Lateral Orbit	Zygomatic Arch
Supraglabella	0.03	0.08	0.09	0.17	0.03	0.21	0.19	0.06	0.15	0.14	0.09	0.00	0.09
Glabella	-0.11	0.09	-0.02	-0.08	-0.02	0.02	0.00	-0.05	-0.05	0.04	-0.11	-0.22	-0.02
Nasion	-0.04	0.07	0.04	-0.21	-0.08	-0.08	-0.12	-0.04	-0.08	0.02	-0.04	-0.13	-0.04
End of Nasals	0.08	0.05	0.00	-0.06	-0.14	-0.04	-0.21	-0.15	0.02	-0.01	0.11	0.05	-0.02
Mid-Philtrum	-0.11	0.06	0.08	-0.19	-0.22	0.05	-0.14	-0.16	-0.19	-0.08	-0.10	-0.17	-0.25
Chin-Lip Fold	-0.16	-0.16	-0.10	-0.04	0.08	-0.20	-0.18	-0.01	-0.13	-0.09	-0.07	-0.15	-0.04
Mental Eminence	0.08	-0.06	-0.03	0.06	-0.07	0.06	-0.04	-0.02	0.14	0.13	0.05	0.04	-0.08
Beneath Chin	0.32	0.20	0.12	0.26	0.12	0.31	0.30	0.17	0.41	0.38	0.30	0.36	0.26
Frontal Eminence	0.10	0.13	0.14	0.26	0.01	0.19	0.26	0.18	0.22	0.27	0.17	0.16	0.20
Supraorbital	0.11	0.09	0.12	0.15	0.02	0.24	0.20	-0.02	0.24	0.19	0.14	0.14	-0.01
Suborbital	-0.20	-0.03	-0.11	-0.26	0.08	-0.13	-0.10	-0.12	-0.24	-0.18	0.04	-0.05	-0.12
Lateral Orbit	0.13	0.05	0.05	0.18	0.12	0.14	0.09	0.06	0.24	0.23	0.13	0.00	0.20
Zygomatic Arch	-0.15	0.01	0.18	-0.16	-0.05	-0.09	-0.13	-0.17	-0.19	-0.10	-0.08	-0.16	-0.16
Basion to Prosthion distance	0.32	0.19	0.27	0.27	-0.12	0.32	0.17	0.08	0.34	0.25	0.04	0.21	0.26
Basion to Nasion distance	0.26	0.10	0.02	0.15	0.02	0.07	0.11	0.04	0.28	0.12	0.02	0.13	0.09
Orbital width	-0.20	-0.16	-0.23	-0.18	-0.03	-0.24	-0.14	-0.29	-0.19	-0.22	-0.14	-0.26	-0.18
Nasal width	0.00	-0.11	-0.16	-0.05	-0.06	-0.07	0.01	-0.09	-0.03	-0.01	-0.06	-0.12	-0.10
Biauricular breadth	-0.09	-0.15	-0.12	0.03	0.12	0.00	-0.01	-0.03	-0.16	-0.19	0.06	-0.02	-0.08
Age	-0.29	-0.21	-0.25	-0.15	-0.28	-0.21	-0.13	-0.28	-0.26	-0.27	-0.08	-0.20	-0.40
Weight	0.65	0.44	0.36	0.37	0.33	0.57	0.55	0.49	0.64	0.64	0.59	0.67	0.72
Height	0.19	0.09	0.15	0.08	-0.04	0.23	0.11	0.03	0.17	0.11	0.03	0.12	0.21
BMI	0.58	0.42	0.38	0.36	0.27	0.60	0.58	0.44	0.57	0.59	0.56	0.64	0.73

Figure 8: Correlation Analysis

As one can see there are only a few useful predictors of tissue thickness available. The greatest correlation with tissue thickness seems to exist with weight and BMI. The bone thickness predictors that may have useful prediction information correspond to correlation coefficients around ± 0.3 or greater.

Modeling Results

The results presented are from the tissue prediction models using the 100 male subject skulls' data collected. The input memory matrix consists of 100 observations and 22 variables. The input variables are the 13 bone thickness measurements, the 5 ethnicity determination measurements, and the 4 demographics (age, weight, height, and BMI). The demographic parameters are rarely provided to the forensic artist to use during the facial reconstruction,

therefore the model's performance will be shown with and without using them as tissue thickness predictors. The output memory matrix contains the 13 facial tissue thicknesses of the 100 skulls. Two non-parametric kernel regression models were constructed using the data from 100 male subjects. A hetero-associative and inferential kernel regression model were built and compared. In order to measure the performance of each model architecture, a Leave One Out Cross Validation (LOOCV) was performed. This validation technique simply takes a single observation in the historical database, one subject's skull, and uses it as the query input for the model. When a particular skull is being used as the input, it is removed from the memory matrix of the model. This done until the model has been run using each of the available observations as the query.

There were several metrics computed to demonstrate the model's performance. A prediction uncertainty was computed for each tissue thickness prediction. It is shown as a percentage of the prediction values. The metric displayed in the result tables are the average prediction uncertainty for the LOOCV. A similarity metric was used that is simply the average of the maximum kernel weights computed for each query input for the LOOCV. The closer the value is to 1 the more similar the query skull is to a skull in the memory matrix and therefore the more confidence we can have in the prediction. The Root Mean Squared Error (RMSE) of the model's predictions and the actual known tissue thicknesses is computed for each query. The mean of the 100 RMSEs from the LOOCV is shown as Model RMSE. Table RMSE is the error of the actual tissue thicknesses measured and the Caucasian tabled tissue thicknesses (Rhine & Moore 1982). The obese tabled values were used due to the majority of the subjects in the model's database are overweight to obese. Figure 9 is a plot of one of the HAKR model predictions with their 95% confidence intervals along with the actual tissue thicknesses.

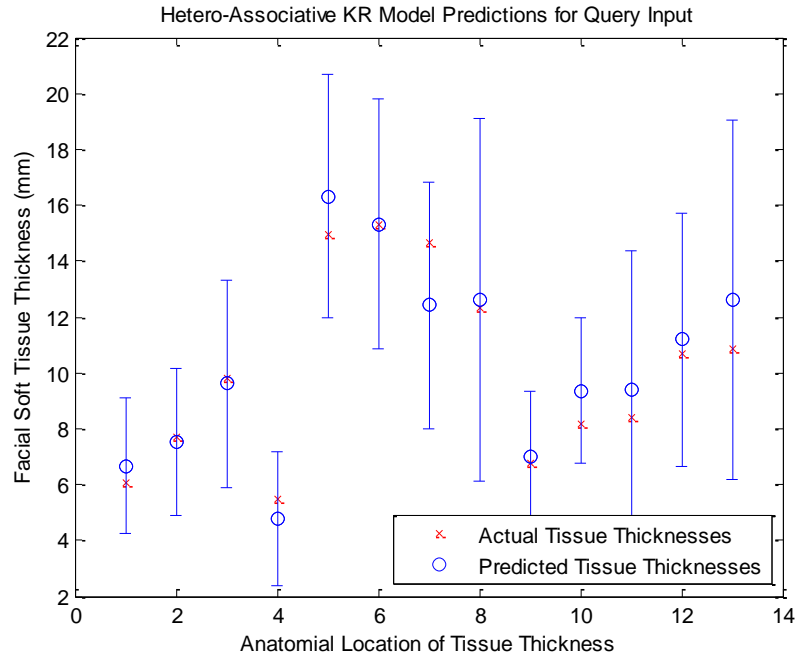


Figure 9: Predictions and Actual tissue thicknesses for HAKR model

Table 1: Average Performance Metrics for HAKR model using demographic predictors

Prediction Uncertainty	Model RMSE	Table RMSE	Similarity
19.73 %	2.04 mm	3.07 mm	0.19

Table 2: Average Performance Metrics for HAKR model without using demographic predictors

Prediction Uncertainty	Model RMSE	Table RMSE	Similarity
19.66%	2.21 mm	3.07 mm	0.41

The tables displayed above convey that the demographics play a role in decreasing the HAKR's prediction error. However, the average similarity metric increases from the model using the demographics to the model not. This can be explained by the fact that the optimal kernel bandwidth also increases; therefore resulting in higher weights given to the more distant skulls in the model's memory. The kernel bandwidth used in the model with demographics was 2.5, while the model without demographics used a bandwidth of 3.1. The HAKR model using the

memory of 100 skulls resulted in a 34% decrease in error when using the demographics and 28% error when not using the demographics when compared to the Table RMSE.

The next non-parametric model investigated used an inferential architecture. This means that 13 separate kernel regression models were built, one for each tissue thickness location predicted. It is expected that this type of model will produce predictions with less error because we can select only the highest correlated predictor variables for each tissue thickness location model. Figure 10 shows a predicted tissue thickness against actual tissue thickness plot. The Model RMSE decreased from that of the HAKR and the similarity metric was also higher than the HAKR's. More importantly the Model RMSE was again lower than the tabled thickness RMSEs, Table RMSE.

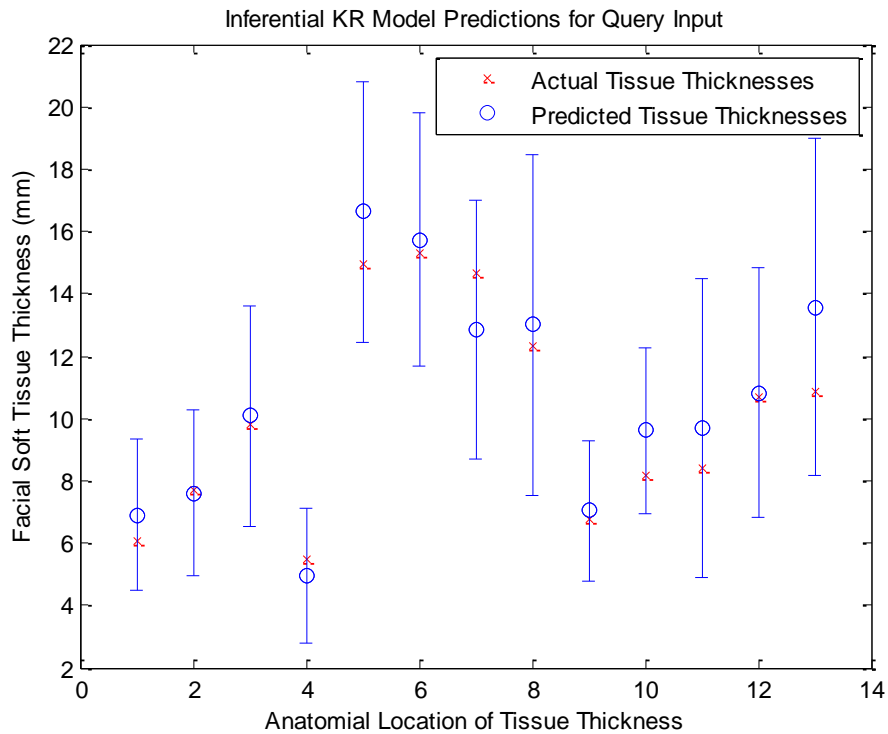


Figure 10: Predictions and Actual tissue thicknesses for inferential model

Table 3: Average Performance Metrics for all Inferential Models using demographics

Prediction Uncertainty	Model RMSE	Table RMSE	Similarity
20.5 %	1.89 mm	3.07 mm	0.81

Table 4: Average Performance Metrics for Inferential modeling without using demographic predictors

Prediction Uncertainty	Model RMSE	Table RMSE	Similarity
20.5 %	2.19 mm	3.07 mm	0.89

The kernel bandwidth used in the inferential model with demographics was 1.3, while the model without demographics used a bandwidth of 1.6. The HAKR model using the memory of 100 skulls resulted in a 38% decrease in error when using the demographics and 29% error when not using the demographics when compared to the Table RMSE.

The William Bass donated collection at the University of Tennessee was used to provide male skulls accompanied with living photos to be used to measure the model’s true abilities. Ms. Joanna Hughes, the project’s forensic artist, has completed all of the facial reconstructions using her normally used techniques, which are the Rhine & Moore facial soft tissue thickness tables for Caucasian males of normal build. Pictures were taken of each completed reconstruction and then the skulls were cleaned so they could be CT imaged and put through our procedures that were developed to analyze the skulls in IDAS. These skulls were analyzed to collect the 18 bone measurements that can be used as the input to the model in order to predict the skull’s tissue thicknesses. The age, weight, height, and BMI were known before death for each of the subjects, but they were not used in one of models in order to show the difference in the resulting reconstructions. The model simply removes those variables from the memory matrix that are not known and makes the best possible predictions with the information it’s given. Since the inferential architecture resulted in the best performance it was used to make the predictions for the test male skulls. The project’s goal was to do reconstructions on 5 male subjects, but the forensic artist had a pregnancy due date during the final 2 reconstructions. Therefore, only 3 reconstructions were completed using the developed model’s predicted tissue thicknesses.

An issue presented itself when the forensic artist began the first reconstruction using the model’s predicted thicknesses. When the forensic artist began using the model's predicted tissue thickness in the reconstruction of subject A she discovered that the value for the Mid-Philtrum location, which is located just below the base of the nasal cavity, was far too large and would interfere with the nose projection. To enable the artist to continue with the reconstruction we elected to not use the model's prediction for this location and result to the normally used tabled values. Since the model only predicts the facial tissue thicknesses for 13 of the 21 craniometrical locations and they are mainly along the midline of the face, the remaining locations needed to be adjusted. The remaining cranial landmarks not predicted using the developed model were scaled to match the magnitude of the model’s predicted values. This was done by computing the ratio of the model’s predictions to the tabled values for the 13 locations and taking the average. The scaling factor is multiplied by the tabled

thickness values that would be used in the reconstruction for the 8 landmarks, to provide new values that better agree with the model's predictions. A single scaling ratio is calculated for each query input to the model. The scaling is necessary because the predicted values are nominally larger than the tabled values, using the tabled values for the remaining locations do not work. Appendix C of the full report contains the exact tissue thicknesses used for the three reconstructions along with the advised scaling factor for subject B and C. The reconstruction of subject B did not use the demographics as inputs.



Figure 11: Old (left) and New (right) reconstruction methods compared to actual living photo (middle) of the subject A

Figure 11 shows the facial reconstruction of male subject A using the tabled values (left), the living photo (middle) and the reconstruction using the model's predicted tissue thicknesses (right). Dr. Richard Jantz provided his interpretation of the comparisons of the reconstructions against the living photos and the following discussions are based on his comments. This male subject was 68 years of age, 85.5 kg in weight, 170 cm in height, and a BMI of 29.6. The table and model reconstructions are similar for subject A, but the model improves the fit a bit. However, it is difficult to say exactly why. The table and model profiles differ in that the model's has a more prominent bridge and nose. Also, the entire face is pulled back a bit more. Overall, the model's predicted tissue thicknesses seem to approximate the face of subject A better than the currently used method. The uncertainty for the 13 predictions was an average of 22.3%. The average similarity metric was 0.91.

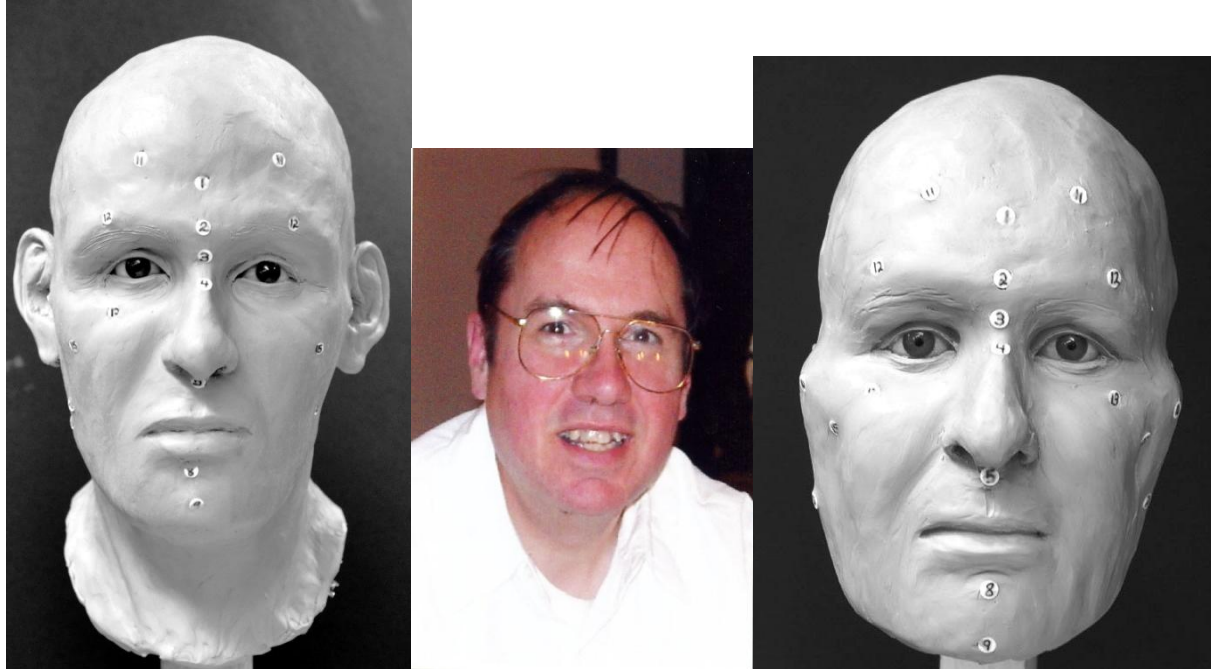


Figure 12: Old (left) and new (right) reconstructions compared to the actual living photo (middle) of the subject B

Figure 12 shows the facial reconstruction of male subject B using the tabled values (left), the living photo (middle) and the reconstruction using the model's predicted tissue thicknesses (right). This male subject was 44 years of age, 112.5 kg in weight, 172.7 cm in height, and a BMI of 37.7. The Zygomatics are too wide in the model's approximation for subject B, requiring the upper facial breadth to retreat, not seen in the photo. The interorbital in model seems to be more accurate than and not quite as narrow as the reconstruction using the tables. Also, the lower face is a bit fuller, which conforms better to actual. The uncertainty for the predictions was an average of 21.5% for all 13 predictions. The average similarity metric was 0.76

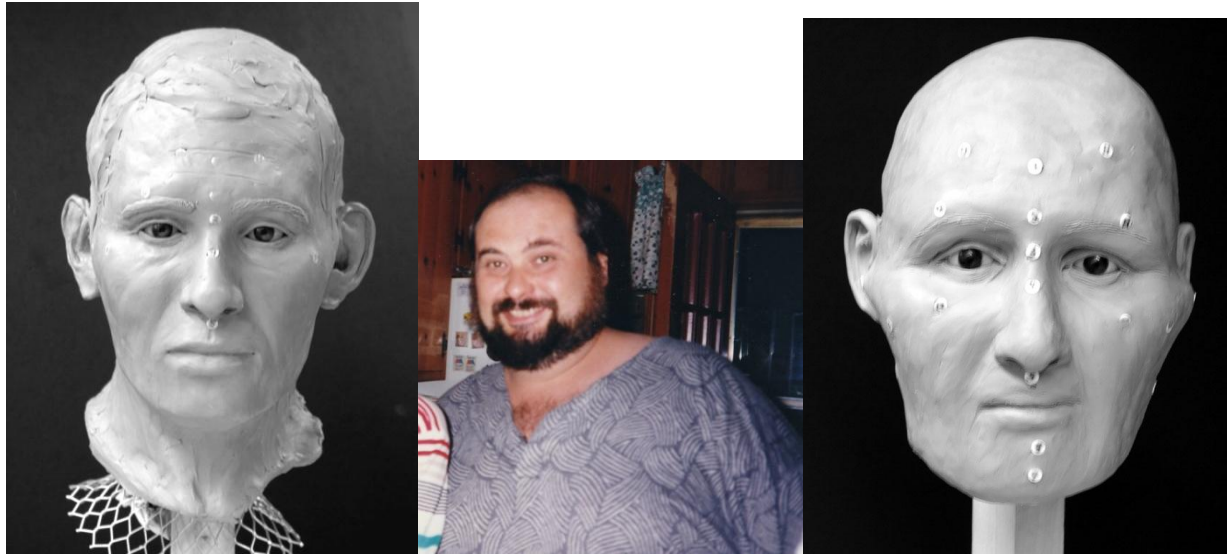


Figure 13: Old (left) and new (right) reconstructions compared to the actual living photo (middle) of the subject C

Figure 13 shows the facial reconstruction of male subject C using the tabled values (left), the living photo (middle) and the reconstruction using the model's predicted tissue thicknesses (right). This male subject was 49 years of age, 180 kg in weight, 179.5 cm in height, and a BMI of 55.9. Examination of the two facial approximations for subject C shows drastic differences. Using table values produces a face too slender. The model version captures the shape of the face a bit better, although it angles too steeply inferiorly and hence not as round as the actual face. The nose and interorbital is a better match to the actual face. In life the nose has a fairly low root and then widens. It does that better in the model version, but still not as much as in life. The uncertainty for the 13 predictions was an average of 16.7%. The average similarity metric was 0.15. This very low similarity was due to the subject's weight and BMI being outside the range of the observations in the memory matrix.

Conclusions

The methodology and procedures required to collect and analyze the cranial data were developed. The setbacks that occurred during the development of the methodology were resolved and with the provided extension through May 2010 the final project objectives were accomplished. With the methodology in place, the collection of the facial tissue thicknesses and bone measurements was much more rapid and consistent using the IDAS software. The HAKR model and inferential models built with the 100 observations both yielded results with less error than the currently used tabled tissue thicknesses. The inferential kernel regression architecture outperformed the hetero-associative kernel regression architecture. The inferential model provided a 38% decrease in error from the tabled thicknesses when using the

demographics as inputs to the model. The demographics, weight and BMI, are the highest correlated predictors of tissue thickness among the 22 predictors used in this pilot study. When the demographics are removed the performance is reduced to a 29% decrease in error. Demographics, weight and BMI especially, are usually not provided to the forensic artist, but technologies could be used in helping to estimate them from skeletal remains (K.Moore, 2008). This could be used to allow these demographics to aid in predicting tissue thickness by using them as input to the inferential model. The clay facial reconstructions resulted in noticeable improvements when using the developed model compared to the currently used tissue thickness tables. However, inaccuracies were presented in the exaggerated thicknesses on the side of the face. This occurred due to the obese and overweight subjects used to build the model and the fact that their measurements were captured with them lying down.

This pilot study revealed that there requires further investigation into possible cranial bone predictors for facial soft tissue thickness. The initial development of IDAS has led to the opportunity to efficiently discover other features that could be used as facial tissue thickness. A more complete data set with ethnic and body mass diversity will allow for more accurate tissue measurements. Each of these concerns must be examined in future work.

Future Work

Future research should include a more complete data set with a wider variety of test subjects, which will allow for additional craniometrical locations to be examined. A source for collecting a more complete data set of crania has been identified and a proposal for future work has been submitted. The proposal titled “Automated Facial Reconstruction Using Empirical Modeling” was submitted for the current NIJ solicitation, Research and Development on Forensic Crime Scene and Medicolegal Death Investigations. The further development of the software package, IDAS, will bring with it many exciting automated feature extraction abilities. This will enable a more exhaustive search for good skin thickness predictors. The more complete data set and automated feature extraction can allow for the kernel based model to be optimized and possibly separated into models based on demographic information. A final objective of future research would be to incorporate the empirical modeling into a computer based facial rendering using the IDAS software.

I. Introduction

Statement of the Problem

Forensic facial reconstruction has been used for many years to identify skeletal remains. The face of the unknown person can be reproduced based upon the soft facial tissue thickness, which overlays the bony structure of the skull. Currently forensic artists place average facial tissue markers at 21 specific anatomical locations on the skull and use clay to model the face based on the length of the markers. The purpose of this study was to develop a new technique for estimating the facial soft tissue thickness at the 21 traditional craniometrical landmarks used in forensic facial reconstruction. The soft tissue thicknesses or marker lengths used in the forensic facial reconstruction are currently the average tissue depths of various examined cadavers of different ethnicity, whereas this technique uses a non-parametric modeling technique to predict the facial tissue depths based on a unique skull input.

Literature Review

Forensic Facial Reproduction

Nearly all facial reproduction techniques rely on the average tissue thickness in the tables produced from past studies of cadavers and are usually presented in sex or different weight categories (Taylor, 2001). The average tissue thicknesses are measured at 21 traditional craniometrical landmarks on the cranium and mandible. Figure 1 displays and numbers the locations of the anthropological landmarks on a skull. The 21 traditional locations used on the reconstructed skull are actually a total of 32 fiducial markers because 11 of the anatomical locations are used on each side of the skull.

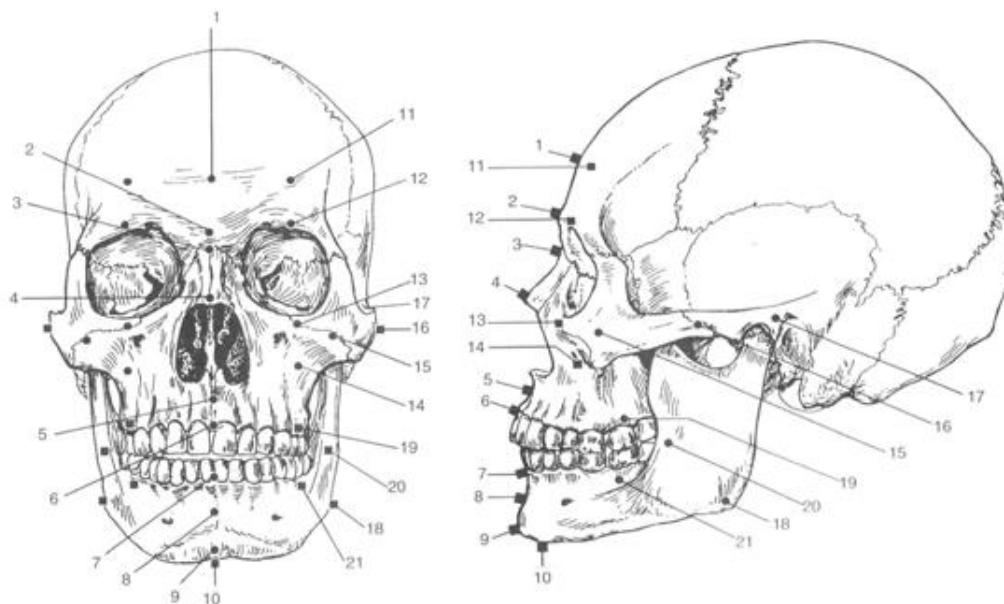


Figure 1: Traditional locations of the fiducial landmarks used in this study (Taylor, 2001)

There are 10 landmarks, numbers 1 through 10, along the midline of the skull, which is a straight line from the center of the forehead to the bottom of the chin. The other 11 facial landmark locations, numbers 11 through 21, are found on the side of the skull and are called bilateral markers. These 11 tissue measurement markers are used on each side of the skull. The numbering system and locations of the tissue depth markers shown in Figure 1 are used throughout this study and were developed by Dr. Stanley Rhine (Taylor, 2001). The anatomical names and numbers corresponding to the facial tissue markers are shown in Table 1. These 21 landmarks are the locations on the skull where the facial tissue depths are to be measured and then predicted on an unknown skull. All 21 landmarks are then used by the forensic artist to reconstruct the face using modeling clay.

Table 1: Traditional landmarks for location of tissue depth markers on the skull (Taylor, 2001)

#	Landmark Name
1	Supraglabella
2	Glabella
3	Nasion
4	End of Nasals
5	Mid-Philtrum
6	Upper Lip Margin
7	Lower Lip Margin
8	Chin-Lip Fold
9	Mental Eminence
10	Beneath Chin
11	Frontal Eminence
12	Supraorbital
13	Suborbital
14	Inferior Malar
15	Lateral Orbit
16	Zygomatic Arch, Midway
17	Supragleniod
18	Gonion
19	Supra M ²
20	Occlusal Line
21	Sub M ²

The above craniometrical landmarks where the tissue depths are measured can display considerable individual variations. A literature study of past work has been completed in the

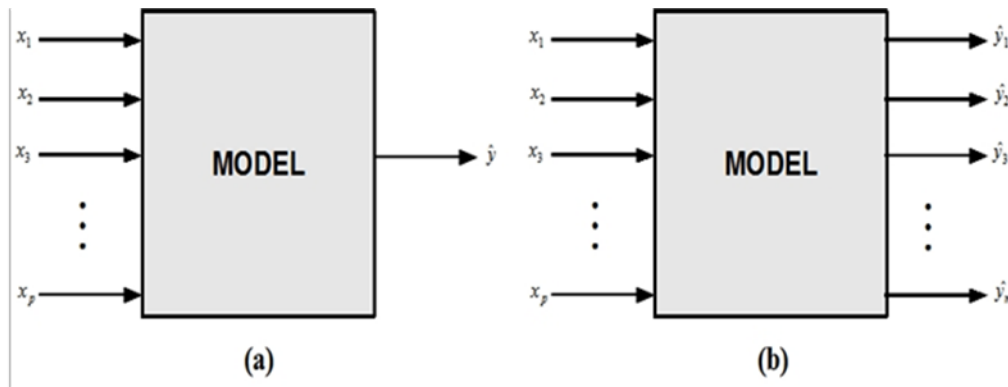
field of forensic facial reconstruction along with empirical modeling techniques. This review of the literature resulted in no studies of the statistical analysis of the relationship between facial and cranial landmarks, and in particular the correlation between bone and soft-tissue landmarks around the eye orbits, nose, mouth and ears (Vargas & Sucar, 2005). The primary purpose of the project is to examine the possible correlations between the bony structure in the cranium and the soft tissue that surrounds it, and then construct an empirical model based on the correlations to predict the facial tissue depth for the 21 landmark locations. As stated in one publication discussing the issues of current facial approximation methods, "The intricacy and complexity of the soft tissues overlaying the skull is significant and to be able to predict them accurately and precisely from the skull alone would definitely be something special" (Stephan 2003).

Background into Empirical Modeling

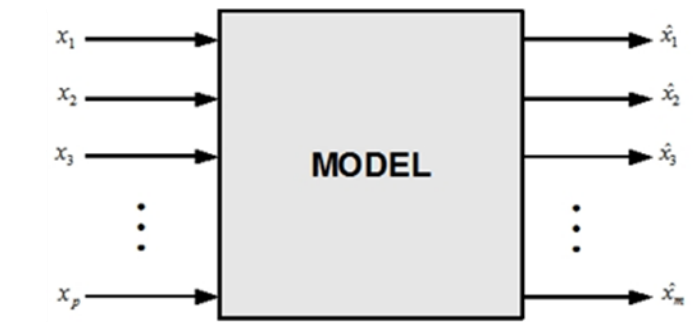
There are two major categories of empirical modeling methods used for prediction: parametric and non-parametric. The parametric methods include linear regression, neural networks and other techniques that map relationships in data by optimizing different parameter values using a data set similar but not exact to future data sets, which is called a training data set. However, once the parameters for the model are identified the training data are no longer used and the model's prediction equation is set. In the forensic facial reconstruction model the parameters that define the model are the facial tissue depths at the traditional anatomical locations. In order improve the facial tissue depths used in a forensic facial reconstruction; the model must be able to change its parameters or weights based on the input to the model. This requires the use of a non-parametric modeling technique.

A non-parametric empirical technique does not use set parameters to define the model like the parametric modeling technique mentioned above. The non-parametric techniques use the actual training data to understand future predictions and store the training data in a "memory matrix". Non-parametric empirical modeling used for forensic facial reconstruction can provide advantages over parametric methods. Non-parametric methods are easily updated as additional data becomes available by simply appending the new data to the historical database or memory matrix. As new facial tissue measurements are made from additional CT images, the data can be added to the historical database and the model predictions become more accurate. There are no training times and no need to optimize the parameter values in the model. This means that new facial tissue measurements can be inserted into an existing model without additional software programming or optimization. As with any prediction method, there is a certain amount of uncertainty involved. Therefore, methods have been developed to produce uncertainty values on non-parametric predictions (Rasmussen & Hines, 2005). This allows the future users of the prediction software to have an estimate of the accuracy of the facial soft tissue thicknesses being used in the reconstruction. The ability to accompany a facial reconstruction with an uncertainty should help forensic investigators decide if the reconstruction should be used in an investigation.

Kernel regression (*KR*) is a technique used in statistics and empirical modeling to estimate a parameter's value by calculating a weighted average of historical observations, also known as exemplars (Atkeson, Moore, & Schaal, 1997b). There are three different *KR* architectures, which are characterized by the number and type of inputs and outputs, shown in Figure 2. These model architectures are inferential, hetero-associative, and auto-associative *KR*. This study uses a hetero-associative model architecture that uses multiple inputs to predict multiple outputs. The multiple inputs in this application consist of demographic information (*sex, age, race, etc...*) facial tissue depths, underlying bone thicknesses, and bone separations along specific anatomical lines collected from the CT images. The number of features collected from a particular subject may be a subset of the features that are considered to be important and that are stored in the historical database. For example, the race may not be known for the test subject. The conventional hetero-associative algorithm will be augmented to work under these cases of missing input variables.



Schematic diagram of (a) inferential and (b) heteroassociative models



Schematic diagram for autoassociative model

Figure 2: Different Kernel Regression (*KR*) Architectures

The empirical modeling architectures used in this project was Hetero-Associative Kernel Regression (HAKR) and Inferential. The HAKR type of modeling architecture is a non-linear, non-parametric, kernel regression model in which the number of inputs does not equal the

number of outputs in the model. The only difference in the inferential type of modeling architecture is the number of outputs from the model is one. Therefore, a separate KR model is constructed for each output exemplar. In this project a total of 13 inferential KR models are built to predict each craniometrical location's facial soft tissue thickness.

The first step in making a prediction using a KR model, regardless of architecture, is to compute how far the query inputs are from the memory matrix, which is built from the known skull data sets. A Euclidean distance operator, Equation 1, is used to determine the distance the query data, q , is from the training data, x . This is used iteratively through each observation in memory, i , through the total number of observations, n .

$$d(x_i, q) = \sqrt{\sum_{i=1}^n (x^i - q)^2}$$

Equation 1: Euclidean distance measure

These distances are then converted to a weight for each training vector. Equation 2 is the Gaussian kernel function used in the modeling architecture. The purpose of the kernel bandwidth, h , is to help optimize which memory vectors are considered similar to the query input and therefore used in the prediction.

$$w = K(d, h) = \frac{1}{\sqrt{2\pi \cdot h^2}} e^{-d^2/2h^2}$$

Equation 2: Gaussian Kernel

The kernel bandwidth must be optimized to reduce the model's error and predictive uncertainty. Figure 3 shows how the kernel bandwidth is used to help find the optimal kernel for the model. As the bandwidth (h) increases the Gaussian kernel widens and incorporates more distant query vectors. This gives a greater weight to more query points. The optimal bandwidth is chosen iteratively while comparing each model's prediction error.

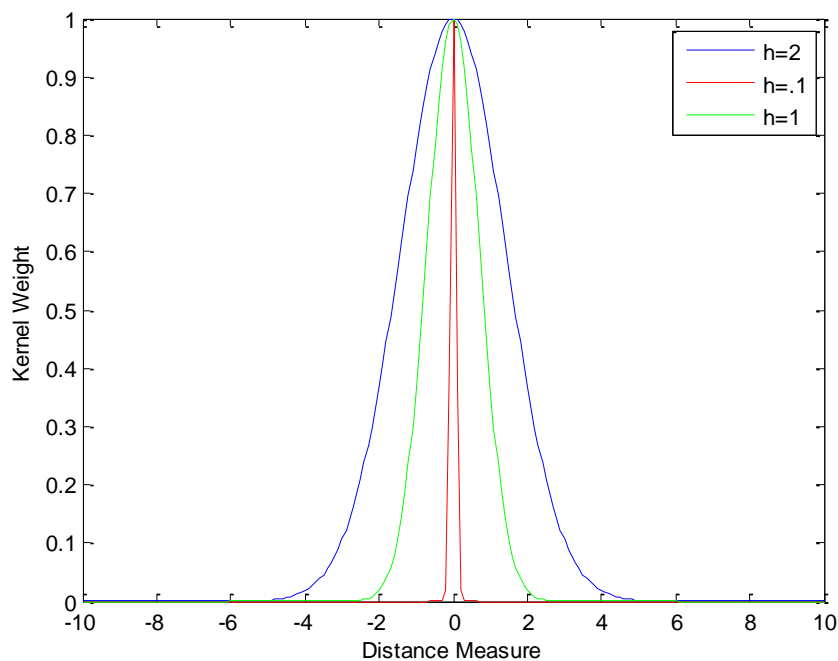


Figure 3: Affect of changing the Kernel bandwidth (h)

The predictions are then computed using Equation 3, which is a weighted sum of the output memory vectors. In the case of the HAKR model used in this study the number of outputs is different than the number of inputs. This requires the prediction to be a weighted sum of the output memory vectors, which are known facial tissue depths measured from the database of male skulls.

$$\hat{y}(q) = \frac{\sum_{i=1:n} y_i w_i}{\sum_{i=1:n} w_i} = \frac{\sum_{i=1:n} y_i K(d(x_i, q))}{\sum_{i=1:n} K(d(x_i, q))}$$

Equation 3: Weighted sum prediction

The prediction outputs are the facial tissue depths for the unknown skull's input parameters. The input parameters used in this study are further discussed in the Additional Predictor Variables section. Methods have been developed to produce uncertainty values and prediction intervals for non-parametric predictions [Rasmussen and Hines 2005]; [Rasmussen 2003]. This allows the users of the tissue prediction model to have a quantitative estimate of the accuracy of the reconstruction. This could help investigators decide if the reconstruction

should be used in an investigation. A prediction uncertainty interval (PI) was calculated for the empirical model predictions in order to present a numerical value investigators could use to determine if the tissue thicknesses should be used. The prediction interval for the empirical model's predictions includes the noise variance in the output data, which makes the PI greater than a confidence interval (CI). This makes a PI more conservative than a CI for uncertainty estimations. The prediction interval for a 95% confidence level was computed using equation 4.

$$\hat{y} \pm 2\sqrt{\hat{\sigma}_e^2 + Var(\hat{y}) + Bias^2}$$

Equation 4: Prediction Uncertainty Interval

The first value within the radical is an estimate of the noise variance in the output, which are the tissue thickness values for each skull in the database. The variance of the prediction is computed analytically using equation 5. The analytical variance calculation incorporates the weights from the prediction and the noise variance for the output memory matrix. The noise variance, σ^2_{noise} , is estimated to be the squared error of the measurements used in the output memory matrix. This value is considered to be the largest dimension of a voxel in the CT images used in measuring the tissue thicknesses, which for this study was 0.6 mm.

$$\sigma^2_{prediction} = W * W' * \sigma^2_{noise}$$

Equation 5: Prediction Variance

The prediction bias is computed using equation 6 below. This analytic bias calculation uses a Bias – Variance Decomposition to analytically compute the prediction variance (Rasmussen 2003).

$$Bias(\hat{x})^2 = MSE(\hat{x}) - Var(\hat{x}) - \sigma_e^2$$

Equation 6: Analytical Prediction Bias

Statement of hypothesis

Facial reconstruction has been a tool used by anthropologists and law enforcement agencies in attempting to identify unidentified human skeletal remains. It is considered by many to be a last resort used in the hope that someone will recognize a resemblance between a missing person and the 3D clay reconstruction. To date, there has never been a statistical analysis of the relationship between facial and cranial landmarks. This pilot study assess the feasibility of using a non-parametric kernel regression model for providing tissue depths based

on underlying bone thicknesses and bone separations which are specific to an individual skull. Bone thicknesses, cranial landmark measurements, and demographics could have prediction information of a subject's soft facial tissue thickness. By predicting more accurate tissue thicknesses from only the skull's bone structure, forensic facial reconstructions can become more accurate at estimating the face of an unknown person.

II. Methods

The methodology and processes needed to begin building the empirical model has been completed. A consistent way to measure the tissue thicknesses of the database of patient crania was found in a software program called IDAS. This software package was developed by Dr. Mohamed Mahfouz at the University of Tennessee in Knoxville. The standardization of producing the surface models for each cranium was needed in order to perform the registration and deformation process in IDAS. The detailed progress of the setbacks that occurred and of what has been accomplished during the methodology development is discussed below.

CT Image Collection

The first step in this project was to find and collect the 100 male subjects' CT data. It was collected in the PET/CT Imaging Department of Thompson Cancer Survival Center West in Knoxville, Tennessee. Only the PET/CT scans labeled as melanoma, bone, and brain were examined as possible subjects to use in the study because their scan procedures should include the complete cranium and mandible. The scans were selected based on the advice from the PET/CT personnel. Also, if any noticeable skull deformations or lesions were found in the scan or if the patient was currently undergoing radiation therapy its data was not used in the study. The patient CT scans were verified to entail the entire cranium and mandible in the Picture Archiving and Communication System (PACS) and then the Digital Image and Communication in Medicine (DICOM) image files were copied onto CDs. The PACS system only contained patient scans as far back as the end of 2007. Therefore, all male subjects on the PACS system that fit the criteria mentioned above were selected for this study. When the quality subjects were exhausted in the PACS system, a more time consuming method was used to find the DICOM images in the cancer center's older data management system. No African American subjects could be positively identified to be used; therefore potentially only Caucasian males were used in this study.

Each subject's DICOM image files consist of upwards of 600 CT slices that make up the volume scanned. The number of slices depends on the slice thickness used for the scan and the section of the body scanned. Each CT slice is a 512 by 512 matrix of values ranging from -1500 to 3000. The units are called Hounsfield Units (HU). An HU is commonly used in medical imaging to represent density values of various tissues in the body. Figure 4 is a chart of the Hounsfield Unit values for various tissues along with water and air.

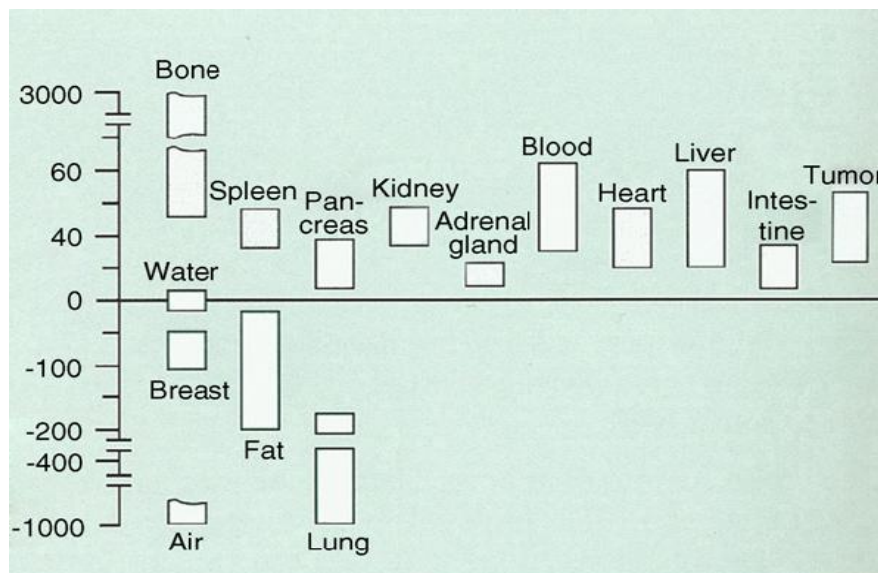


Figure 4: Hounsfield Unit (HU) values for human body tissue along with water and air (Poulsen & Simonsen, 2007)

The CT patient data did not have consistent slice thicknesses and pixel spacing. The slice thicknesses ranged from 1mm to 5mm. The pixel spacing or resolution ranged from 0.5mm by 0.5mm to 1mm by 1mm. These values create what is called the voxel size of an image. It is simply the three dimensions stated above, which creates a small cubic pixel that makes up the complete volume of the subject. The smaller the slice thickness and pixel spacing the clearer the image and the more accurate tissue measurements. A slice thickness of less than 5mm is recommended for accurate facial tissue measurements (Kee-Doeg, Ruprecht, & Wang, 2005). However, the large and inconsistent voxel sizes in the images created a problem in the segmentation process.

Before the empirical model could be constructed, the facial soft tissue thicknesses at the 21 craniometrical landmarks and the possible cranial features that correlate well with the tissue thicknesses had to be measured for each male subject. An extensive exploration in using the MATLAB computing language for a viable answer to registering the CT images and extracting the data needed to build a kernel regression model was performed, but no solution was found. Therefore, contact was made with Dr. Mohamed Mahfouz and The Center for Musculoskeletal Research (CMR) in the Biomedical Engineering Department at The University of Tennessee. He was contacted because of his extensive work in the medical imaging field and experience in computed tomography (CT) image analysis. A software package created by Dr. Mahfouz, *IDAS*, proved to be the best option for collecting the facial thickness and skull feature data. The software has been created for many different bones or joints in the human body, like the femur and hip, but is currently being developed for the cranium. The creation of a cranial registration and deformation package is headed by one of Dr. Mahfouz's PhD students, Emam ElHak Abdel Fatah. This software allowed the measurement of the tissue thicknesses and other features to

be made automatically, which helps remove the variance of manually performing the measurements.

Before the cranial measurements could be made, the bone structure had to be separated or segmented from the rest of the facial tissue in separate image analysis software called *Amira*. Segmentation is the process of separating the cranium and mandible bone from the surrounding facial soft tissue. The segmentation process creates a surface model of the cranium and mandible that is used in the registration and deformation software. Several problems occurred during the first attempts to segment the bone. The inconsistent voxel sizes of the CT image sets resulted in errors in the segmented surface models. These inconsistencies resulted in incorrect bone segmentations and therefore could not be accurately analyzed in *IDAS*.

The segmented skulls are then analyzed in *IDAS* where they are aligned and morphed to the base segmented skull, which has the 32 fiducial markers placed at the 21 anatomical locations. This will allow the correct craniometrical location of each of the markers to be selected for each skull in the model's database. Figure 5 shows the *Amira* surface mesh of the segmented base skull used in the study. This skull is just a normal male skull, which was selected by Dr. Lee Meadows Jantz of the Anthropology Department at The University of Tennessee to be used as the base skull for the registration and morphing process. The teeth are missing from the surface model because of the scattering artifacts that occur when metal objects are imaged with computed tomography. Since the base skull had metal caps in his teeth, all skulls in this study were segmented without the teeth to provide some consistency among the surface models.

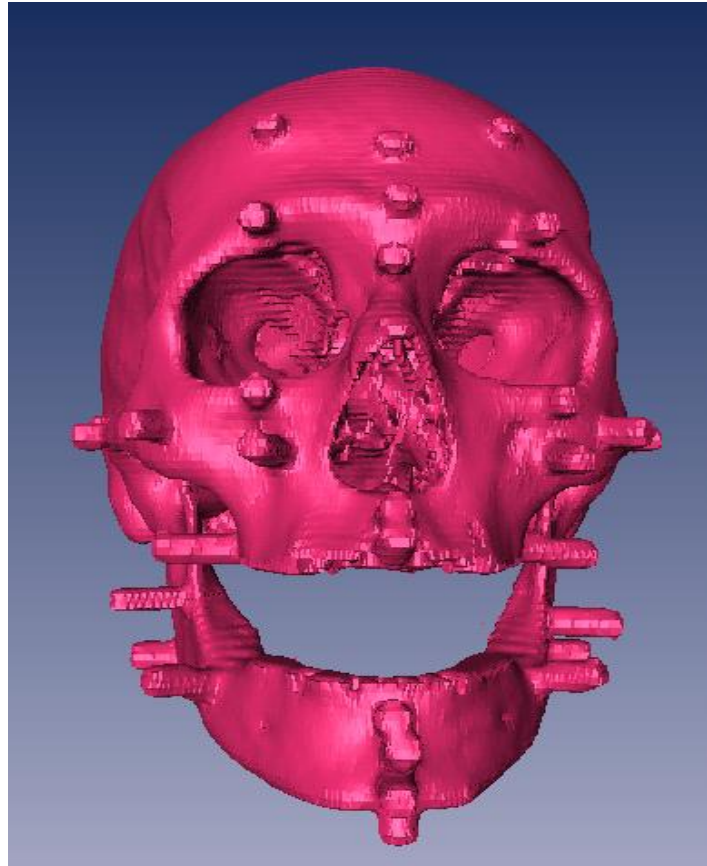


Figure 5: Segmented base skull with the 32 fiducial markers

An essential concern in the segmentation of the CT images was selecting the data window and threshold to be used throughout the data set. A data window is the range of pixel values used when viewing the CT image. The data window can be adjusted to exclude certain pixel values in the CT images from being shown to enhance the more important features, which in segmenting is the bone. The data windowing and thresholding step in segmentation is very important to the accuracy of the future non-parametric model. Therefore, consistency in the data window and threshold values used in segmenting the CT images is vital to finding any possible correlations between bony structure and soft tissue depth. In the CT images used in this study the pixel values range from -1500 to 3000. The difference between the HU values of facial soft tissue and bone can be minimal and hard to define in a CT image. The purpose of this study was not to investigate how to accurately measure facial tissue depths using CT imaging, but instead to find correlations among the cranial bone features and the soft facial tissue. Therefore, consistency was most important when performing the segmentations so that any potential correlations were not lost.

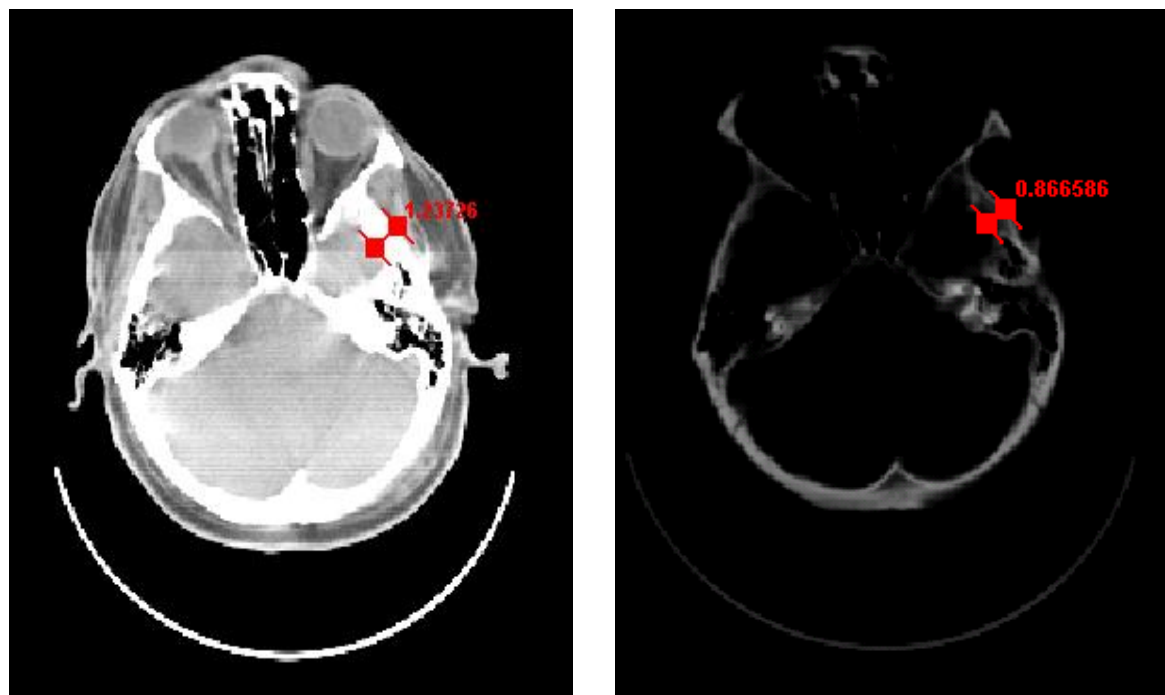


Figure 6: Effect of data window setting on bone thickness measurement. Thickness measured in cm.

Figure 6 shows the effect of data window selection on the appearance of bone thickness in an axial CT image. The image on the left has the default centered data window setting in Amira of -200 to 200. The image on the right has a data window setting of 100 to 3000. According to the Hounsfield Unit scale, the bone should lie in pixel values ranging from about 100 to 3000. As one can see when the data window is changed to a window only including pixel values for bone, the visual thickness of the bone in the cranium is less. However, which is the correct bone thickness? The live tissue CT images are much more difficult to segment due to the soft tissue, cartilage, etc... that can interfere with correctly distinguishing between bone and other tissue. After much trial and error it was decided that once the data is re-sampled to a 0.6mm slice thickness, the default data window would be used in order to keep all segmentations as consistent as possible. This should keep any possible correlation among the soft tissue thickness and various features in the cranium and mandible from being lost due to large variability in each surface model.

To improve the detail visible in the CT image volume, the DICOM data sets were first analyzed in *Mimics 10.1* before being transferred to *Amira* for segmentation. This was done because of abnormal artifacts that were present when loading the DICOMS in *Amira*. Once all the skulls' DICOM images were exported from *Mimics*, they were sent to *Amira 4.0*. In *Amira* the DICOM image volumes were cropped down to only include the cranium and mandible in order to reduce to amount of data being processed. Also, before the segmentation process began the DICOM images were all re-sampled to have consistent slice thicknesses of 0.6mm.

This increases the clarity of the images and makes the segmentation of the skull more accurate and consistent. Another decision was made to reduce the pixel range to unsigned 8-bit. This made the pixel values range from 0 to 255, therefore removing unneeded values. Figure 7 is a simple depiction of the steps from a single DICOM image slice of the skull to a segmented surface model of the cranium and mandible bone.

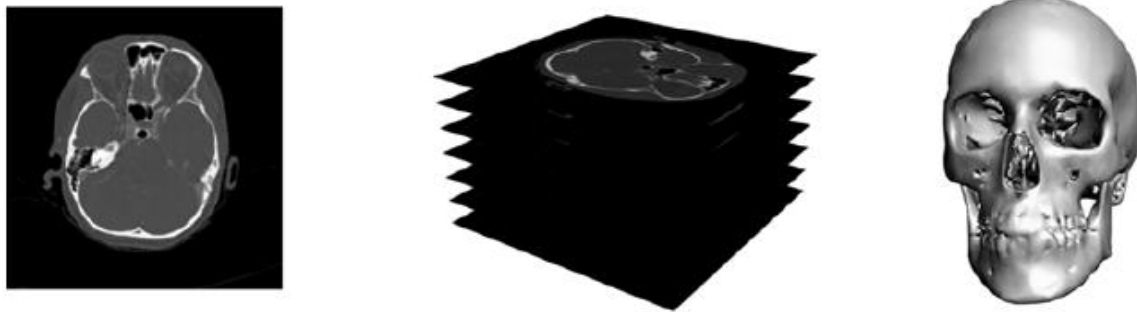


Figure 7: DICOM slice to 3D surface model

The detailed procedure being used to perform the preparation of the DICOM images is shown in Appendix A. This procedure provides a guideline to follow when preparing each data set for the next step performed, which was to segment the bone from the facial tissue. A consistent bone surface model for the entire subject database is vital for the registration and morphing software to work correctly. A flowchart of the steps taken from CT image collection to surface model registration is displayed in Figure 8.

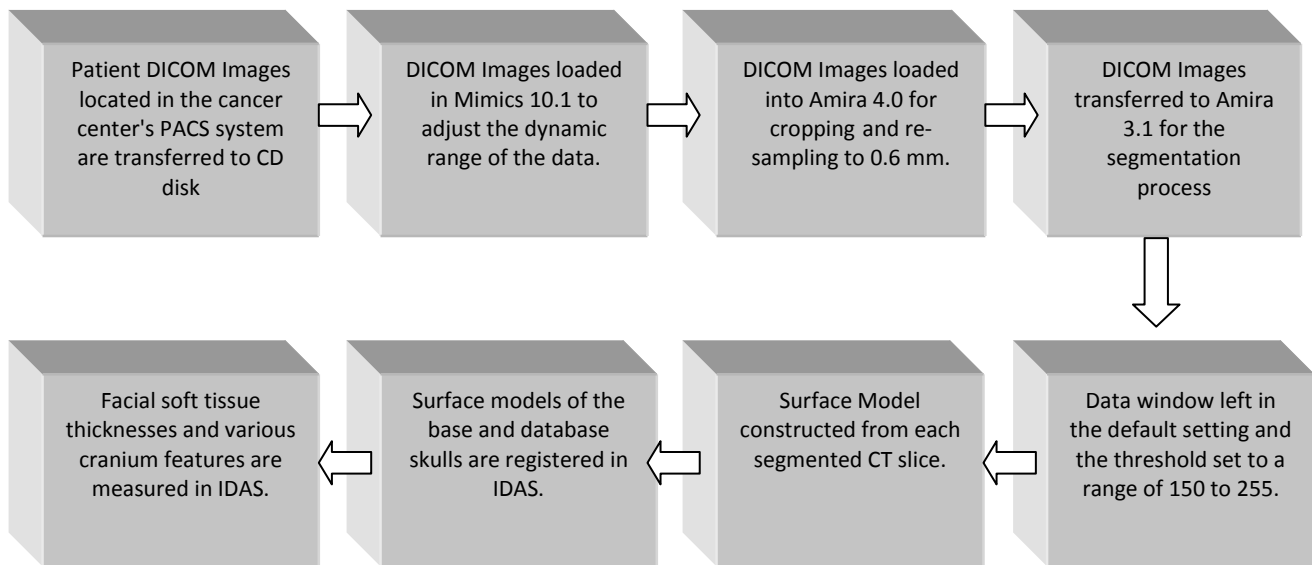


Figure 8: Flowchart for the Data Collection and Analysis Process

The above flow chart displays the steps taken to transform the CT volumes collected at Thompson Cancer Survival Center to a segmented bone surface model that can be analyzed in the IDAS software. The procedure developed to correctly prepare the CT volume data will enable that accurate tissue and bone measurements can be made and allows for future CT data to be processed properly.

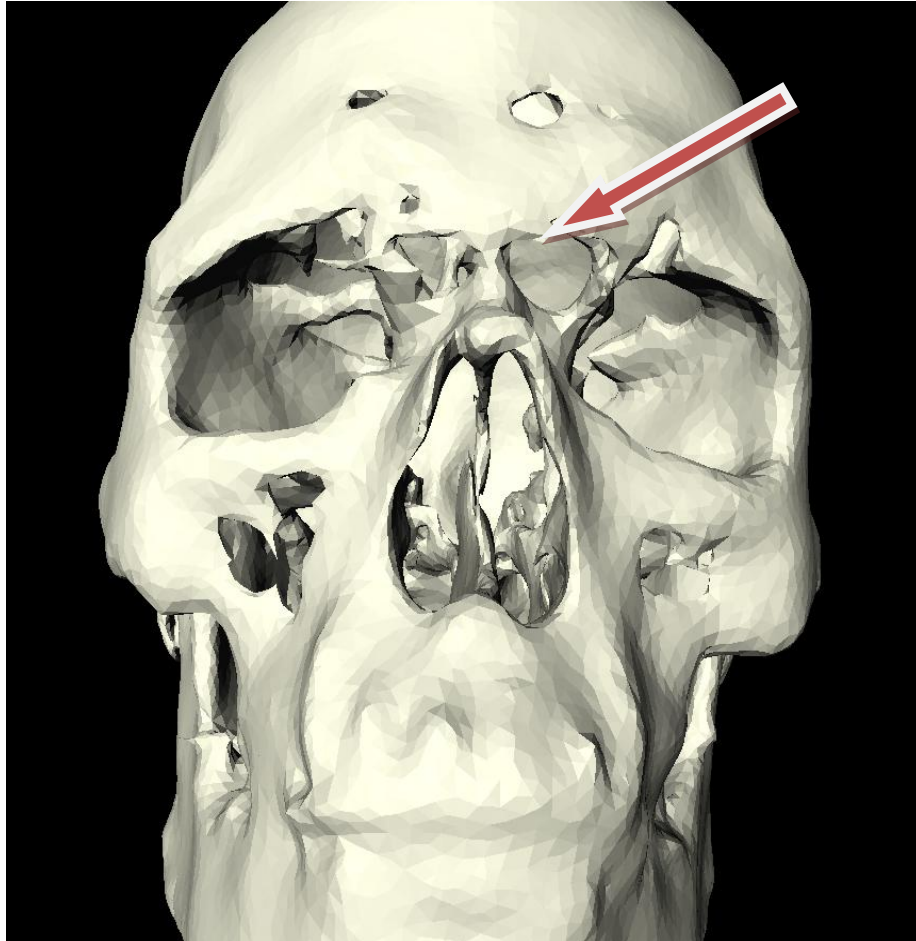


Figure 9: Surface model with holes due to poor segmentation

Even with the procedure mentioned above to increase the DICOM volume resolution, some segmented surface models of the skull had holes in the areas of thin bone thickness. These locations are generally in the lower forehead region where the frontal sinus creates thin bone thickness and in the cheek region where again the sinuses create thin bone thicknesses. The thin bone thicknesses make segmenting the bone from the live tissue very difficult and result in holes in the surface model as shown above in Figure 9. In the surface models where this occurred, the tissue and bone thicknesses could not be made at those locations. However, the chosen craniometrical locations where tissue and bone thickness measurements would be made generally do not lie at the same locations as the surface model errors. This is the case

because after correct DICOM procession and re-sampling the holes that still occur are always in the sinus regions, which are not located where the tissue measurements are taken.

Surface Model Morphing and Registration

The registration and morphing software, *IDAS*, is currently being developed by Center for Musculoskeletal Research (CMR) in the Biomedical Engineering Department at The University of Tennessee, Knoxville. This software will allow the user to select a desired measurement on the base skull to be then propagated throughout the whole atlas of skulls and return that measurement values for each skull. However, the finished software package using this technique for the cranium is not yet complete. In order to move forward in the project and start collecting the tissue thickness data, a simpler method was used to register a database skull to the base skull model, this type method is called affine transformation. It was used in order to start measuring skin thicknesses for the 100 male skulls in the database. This transformation attempts to rigidly align the two skull surface models and put them in the same scale. After a male skull in the database and the base male skull with the fiducial markers are registered to one another, an elastic deformation is used to stretch the database skull to fit the base skull. The elastic deformation will try to match the 32 total fiducial markers on the base skull to the correct craniometrical locations on the database skull where the soft tissue thicknesses will be measured. This method can only be performed one skull at a time. The process of registering and making measurement is discussed throughout this section.

The *IDAS* software home screen is shown in Figure 10. Before any tissue or bone measurements can be made, a single skull's DICOM image set must be loaded into *IDAS*. Along with the DICOM image volume of a particular subject in the database, the subject's surface mesh model must be loaded into *IDAS*.

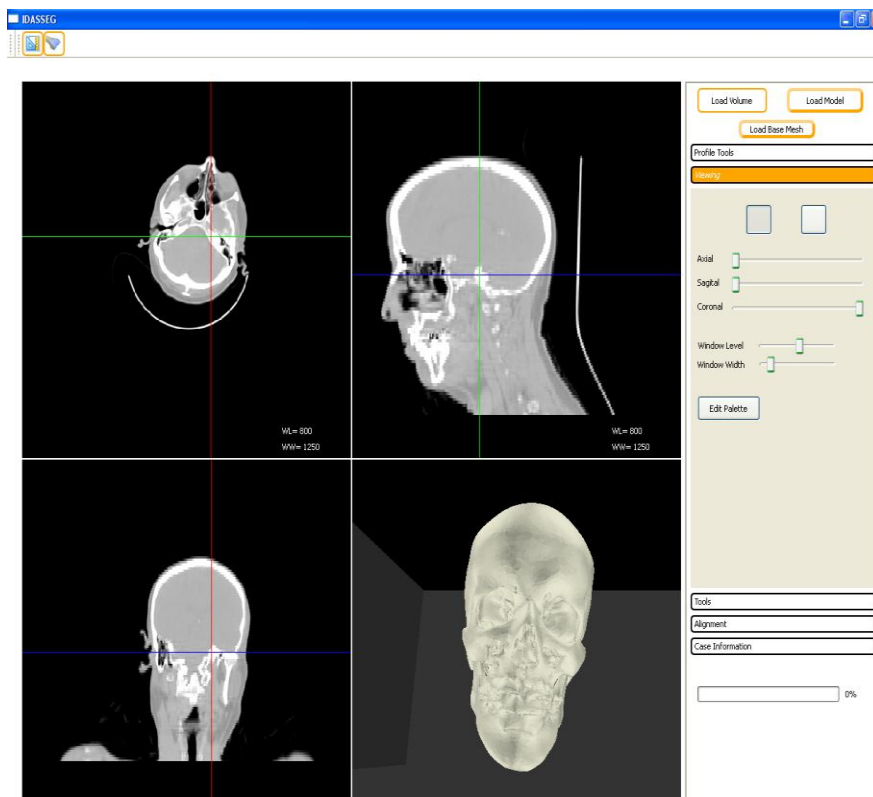


Figure 10: IDAS software home screen with subject volume and model loaded

After the DICOM volume and surface model have been loaded, the IDAS home screen displays the DICOM volume in three different views (axial, sagittal, and coronal). In the lower right quadrant of the home screen the surface model of the segmented bone is correctly placed within the DICOM volume. The next step in using the IDAS software is to load the base mesh and register it to the previously loaded surface model. The registration method used in IDAS for the cranium consists of four steps: scaling, rigid alignment, affine transformation, and morphing (Mahfouz, 2007). The surface model scaling step attempts to align the new surface model mesh with base mesh model and then scales the base mesh to match the dimensions of the new mesh model. The second step in the registration and deformation process is a rigid alignment of the base model to the new model. The rigid alignment is performed using a standard vertex-to-vertex iterative closest point (ICP) algorithm (Besl, 1992). The ICP algorithm works to minimize the distance between a set of points from the 100,000 triangles that make up the base surface model and the new surface model. The algorithm continues to compute the closest point then compute the registration and then apply the registration until the root mean square error between the base model and the new model falls below a set threshold. Figure 11 shows the IDAS screen as the ICP algorithm is working to register the base mesh to the displayed new model.

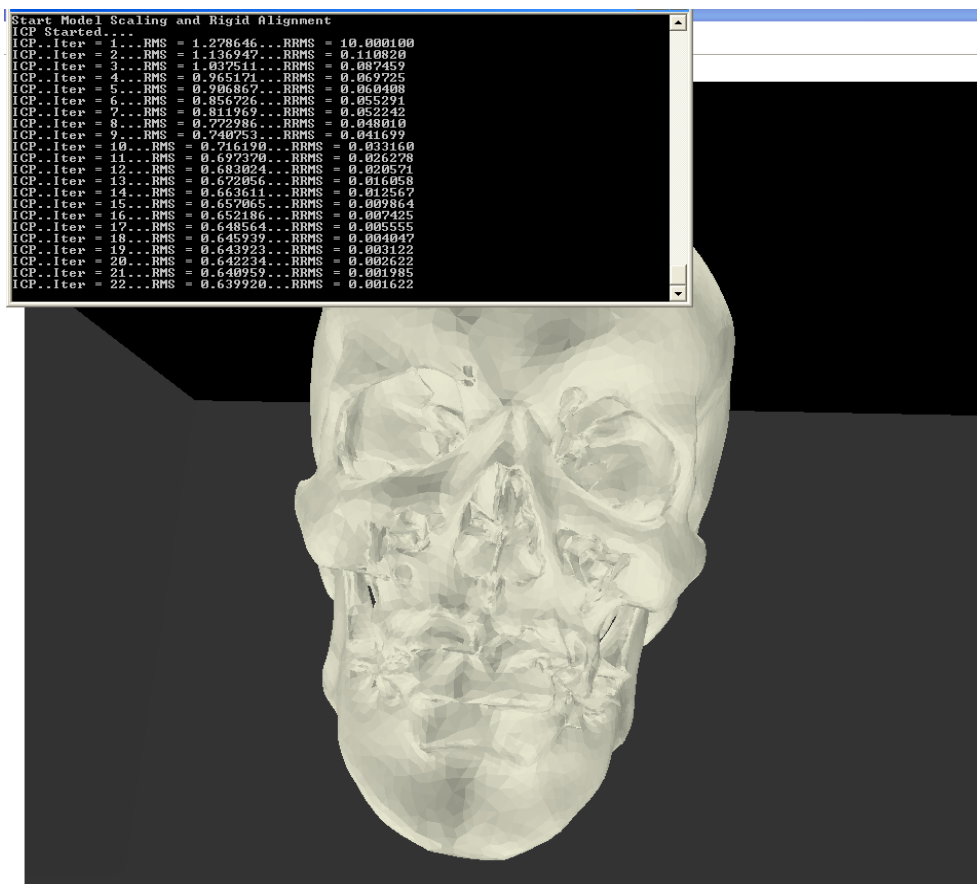


Figure 11: ICP algorithm in IDAS

The third step is to perform a general affine transformation without iteration. The affine transformation method is used to align the base model with new model using 12 degrees of freedom (rotations, translations, scaling, and shear). After the affine transformation the linear transformation limits have been reached, therefore another method must be used to register local portions that are still distant from one another. The last step is a morphing or warping process that tries to create new points on the surface of the new model that has similar local spatial characteristics as the base model. This method used in IDAS is termed mutual correspondence warping (MCW) (Mahfouz, 2007). The MCW in the current version of IDAS for the cranium is not completely done. Figure 12 below shows the registered base model (green) with the underlying new model, which has the red profiles of the tissue thickness measurements. As one can see there are errors in the deformation (MCW) step of the registration; for example around the orbits and mandible. Because of these errors, the base model was used as a guide in finding the locations to measure the tissue thicknesses each new model analyzed.

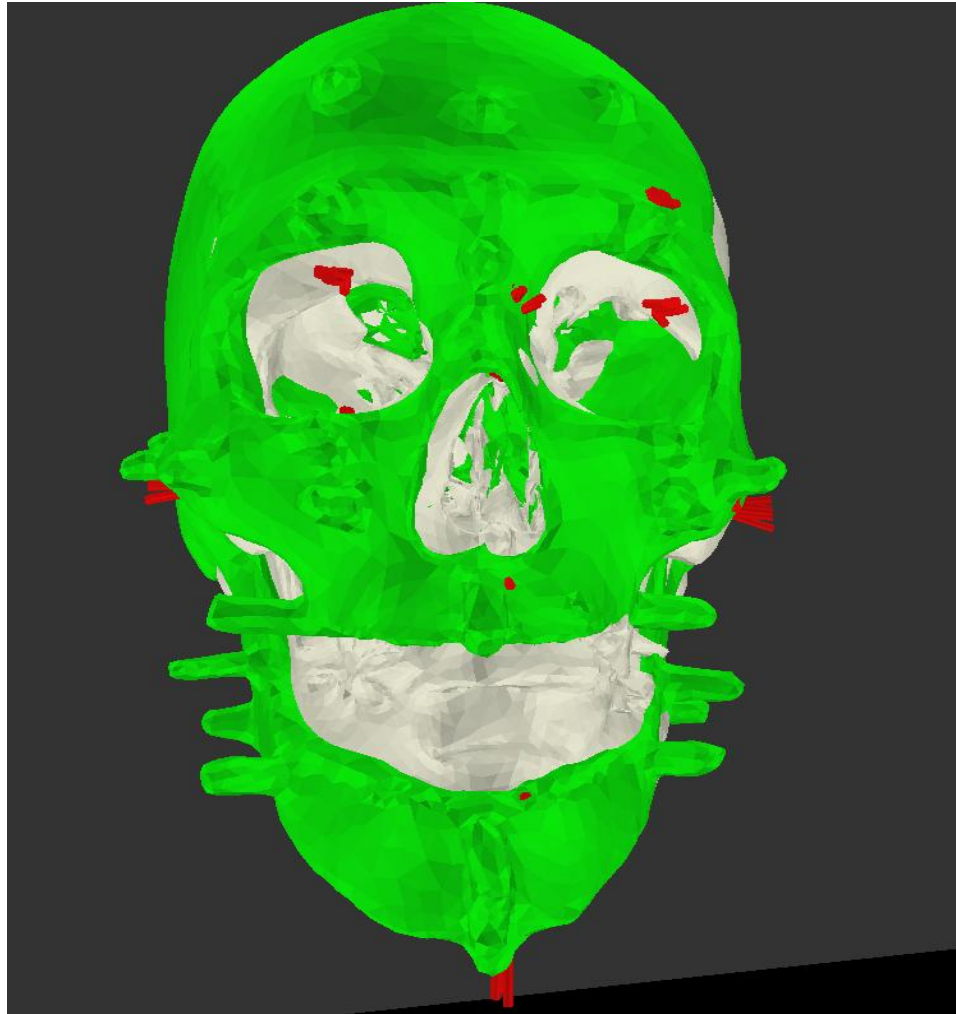


Figure 12: Registered base model and new model in IDAS

The next step in using IDAS to make the tissue and bone measurements is to select the craniometrical location at which to measure the tissue thickness and bone thickness. In IDAS under the Profile Tools tab one can select the Pick button. This allows the user to then pick any number of points on the new surface model to where a measurement will be made. Figure 13 shows a collection of points (pink) selected on the subject's model at a particular anatomical location, which is the glabella in this instance. The error in locating the correct position of each landmark was not determined in this study. This analysis would need to be performed in future studies in order to determine the error and uncertainty associated with measuring the correct tissue thicknesses.

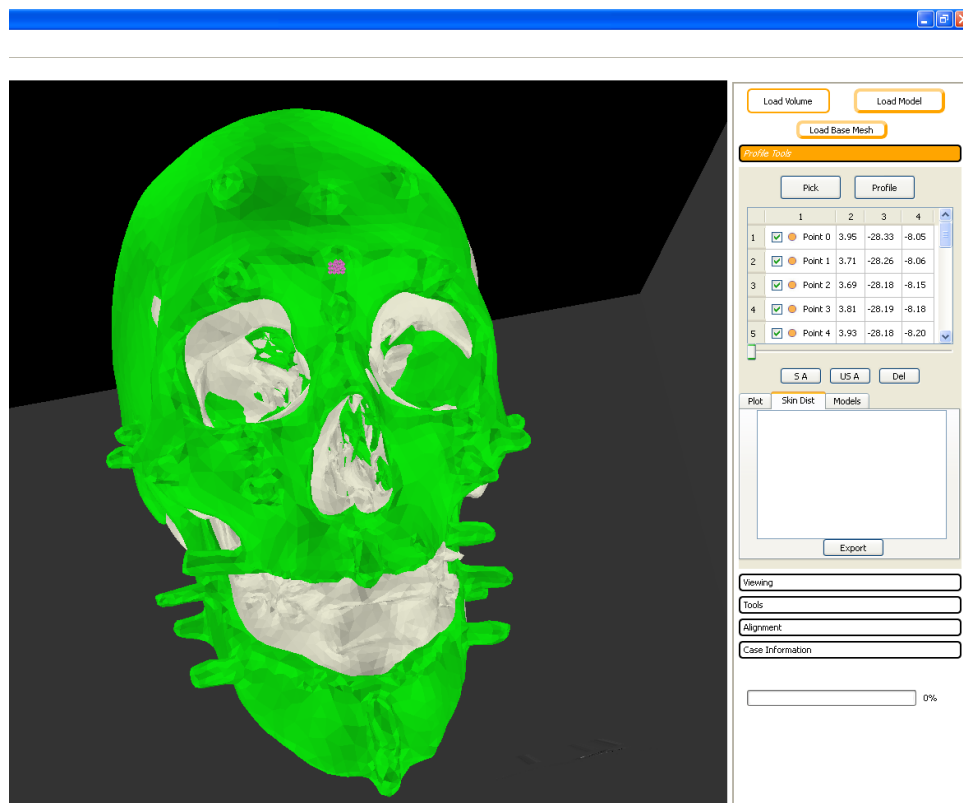


Figure 13: Picking points in IDAS for tissue and bone thickness measurement

To help ensure the most accurate measurements possible, about 20-40 points are picked at each location. This will allow for an average tissue thickness and bone thickness to be calculated from the 20-40 points for a single location on the skull. The tissue thickness and bone thickness measurement for each point is computed by selecting the profile button in IDAS after all points have been picked for a single location. IDAS computes the tissue thickness and underlying bone thickness for each picked point by extending a profile line through the point on the surface model. The tissue thickness is the distance in centimeters from the point picked on the model's surface along the profile line until the pixel value in the DICOMs drops to zero, which is equivalent to air. The bone thickness measurement in IDAS is calculated similarly to the tissue measurement. It finds the distance, in centimeters, from the point picked on the model's surface along the profile line in the direction into the cranium until the surface model at that location ends. Bone thicknesses were selected due to their ability to be easily measured in the IDAS software. The lack of previous studies in the potential of skull bone features being predictors of overlaying soft facial tissue prevented a more guided search. Therefore, bone thicknesses and bone measurements were chosen. How the bone measurements were performed is discussed below.

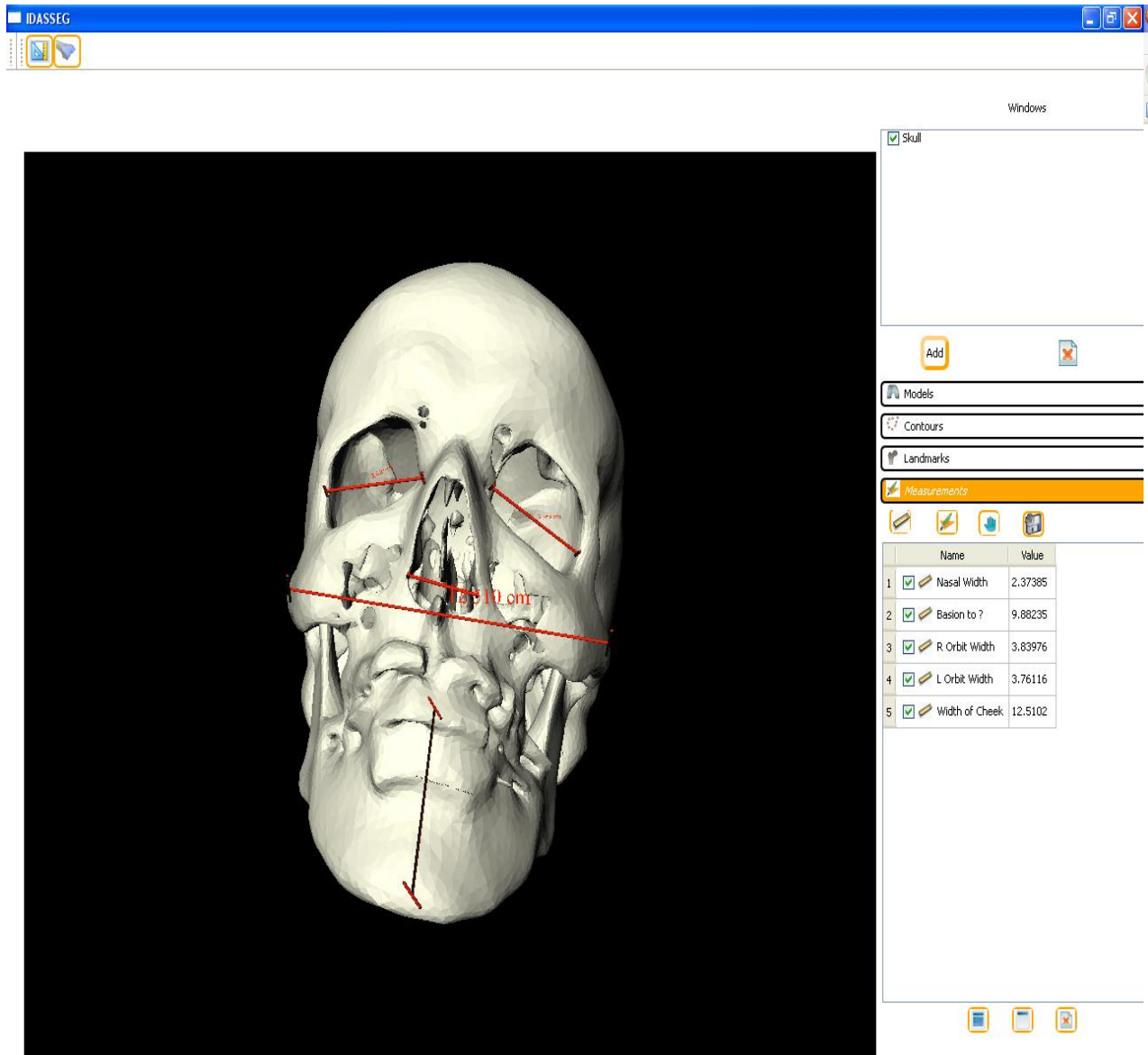


Figure 14: Cranial bone measurements in IDAS

Another tool available in the IDAS software is the surface model measurement tool. This tool allows the user to measure any linear distance on the segmented cranium model. Figure 14 shows the tool being used on a subject skull. The distance tool also allows for any angle to be measured on the skull. These measurements can then be used as possible predictors in the kernel regression model used in this project. The initial bone measurements that were acquired were those needed to possibly estimate a skull's Caucasian or African American ancestry and therefore could also be potential predictors of facial tissue thickness.

Additional Predictor Variables

Consultation with Dr. Richard Jantz and Dr. Lee Meadows Jantz from the Anthropology Department at the University of Tennessee was performed in order to help find more possible cranial features that may correlate to facial tissue thickness. The consultation also determined that none of the 100 male subjects in our database could be estimated as black when analyzed by the Anthropology Department. This was accomplished by viewing the rendered volumes of the faces all 100 subjects. Therefore, the model developed in this study is based on data from all Caucasian males. However, The University of Tennessee's Anthropology Department has developed a method of predicting the ethnicity of an unknown skull, Caucasian or African American, by using several craniometrical measurements on the skull. These measurements were chosen to be additional predictor variables to find out if they are helpful in predicting facial tissue thicknesses.

There are 5 measurements that were chosen to be measured in IDAS. These skull landmark distance measurements shown below can be used to help discriminate between Caucasian and African American by almost 90% based on data from UT's Anthropology Department. These particular measurements, Table 2, were chosen due to their ability to be measured easily from CT images in IDAS and could be measured by a forensic anthropologist physically on the skull. The exact definitions of the craniometrical measurements made for each subject's skull in the database were drawn from Dr. William Bass's *Human Osteology* book (Bass, 1995). The first measurement was the Basion to Prosthion distance. Figure 15 shows the measurement being made in IDAS.

Table 2: Bone Measurements

1. Basion – Prosthion
2. Basion – Nasion
3. Orbit Height
4. Nasal Breadth
5. Biauricular Breadth

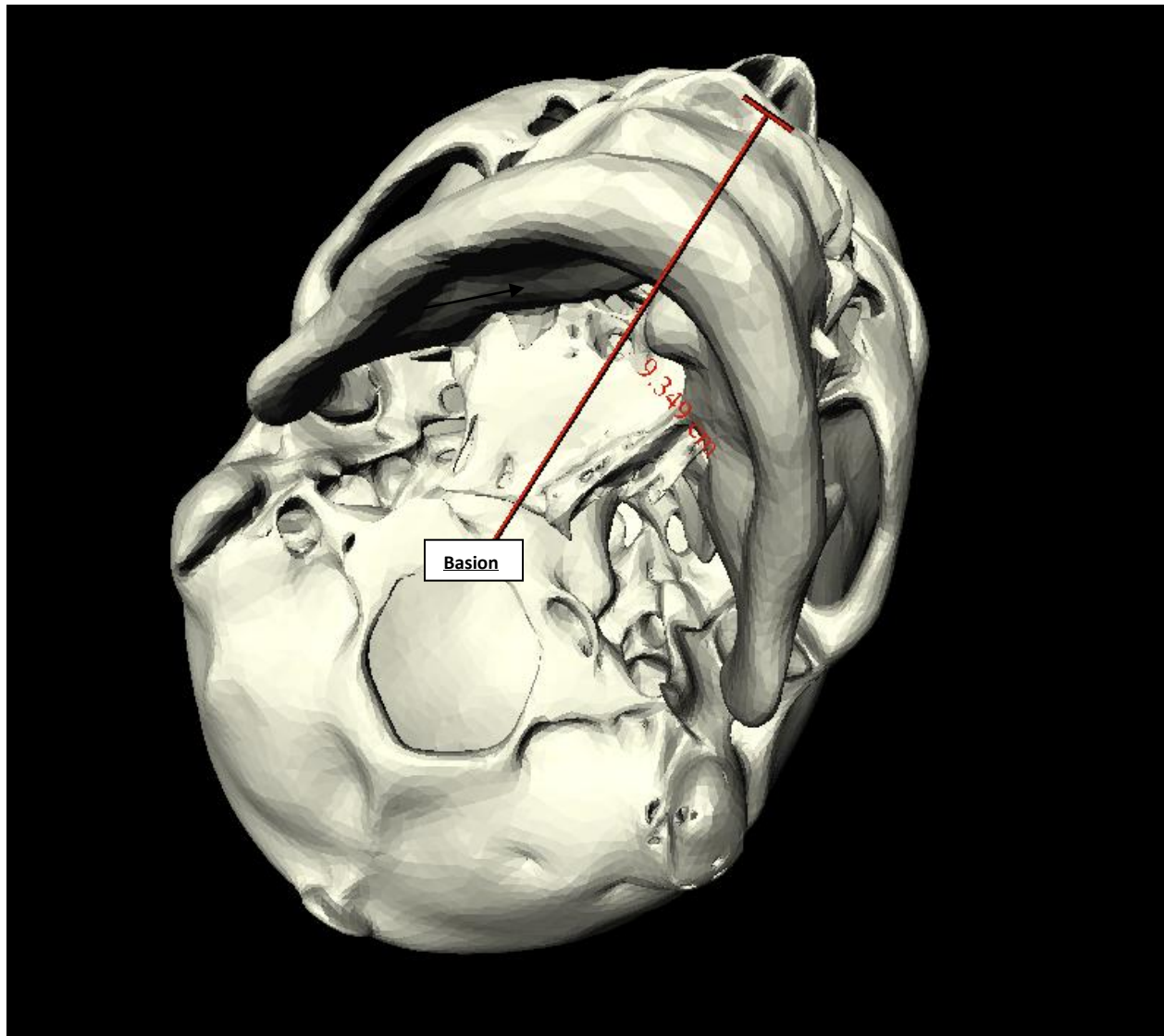


Figure 15: Basion-Prosthion Distance Measurement in IDAS

The Basion location is labeled in Figure 15, but the prosthion location is hard to see. Therefore, a figure from Bass's book is provided to show where the prosthion landmark is located on the cranium. Figure 16 shows the prosthion (pr) landmark just above the upper teeth along the midline of the cranium. Since many of the skulls in our database did not have teeth or the teeth could not be correctly segmented when constructing the surface model, the prosthion landmark was difficult to accurately locate. This measurement was still performed as accurately as possible, but its reliability and measurement error are unknown.

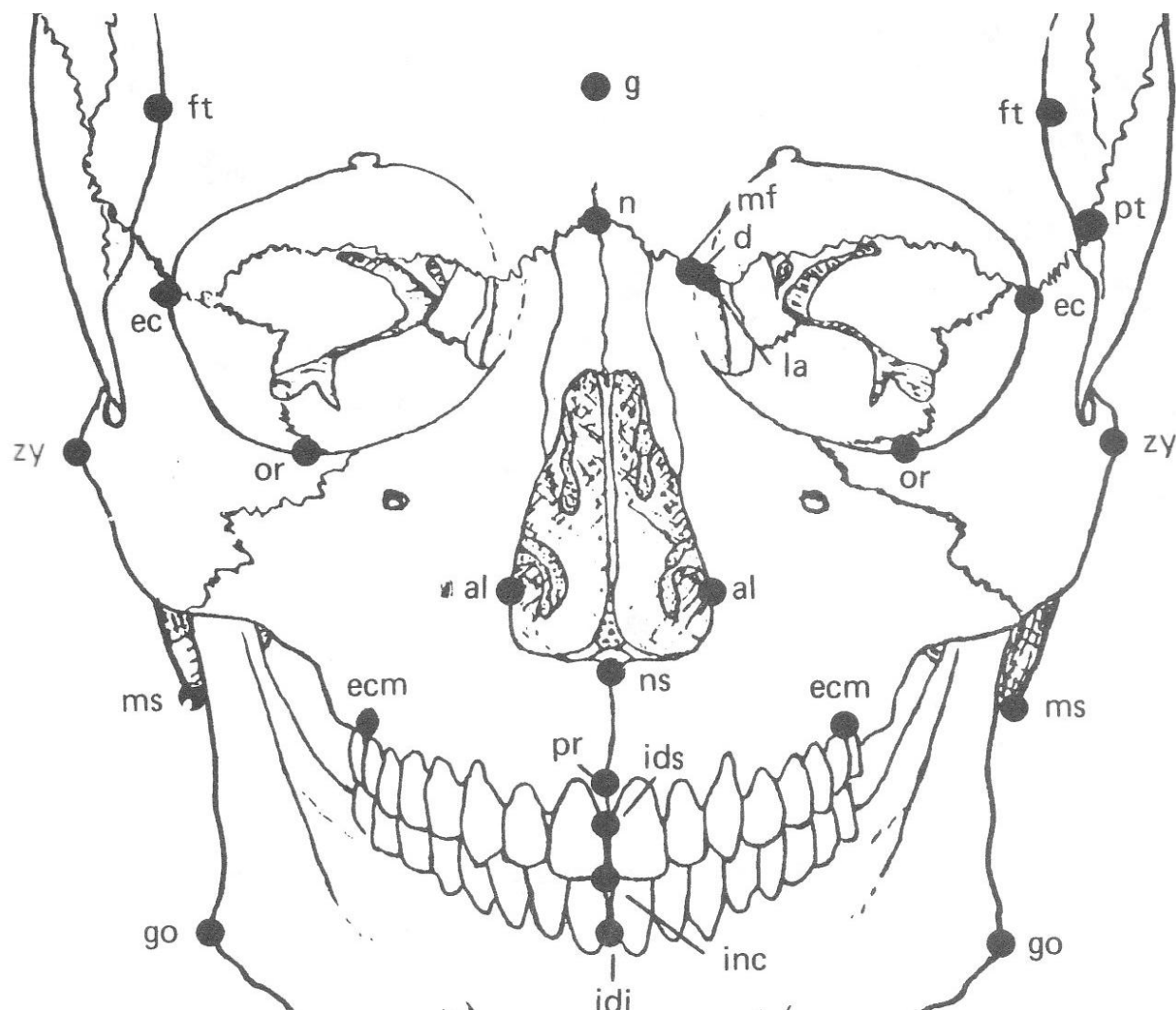


Figure 16: Frontal cranial landmarks

The next bone measurement performed was the Basion to Nasion (n) distance. This distance measurement was more accurate and easy to perform due to the consistent ability to locate the Basion and Nasion landmarks. The Nasion craniometrical landmark is the same location as mentioned earlier when discussing the facial tissue landmarks. Figure 17 is a screenshot of the Basion to Nasion distance measurement being performed in IDAS. The third bone measurement collected in IDAS was the Orbit height. The orbit height is the maximum height from the upper to lower orbital borders perpendicular to the horizontal axis of the orbit. Figure 18 shows the Orbit height measurement in IDAS.

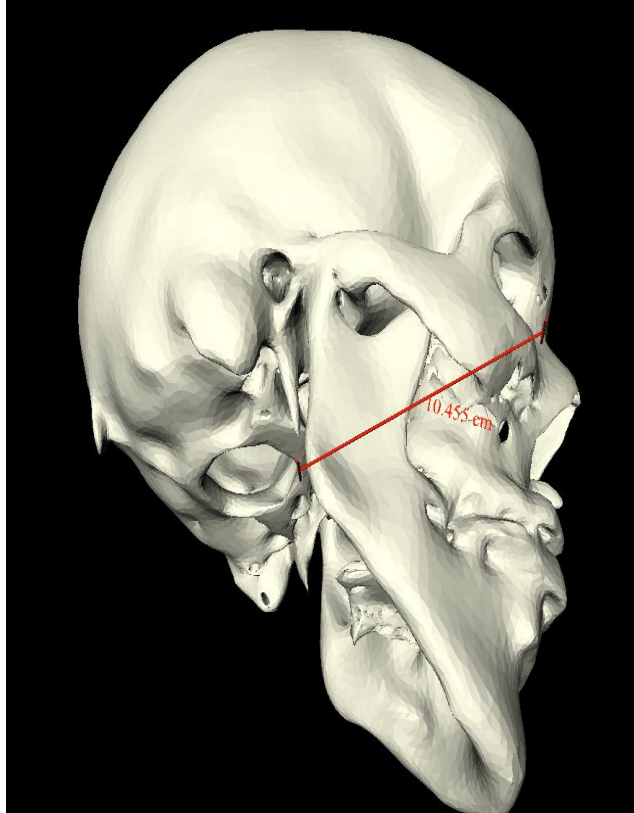


Figure 17: Basion-Nasion distance measurement in IDAS

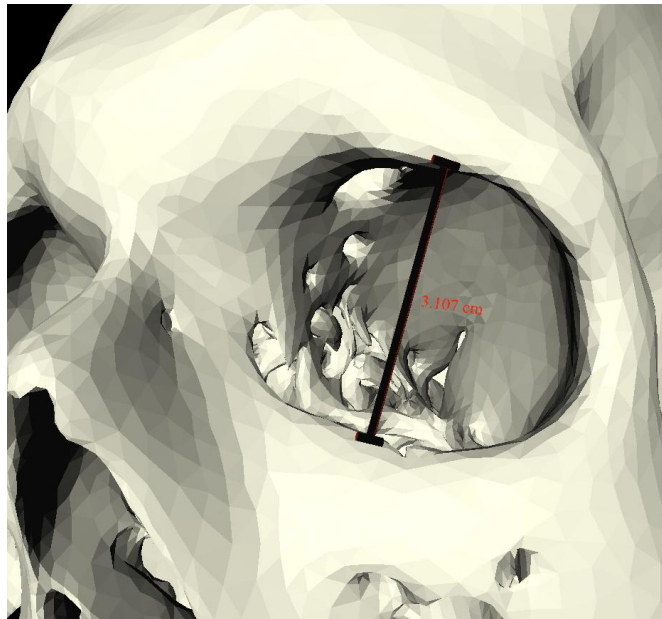


Figure 18: Orbit Height measurement in IDAS

The fourth bone measurement performed in IDAS was the Nasal Breadth. The Nasal Breadth is defined as the maximum breadth of the nasal cavity. It is measured at a right angle to the height of the nasal cavity from craniometrical locations alare to alare (al), which are shown in Figure 16. The nasal breadth measurement being performed in IDAS is shown below in Figure 19.

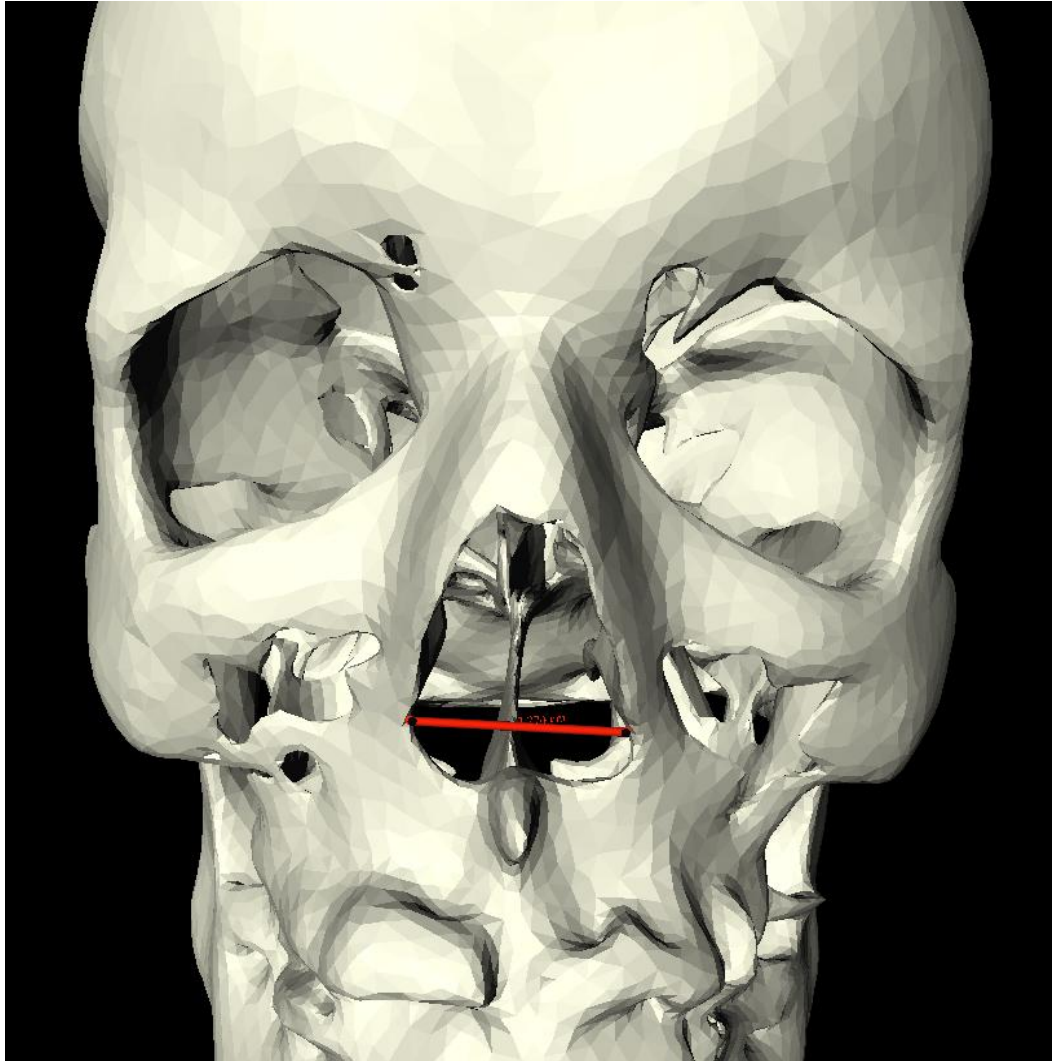


Figure 19: Nasal Breadth measurement in IDAS

The fifth and final bone measurement that was used was the Biauricular Breadth. This distance is defined as the least breadth across the roots of the zygomatic processes, which is the porion landmark. The porion landmarks are located just above the ear openings on each side of the skull. Figure 20 shows the measurement in IDAS.

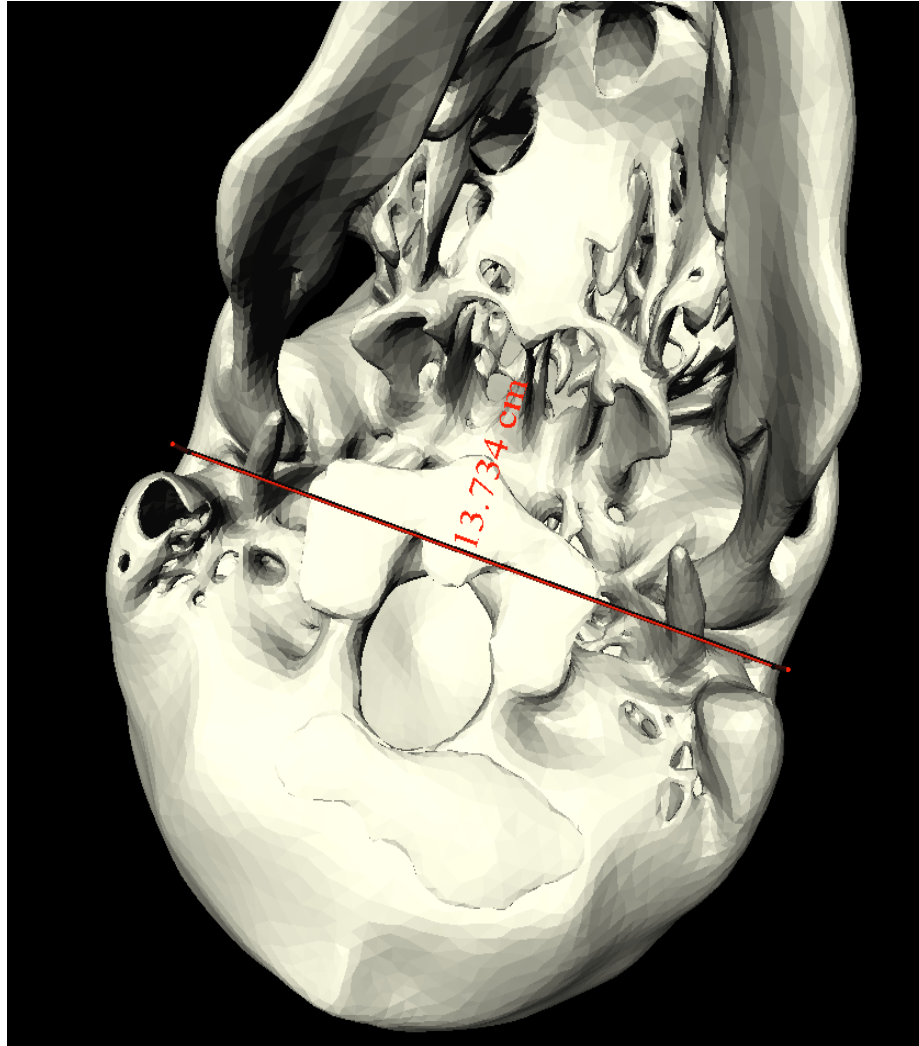


Figure 20: Biauricular Breadth measurement in IDAS

The five bone measurements collected in IDAS are then exported from the IDAS software in a text file with each of the measurements in the units of centimeters. The text file is saved with the name of the skull which was analyzed. These five bone measurements are used along with the bone thickness measurements and subject demographics as the inputs in the model to predict facial tissue thicknesses. The demographic information (age, weight, height, and Body Mass Index) was collected for each of the subjects used in this study if it were available. The demographic information is not normally provided in a forensic facial reconstruction case, so the performance of the developed model will be shown with and without using these inputs. However, research has shown that body mass can be estimated from using only skeleton structure (K.Moore, 2008). As shown in the results section of this report, the use of demographics in the model input improves the tissue thickness prediction

accuracy. How the data collected using IDAS is being used in a kernel regression model to predict an unknown skull's facial tissue thicknesses is discussed in the next section.

Forensic Facial Soft Tissue Kernel Regression Model

The Kernel Regression estimation process for forensic facial tissue prediction is depicted in Figure 21. The figure shows the steps taken in making a prediction of unknown skulls' facial tissue thicknesses: calculate distance, kernel weighting, and weighted averaging.

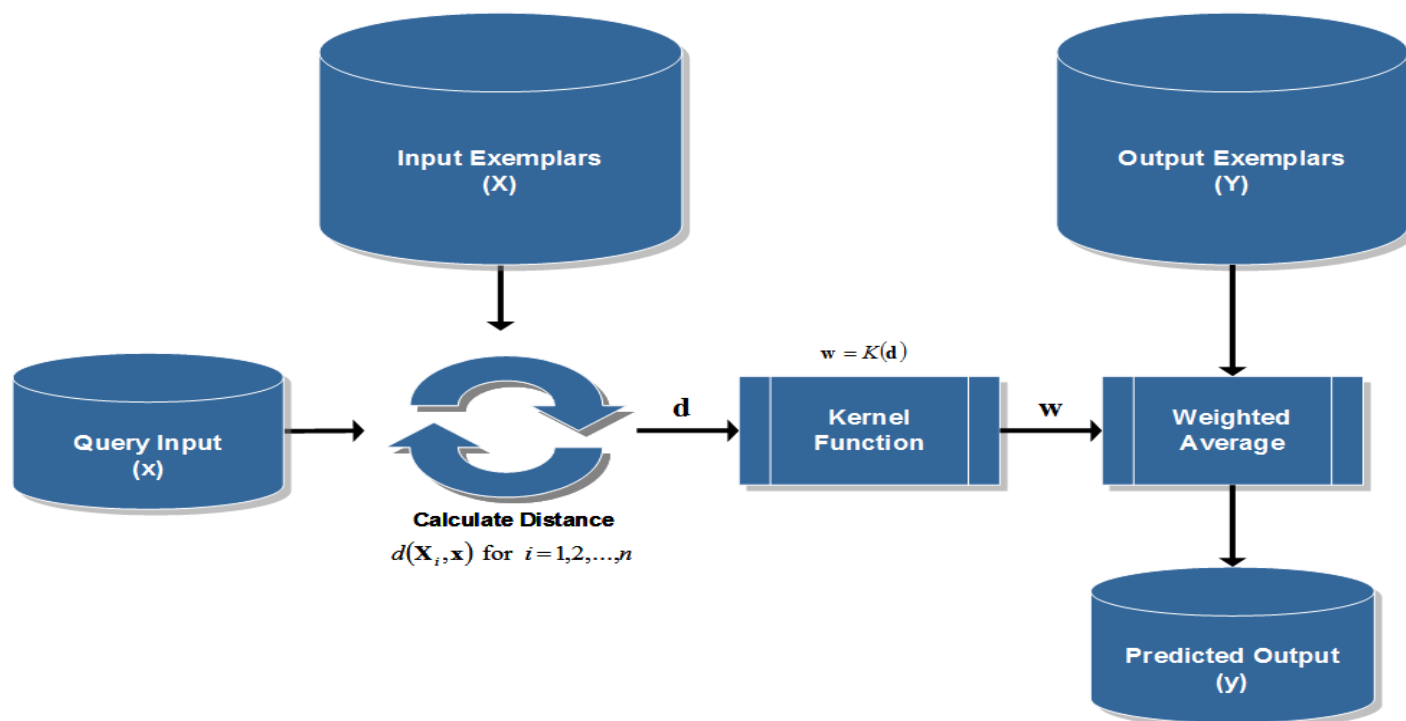


Figure 21: Kernel Regression Process

The input and output exemplars are a database of measured anatomical and demographic data measured from the CT imaging of each of the male subjects. For these subjects, the facial characteristics and underlying anatomy are known through the analysis performed in the *IDAS*. The input exemplars (X) or input memory matrix consists of the underlying bone thicknesses, and bone separations along specific anatomical lines collected from the analysis of the patient CT images. The output exemplars (Y) or output memory matrix are the facial tissue depths at specific anatomical points collected from analysis of the CT images for each of the male subjects. The query input (x) is the underlying bone thicknesses and bone separations along specific anatomical lines collected from the CT images of an unknown skull. Also, if the race and age of the subject are known then that information could be included in the query vector. The predicted output is the predicted facial tissue depths for the unknown skull.

The Kernel Regression estimation process for forensic facial reconstruction is structured into three steps. The first step in the Kernel Regression facial reconstruction is to calculate the distance of the new query, which is an unknown skull's facial features, from each of the input exemplars, which are the known database of skulls features. Next, the distances are supplied as inputs to a kernel similarity function, which converts the distances to weights. Finally, the weights are used to predict the model output as a weighted average of the output exemplars. The entire matrix setup and process used the Hetero-Associative Kernel Regression model is shown in Figure 22.

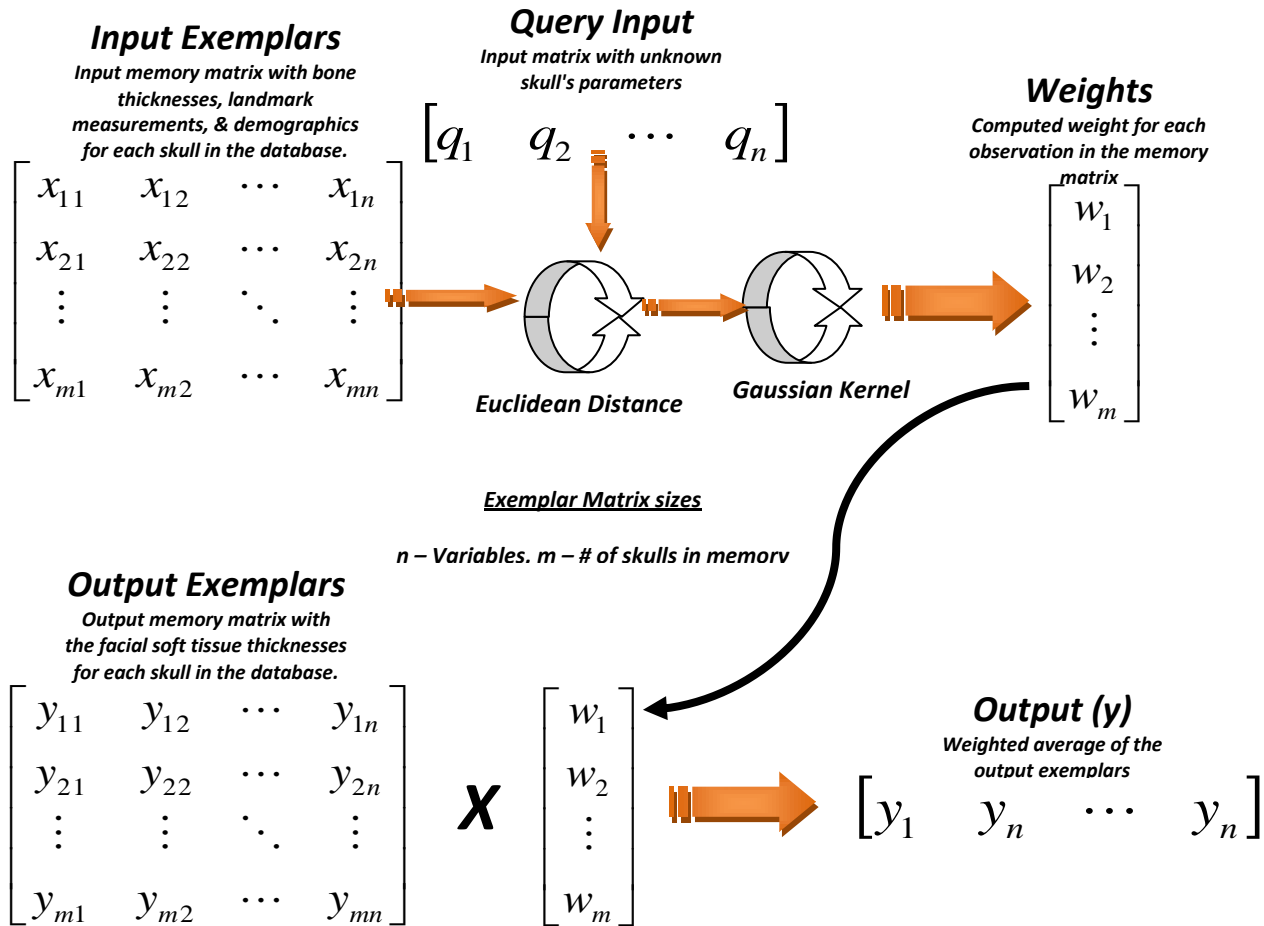


Figure 22: Hetero-Associative Kernel Regression Model flowchart

To measure the performance of the model a leave one out cross validation (LOOCV) technique was used to evaluate the performance of the facial reconstruction model with different combinations input data. The LOOCV works for each test case by running the model using a particular observation as the input and the remaining test data as training data. The predicted and actual facial tissue depths will be compared for each test case. The accuracy of

the model's predictions is represented by the Root Mean Squared Error (RMSE), equation 7. The equation used to calculate the RMSE for a single output variable is shown in Equation 7 below.

$$RMSE(i) = \sqrt{\frac{\sum (\hat{y}_i - y_i)^2}{N}}$$

Equation 7: Root Mean Squared Error (RMSE)

\hat{y}_i is the model prediction of the i th output variable

N = Number of output variables

y_i is the i^{th} variable of the output exemplar for the observation not in the test data.

Rhine's Caucasian average tissue thickness table (Rhine & Moore, 1982) is also compared to the actual tissue thicknesses used in the model. Rhine's current table is used by the forensic artist on this project when reconstructing white male faces. The comparison will provide a Root Mean Squared Error (RMSE) for our model's predicted tissue thicknesses and a RMSE for the tabled facial thicknesses that are used in today's forensic facial reproductions for each skull in our memory matrix. This will provide a quantitative comparison between the developed model's predicted tissue thicknesses for all the 100 query skulls and the current tabled tissue thicknesses for the same 100 query skulls. The goal is for the RMSE of the model to be lower than that of the current tabled thicknesses.

III. Results

Tissue and Bone Thickness Measurement Results

After completing all the tissue thickness and bone measurements for all 100 skulls in our database, the input and output training matrices were constructed. The input memory matrix consists of 100 observations and 22 variables. The input variables are the 13 bone thickness measurements, the 5 ethnicity determination measurements, and the 4 demographics (age, weight, height, and BMI). The demographic parameters are rarely provided to the forensic artist to use during the facial reconstruction, therefore the model's performance will be shown with and without using them as tissue thickness predictors. The output memory matrix contains the 13 facial tissue thicknesses of the 100 skulls.

The number of variables in the output matrix was limited to only 13 craniometrical locations due to the concern that arose from the high number of older and obese subjects in the database. This concern was in the ability to accurately measure the tissue thicknesses in the cheek and side of the mandible locations. Therefore, locations mainly along the midline of the skull and forehead were chosen because of their absence from areas where skin sagging due to aging and obesity is prominent. The average BMI for the 100 subjects in our database is

29.0449 kg/m². This BMI is considered overweight and a person with a BMI of greater than 30 is considered obese. With subjects that are obese or overweight their tissue thicknesses on the side of their skull when lying down to have a CT scan can be much different from their correct facial tissue thicknesses. Figure 23 is a plot of the BMIs for all 100 male subjects used in the study. The red line in the plot is placed at the obesity cutoff (>30) and shows that about 50% of the subjects used can be considered obese by the BMI scale.

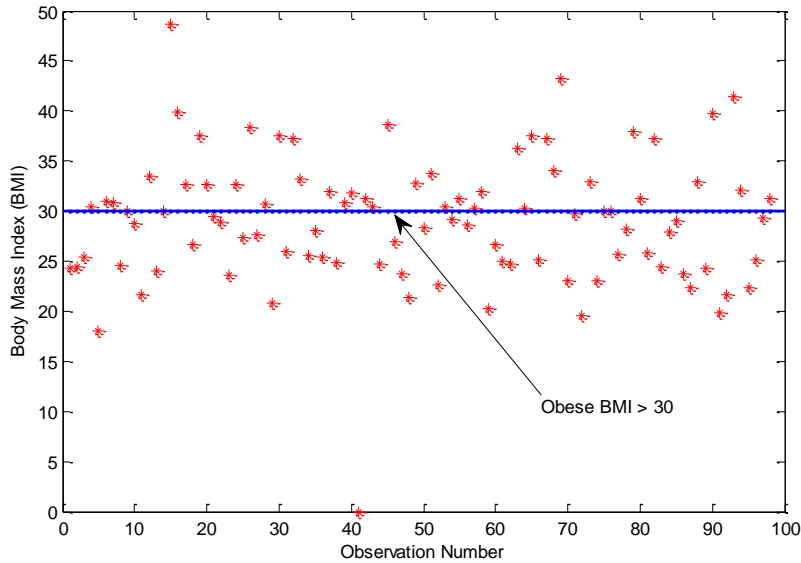


Figure 23: Body Mass Index of the 100 subjects

Table 3: Craniometrical Landmarks where tissue thickness measurements were made to build kernel regression model

#	Landmark Name
1	Supraglabella (1)
2	Glabella (2)
3	Nasion (3)
4	End of Nasals (4)
5	Mid-Philtrum (5)
6	Chin-Lip Fold (8)
7	Mental Eminence (9)
8	Beneath Chin (10)
9	Frontal Eminence (11)

10	Supraorbital (12)
11	Suborbital (13)
12	Lateral Orbit (15)
13	Zygomatic Arch, Midway (16)

The 13 craniometrical locations used in the tissue thickness measurements are shown in Table 3. The numbers in parentheses to the right of the landmark names corresponds to the numbers used in Figure 24 (Taylor, 2001). These locations are mostly along the midline of the skull with the exception of the frontal eminence, supraorbital, suborbital, lateral orbit, and zygomatic arch landmarks. Using only 13 of the 21 landmarks should still provide adequate results to construct a facial reproduction. The remaining 8 landmarks were scaled to match the magnitude of the model's predictions for the 13 mentioned landmarks and this is discussed further, later in the report.

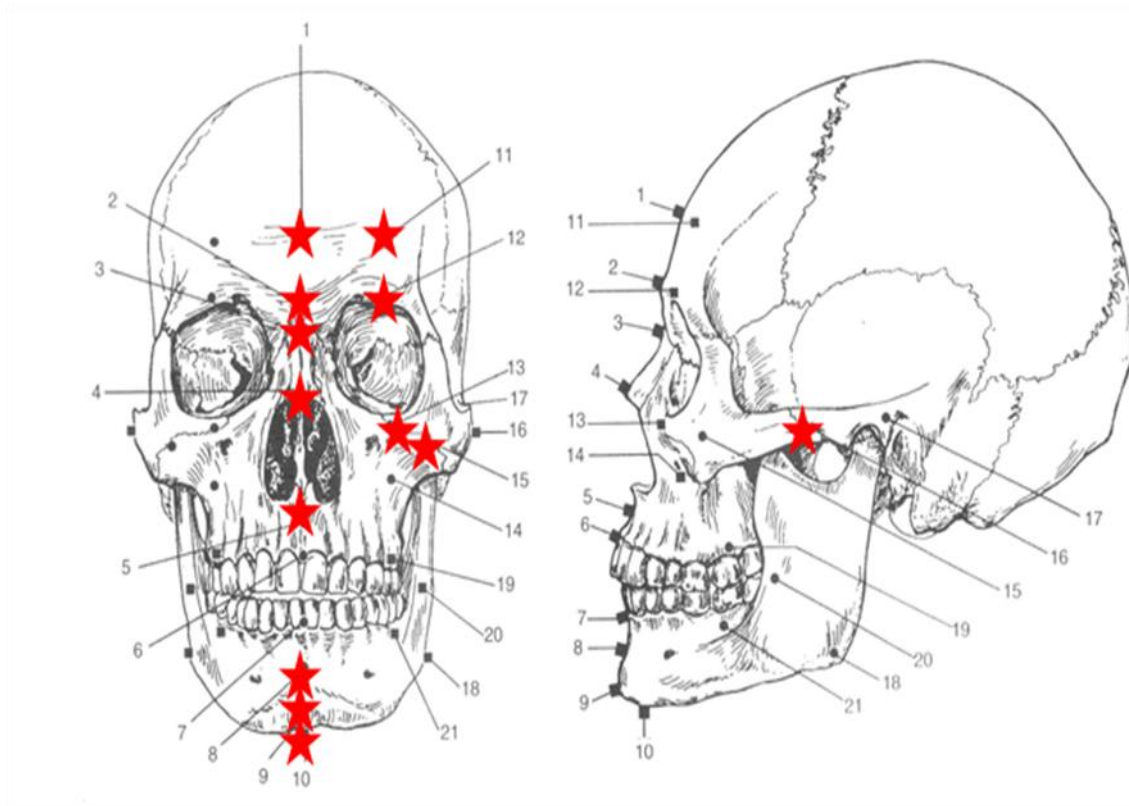


Figure 24: Craniometrical Locations that will be predicted using the KR model

Figure 24 shows the tissue thickness landmarks being measured on a subject's skull in IDAS. The bilateral measurements where there is a left and right landmark, the left landmark was used in building the memory matrices for the model. All the different measurements were loaded into MATLAB in order to build the input and output memory matrices for the Kernel regression model. The MATLAB function created to do this is called 'dataload' and is shown in Appendix B. In building the tissue thickness memory matrix a trimmed mean was performed on the 30-40 points measured for each the 13 anatomical locations to produce a single tissue thickness for each location. The trimmed mean was set to remove the upper and lower 5% of the data before computing the mean. The building of the input memory matrix is performed the same way in using a trimmed mean to compute a single bone thickness measurement from the 30-40 points from each of the 13 locations. Along with the 13 bone thickness measurements, numbered as shown in Table 3, the 5 cranial landmark distance measurements discussed previously, and the 4 demographics (age, weight, height, and BMI) are added onto the matrix to make the 22 predictor variables.

	Supraglabella	Glabella	Nasion	End of Nasals	Mid-Philtrum	Chin-Lip Fold	Mental Eminence	Beneath Chin	Frontal Eminence	Supraorbital	Suborbital	Lateral Orbit	Zygomatic Arch
Supraglabella	0.03	0.08	0.09	0.17	0.03	0.21	0.19	0.06	0.15	0.14	0.09	0.00	0.09
Glabella	-0.11	0.09	-0.02	-0.08	-0.02	0.02	0.00	-0.05	-0.05	0.04	-0.11	-0.22	-0.02
Nasion	-0.04	0.07	0.04	-0.21	-0.08	-0.08	-0.12	-0.04	-0.08	0.02	-0.04	-0.13	-0.04
End of Nasals	0.08	0.05	0.00	-0.06	-0.14	-0.04	-0.21	-0.15	0.02	-0.01	0.11	0.05	-0.02
Mid-Philtrum	-0.11	0.06	0.08	-0.19	-0.22	0.05	-0.14	-0.16	-0.19	-0.08	-0.10	-0.17	-0.25
Chin-Lip Fold	-0.16	-0.16	-0.10	-0.04	0.08	-0.20	-0.18	-0.01	-0.13	-0.09	-0.07	-0.15	-0.04
Mental Eminence	0.08	-0.06	-0.03	0.06	-0.07	0.06	-0.04	-0.02	0.14	0.13	0.05	0.04	-0.08
Beneath Chin	0.32	0.20	0.12	0.26	0.12	0.31	0.30	0.17	0.41	0.38	0.30	0.36	0.26
Frontal Eminence	0.10	0.13	0.14	0.26	0.01	0.19	0.26	0.18	0.22	0.27	0.17	0.16	0.20
Supraorbital	0.11	0.09	0.12	0.15	0.02	0.24	0.20	-0.02	0.24	0.19	0.14	0.14	-0.01
Suborbital	-0.20	-0.03	-0.11	-0.26	0.08	-0.13	-0.10	-0.12	-0.24	-0.18	0.04	-0.05	-0.12
Lateral Orbit	0.13	0.05	0.05	0.18	0.12	0.14	0.09	0.06	0.24	0.23	0.13	0.00	0.20
Zygomatic Arch	-0.15	0.01	0.18	-0.16	-0.05	-0.09	-0.13	-0.17	-0.19	-0.10	-0.08	-0.16	-0.16
Basion to Prosthion distance	0.32	0.19	0.27	0.27	-0.12	0.32	0.17	0.08	0.34	0.25	0.04	0.21	0.26
Basion to Nasion distance	0.26	0.10	0.02	0.15	0.02	0.07	0.11	0.04	0.28	0.12	0.02	0.13	0.09
Orbital width	-0.20	-0.16	-0.23	-0.18	-0.03	-0.24	-0.14	-0.29	-0.19	-0.22	-0.14	-0.26	-0.18
Nasal width	0.00	-0.11	-0.16	-0.05	-0.06	-0.07	0.01	-0.09	-0.03	-0.01	-0.06	-0.12	-0.10
Biauricular breadth	-0.09	-0.15	-0.12	0.03	0.12	0.00	-0.01	-0.03	-0.16	-0.19	0.06	-0.02	-0.08
Age	-0.29	-0.21	-0.25	-0.15	-0.28	-0.21	-0.13	-0.28	-0.26	-0.27	-0.08	-0.20	-0.40
Weight	0.65	0.44	0.36	0.37	0.33	0.57	0.55	0.49	0.64	0.64	0.59	0.67	0.72
Height	0.19	0.09	0.15	0.08	-0.04	0.23	0.11	0.03	0.17	0.11	0.03	0.12	0.21
BMI	0.58	0.42	0.38	0.36	0.27	0.60	0.58	0.44	0.57	0.59	0.56	0.64	0.73

Figure 25: Correlation matrix of model predictors and responses from 100 skulls

Using the input and output memory matrices created from the IDAS measurements, a correlation analysis was performed in order to try and discover any linear correlations among the predictors (bone measurements and demographics) and the responses (facial tissue thicknesses). Figure 25 shows a correlation matrix for the 13 tissue thicknesses (columns) and the 22 predictors (rows) for the 100 skulls. The values computed are the correlation coefficients for the each predictor and response combination, with ± 1 being the greatest correlation possible. We consider most useful predictors have an absolute correlation coefficient of 0.3 or greater. As one can see there are only a few useful predictors of tissue thickness available. The greatest linear correlation with tissue thickness seems to exist with weight and BMI. The bone thickness predictors that may have useful information in them are corresponding to correlation coefficients around ± 0.3 . The full symmetric correlation matrix from all 35 variables (13 responses + 22 predictors) is presented in Appendix D. Due to its large size one may have to zoom in on the table to clearly view the values.

This metric along with the similarity would be used to help investigators determine if the predictions should be used in an investigation. The bias computation was performed using the MSE and the variances from a LOOCV of all 100 observations. In using kernel regression we are assuming a normal distribution of the error, which is shown in Figure 26 (right). Also, in Figure 26 (left), a probability plot was constructed for the error of the model. The assumed normal distribution did not hold true in the lower 5% of the distribution of the error data. This extended tail on the Gaussian fit of the error metric causes a substantial increase in the mean of the bias calculations. To help remove this added bias a trimmed mean was used to compute the MSE during the bias calculation.

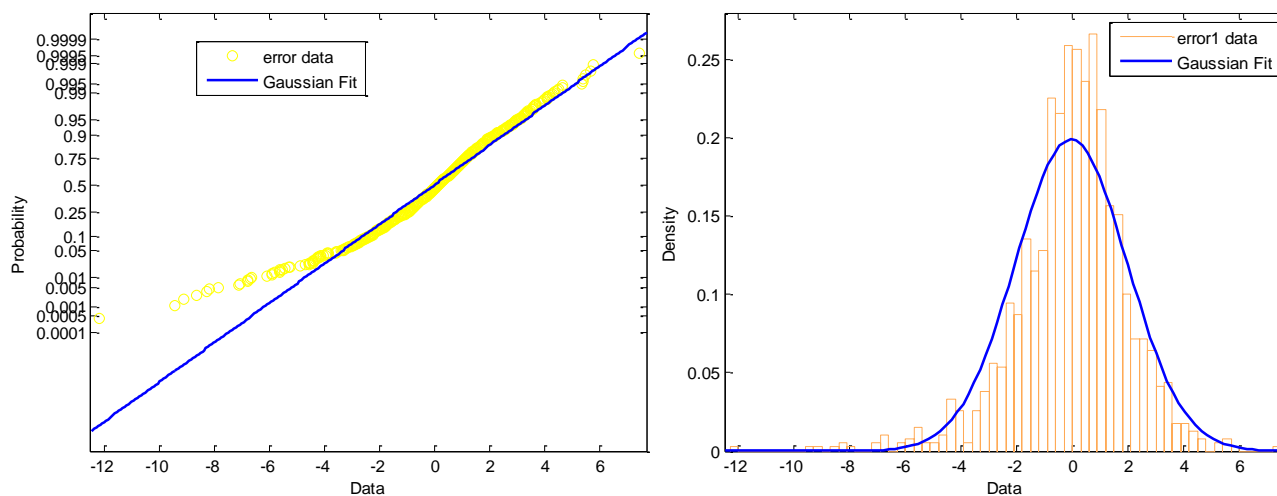


Figure 26: Model's MSE distribution

Initial Kernel Regression Model Results

The first preliminary model constructed was a hetero-associative kernel regression (HAKR) model. The first step taken was to standardize the data. Since there are a wide range of values from one variable to another standardizing the data was needed. This function, 'zscore1', was used to mean center and unit variance the input and output data, shown in Appendix B. Another MATLAB function, 'unscore', was used to take the predictions back to their original scale, shown in Appendix B. The next step was to optimize the bandwidth (h) for the Gaussian kernel used in the model. This optimization parameter (h) is used to minimize the Root Mean Squared Error (RMSE) of the model's predicted tissue thicknesses and the actual measured tissue thicknesses. To select the optimal bandwidth, values ranging from 0.5 to 10 with intervals of 0.5 are iteratively used in the Leave One Out Cross Validation (LOOCV) algorithm. Figures 27 & 28 below show the plots of the Root Mean Squared Error (RMSE) versus each bandwidth used in the optimization for the Hetero-Associative Kernel regression model. Figure 27 is the bandwidth optimization plot for the model using the demographics as predictors and Figure 28 is from the model not using the demographics.

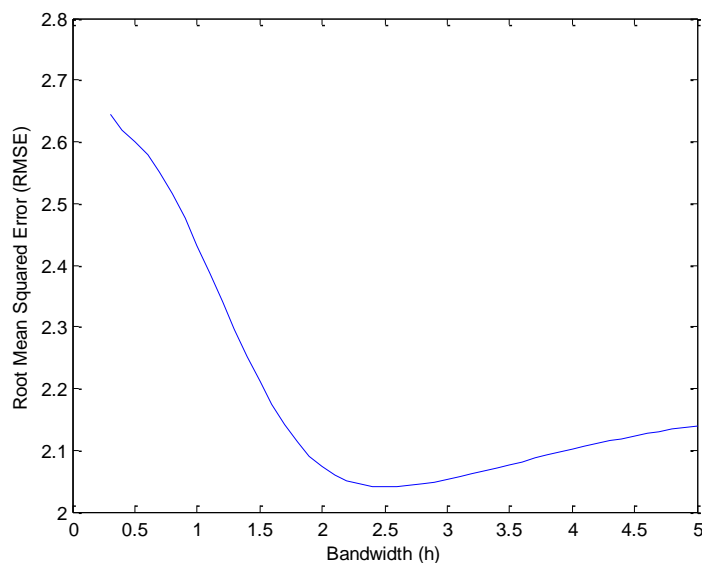


Figure 27: Bandwidth Optimization for HAKR using demographics

The optimal kernel bandwidth was 2.5 when using demographics as a predictor and then 3.1 when not using them. This is expected since the correlations between the demographics (age, weight, height, and BMI) are the greatest among the 22 predictors. By removing them, the model loses substantial predicting power and therefore the kernel bandwidth must be increased to incorporate more distant specimen. However, this moves the model's prediction to a near simple average of the tissue thicknesses. This can be seen in

Figure 28 where the optimal bandwidth chosen for the model not using demographics, 3.1, has a nearly identical RMSE (y-axis) as the largest bandwidth used in the optimization.

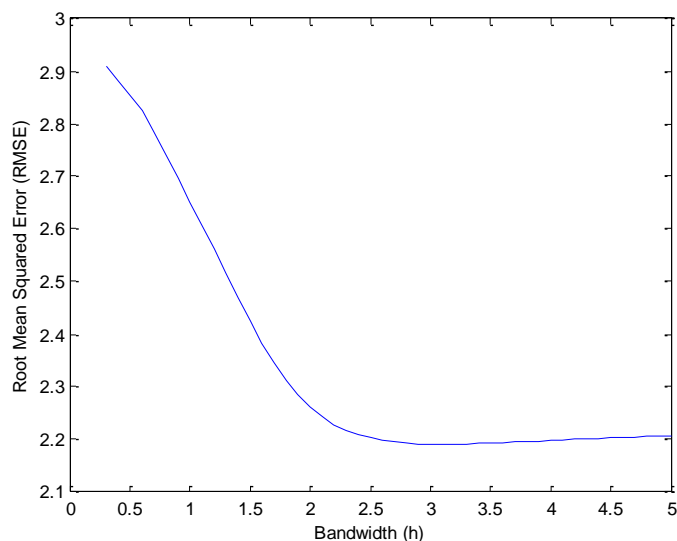


Figure 28: Bandwidth Optimization for HAKR without using demographics

To measure the performance of the models' ability to predict the 13 facial tissue thicknesses, two metrics are used. The first, model RMSE, is a root mean squared error of the model's predictions and the actual measured tissue thicknesses. The second, Table RMSE, is a root mean squared error of the model's actual tissue thicknesses in its memory matrix and the obese tabled tissue thicknesses used in current forensic facial reconstructions. The obese tabled values were used due to the majority of the subjects in the model's database are overweight to obese in stature. The similarity metric used is simply the average of the maximum kernel weights computed for the query input. The closer the value is to 1 the more similar the query is to a skull in the memory matrix. The model's prediction uncertainty was also computed. It is shown as a percentage of the prediction values. The metrics displayed in the result tables are the average for the LOOCV that was performed.

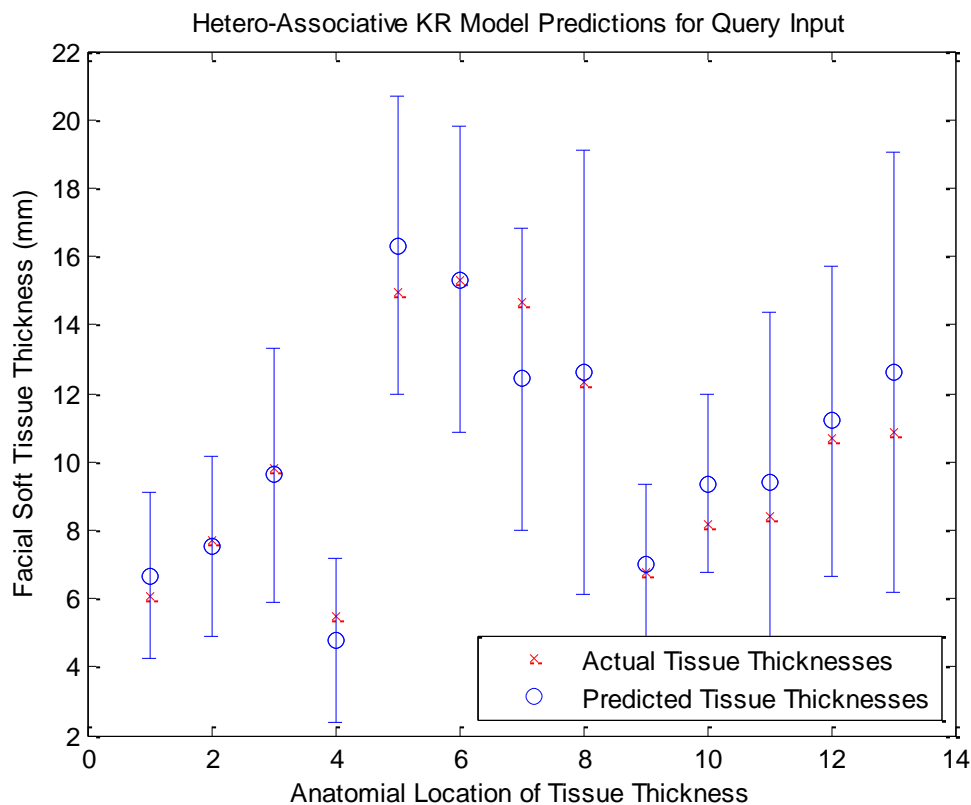


Figure 29: Predictions and Actual tissue thicknesses for HAKR model

One of the skull’s predictions from HAKR model using demographics was plotted against the actual known tissue thicknesses in Figure 29. The graph shows the model’s prediction along with their respective 95% prediction intervals plotted on top of the actual tissue thickness values for that observation. Since in most forensic investigative situations the forensic artist is not provided any demographic information, the LOOCV was performed with and then without using demographics as predictors. The performance metrics from the HAKR model using and not using demographics as predictors are shown in Table 4 and Table 5, respectively.

The tables displayed below convey that the demographics play a role in decreasing the HAKR's prediction error. However, the average similarity metric increases from the model using the demographics to the model not. This can be explained by the fact that the kernel bandwidth also increases; therefore resulting in higher weights given to the more distant skulls in the model's memory. The HAKR model using the memory of 100 skulls resulted in a 34% decrease in error when using the demographics and 28% error when not when compared to the Table RMSE.

Table 4: Average Performance Metrics for all HAKR models using demographic predictors

Prediction Uncertainty	Model RMSE	Table RMSE	Similarity
19.73 %	2.04 mm	3.07 mm	0.19

Table 5: Average Performance Metrics for all HAKR models without using demographic predictors

Prediction Uncertainty	Model RMSE	Table RMSE	Similarity
19.66%	2.21 mm	3.07 mm	0.41

In order to identify the optimal kernel regression architecture, an inferential kernel regression model was also used to predict the 13 soft facial tissue thicknesses. This type of architecture has a single output; therefore 13 separate prediction models are needed to estimate the 13 desired tissue thicknesses. The LOOCV was again performed using the inferential architecture. The same performance metrics were also measured. In the Inferential architecture, a correlation analysis is used to discover if any linear relationships among the predictors and responses exist. The correlation analysis was used to find out if there are any underlying relationships between the predictors (bone thicknesses, measurements and demographic information) and the response variables (tissue thicknesses) for each inferential model. Predictors with an absolute correlation coefficient of 0.3 or greater were selected as input variables for each respective inferential model. Adding unneeded inputs to the model increases the outputs' variance. However, by not including important inputs in the model increases the outputs' bias. As with the HAKR model, the kernel bandwidth can be iteratively optimized for the least RMSE of the predictions. Figure 30 is a plot of the bandwidth values used versus the RMSE of the predictions when using that respective bandwidth. Figure 31 is the bandwidth optimization when not using the demographics in the inferential model's input.

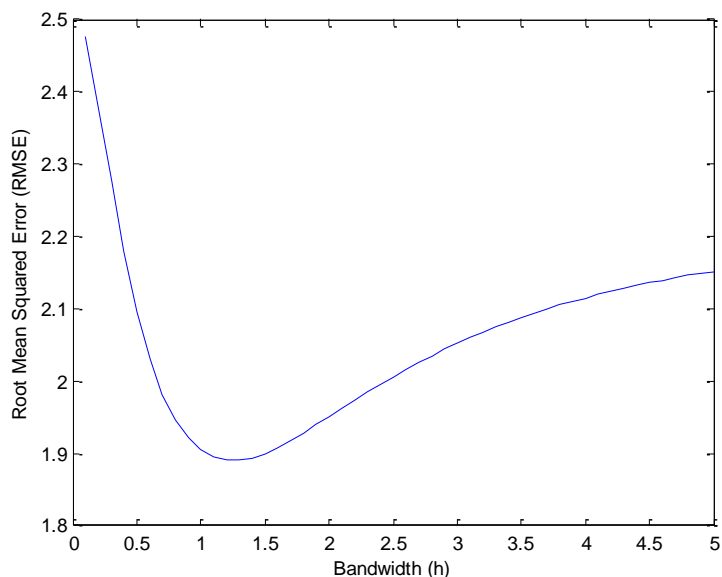


Figure 30: Optimal Bandwidth for the Inferential Model using demographics

The optimal bandwidth for the Inferential modeling architecture with and without using demographics in the model was 1.3 and 1.6, respectively. Again as shown in the HAKR model results, by removing the demographics from the model's input the optimal bandwidth increases and the curve flattens out shortly after reaching the minimum RMSE possible.

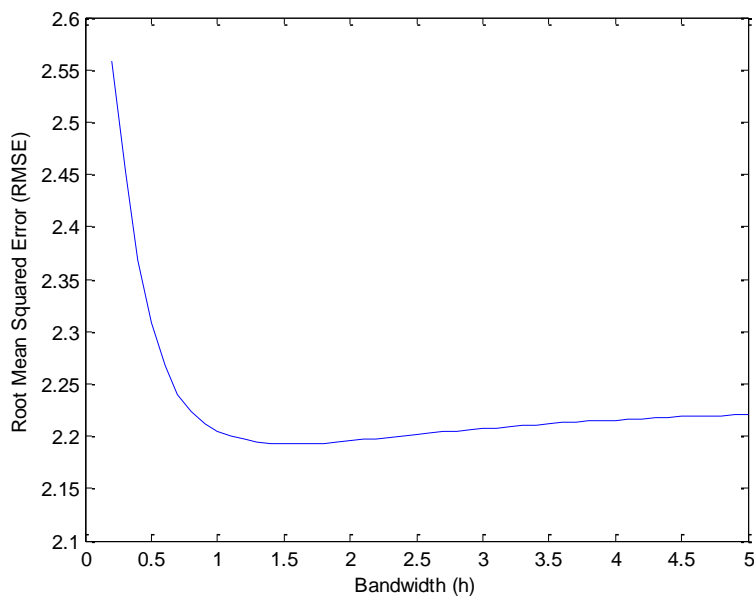


Figure 31: Optimal Bandwidth for the Inferential Model without using demographics

The optimal bandwidth for the Inferential modeling architecture with and without using demographics in the model's input was 1.3 and 1.6, respectively. The same observation's predictions shown in the HAKR modeling, Figure 29, were used for the inferential model's predictions plot shown in Figure 32. Tables 6 and 7 show the performance metrics calculated after the LOOCV for the Inferential model using demographics as a predictor and then without. Appendix B displays all MATLAB code used in this study.

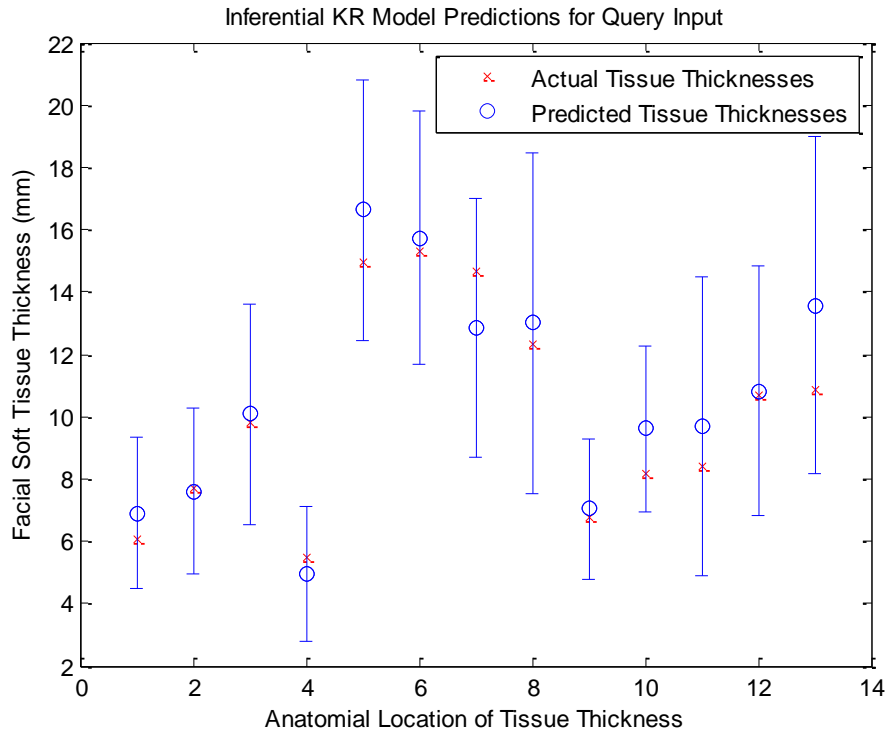


Figure 32: Predictions and Actual tissue thicknesses for inferential model

The results shown in Tables 6 & 7 provide evidence that the inferential architecture provides predictions with less error than the hetero-associative architecture. This is particularly true when using the demographics as additional inputs to the model. There was a 38% decrease in the RMSE from the Table RMSE when using the demographics. The decrease in RMSE was reduced to 29% when not using the demographics as predictors in the inferential model. The increase in the average similarity metric was again due to the increase in the kernel bandwidth used.

Table 6: Average Performance Metrics for Inferential modeling using demographic predictors

Prediction Uncertainty	Model RMSE	Table RMSE	Similarity
20.5 %	1.89 mm	3.07 mm	0.81

Table 7: Average Performance Metrics for Inferential modeling without using demographic predictors

Prediction Uncertainty	Model RMSE	Table RMSE	Similarity
20.5 %	2.19 mm	3.07 mm	0.89

Furthermore, the inferential model's RMSE decreased from that of the HAKR and the similarity was also higher than the HAKR's. More importantly the model's error was again lower than the tabled tissue thickness error. The similarity and error metrics should improve with the addition of more observations to the model's memory matrices. To show that the addition of more skulls to the model's memory matrices can improve the performance of the model, the LOOCV was run on using only 30 of the 100 observations in the input and output memory matrices for the inferential architecture using the demographics. Table 8 has the average performance metrics for the Inferential KR model using only the 30 skulls. Comparing Table 8 to Table 6 one can see that both the model RMSE and similarity metrics worsen when only using 30 observations. The more observations the model has to compare a given query to, the more likely a similar skull will be found and more accurate tissue thicknesses can be predicted.

Table 8: Performance Metrics for Inferential modeling using only 30 observations

Prediction Uncertainty	Model RMSE	Table RMSE	Similarity
20.5 %	2.14 mm	3.07 mm	0.34

3D Clay Facial Reproductions

The William Bass donated collection at the University of Tennessee was used to provide male skulls accompanied with living photos to be used to measure the model's true abilities. Ms. Joanna Hughes, the project's forensic artist, has completed all of the facial reconstructions using her normally used techniques, which are the Rhine & Moore facial soft tissue thickness tables for Caucasian males of normal build. Pictures were taken of each completed reconstruction and then the skulls were cleaned so they could be CT imaged and put through our procedures that were developed to analyze the skulls in IDAS. These skulls were analyzed to collect the 18 bone measurements that can be used as the input to the model in order to

predict the skull's tissue thicknesses. The age, weight, height, and BMI were known before death for each of the subjects, but they were not used in one of models in order to show the difference in the resulting reconstructions. The model simply removes those variables from the memory matrix that are not known and makes the best possible predictions with the information it's given. Since the inferential architecture resulted in the best performance it was used to make the predictions for the test male skulls. The project's goal was to do reconstructions on 5 male subjects, but the forensic artist had a pregnancy due date during the final 2 reconstructions. Therefore, only 3 reconstructions were completed using the developed model's predicted tissue thicknesses.

An issue presented itself when the forensic artist began the first reconstruction using the model's predicted thicknesses. When the forensic artist began using the model's predicted tissue thickness in the reconstruction of subject A she discovered that the value for the Mid-Philtrum location, which is located just below the base of the nasal cavity, was far too large and would interfere with the nose projection. To enable the artist to continue with the reconstruction we elected to not use the model's prediction for this location and result to the normally used tabled values. Since the model only predicts the facial tissue thicknesses for 13 of the 21 craniometrical locations and they are mainly along the midline of the face, the remaining locations needed to be adjusted. The remaining cranial landmarks not predicted using the developed model were scaled to match the magnitude of the model's predicted values. This was done by computing the ratio of the model's predictions to the tabled values for the 13 locations and taking the average. The scaling factor is multiplied by the tabled thickness values that would be used in the reconstruction for the 8 landmarks, to provide new values that better agree with the model's predictions. A single scaling ratio is calculated for each query input to the model. The scaling is necessary because the predicted values are nominally larger than the tabled values, using the tabled values for the remaining locations does not work. Appendix C contains the exact tissue thicknesses used for the three reconstructions along with the advised scaling factor for subjects B and C. The reconstruction of subject B did not use the demographics as inputs.



Figure 33: Old (left) and New (right) reconstruction methods compared to actual living photo (middle) of the subject A

Figure 33 shows the facial reconstruction of male subject A using the tabled values (left), the living photo (middle) and the reconstruction using the model's predicted tissue thicknesses (right). Dr. Richard Jantz provided his interpretation of the comparisons of the reconstructions against the living photos and the following discussions are based on his comments. This male subject was 68 years of age, 85.5 kg in weight, 170 cm in height, and a BMI of 29.6. The table and model reconstructions are similar for subject A, but the model improves the fit a bit. However, it is difficult to say exactly why. The table and model profiles differ in that the model's has a more prominent bridge and nose. Also, the entire face is pulled back a bit more. Overall, the model's predicted tissue thicknesses seem to approximate the face of subject A better than the currently used method. The uncertainty for the 13 predictions was an average of 22.3%. The average similarity metric was 0.91.

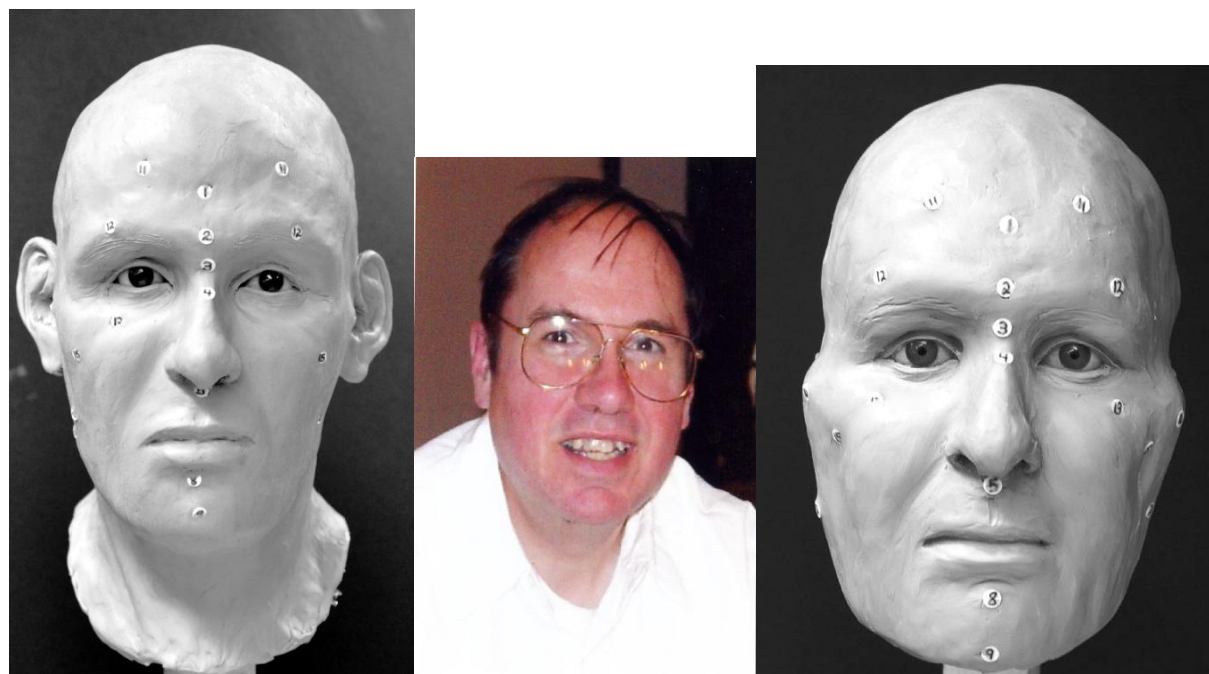


Figure 34: Old (left) and new (right) reconstructions compared to the actual living photo (middle) of the subject B

Figure 34 shows the facial reconstruction of male subject B using the tabled values (left), the living photo (middle) and the reconstruction using the model's predicted tissue thicknesses (right). This male subject was 44 years of age, 112.5 kg in weight, 172.7 cm in height, and a BMI of 37.7. The Zygomatics are too wide in the model's approximation for subject B requiring the upper facial breadth to retreat, not seen in the photo. The interorbital in the model reconstruction seems to be more accurate than and not quite as narrow as the reconstruction using the tables. Also, the lower face is a bit fuller, which conforms better to actual. The uncertainty for the predictions was an average of 21.5% for all 13 predictions. The average similarity metric was 0.76.

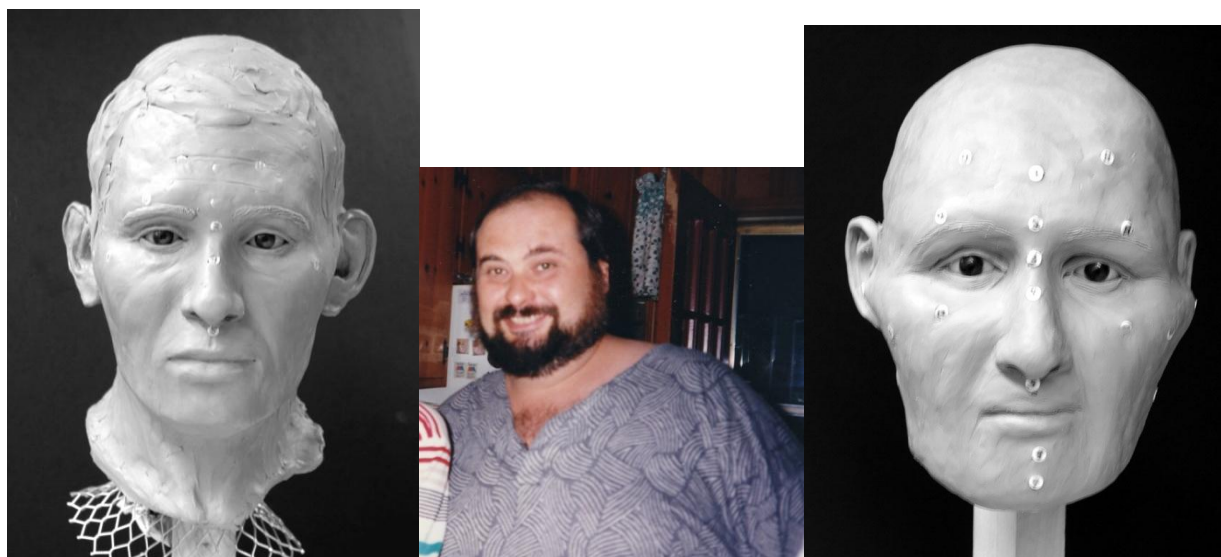


Figure 35: Old (left) and new (right) reconstructions compared to the actual living photo (middle) of the subject C

Figure 35 shows the facial reconstruction of male subject C using the tabled values (left), the living photo (middle) and the reconstruction using the model's predicted tissue thicknesses (right). This male subject was 49 years of age, 180 kg in weight, 179.5 cm in height, and a BMI of 55.9. Examination of the two facial approximations for subject C shows drastic differences. Using table values produces a face too slender. The model version captures the shape of the face a bit better, although it angles too steeply inferiorly and hence not as round as the actual face. The nose and interorbital is a better match to the actual face. In life the nose has a fairly low root and then widens. It does that better in the model version, but still not as much as in life. The uncertainty for the 13 predictions was an average of 16.7%. The average similarity metric was 0.15. This very low similarity was due to the subject's weight and BMI being outside the range of the observations in the memory matrix.

IV. Conclusions

Discussion of Findings

The methodology and procedures required to collect and analyze the cranial data were developed. The setbacks that occurred during the development of the methodology were resolved and with the provided extension through May 2010 the final project objectives were accomplished. With the methodology in place, the collection of the facial tissue thicknesses and bone measurements was much more rapid and consistent using the IDAS software. The HAKR model and inferential models built with the 100 observations both yielded results with less error than the currently used tabled tissue thicknesses. The inferential kernel regression

architecture outperformed the hetero-associative kernel regression architecture. The inferential model provided a 38% decrease in error from the tabled thicknesses when using the demographics as inputs to the model. The demographics, weight and BMI, are the highest correlated predictors of tissue thickness among the 22 predictors used in this pilot study. When the demographics are removed the performance is reduced to a 29% decrease in error. Demographics, weight and BMI especially, are usually not provided to the forensic artist, but technologies could be used in helping to estimate them from skeletal remains (K.Moore, 2008). This could be used to allow the demographic information to aid in predicting tissue thickness by using them as inputs to the inferential model. The three-dimensional clay reconstructions resulted in noticeable improvements when using the developed model compared to the currently used "normal" tissue thickness tables. However, possible inaccuracies were presented in the exaggerated thicknesses on the side of the face. This most likely occurred due to the obese and overweight subjects used to build the model and the fact that their measurements were captured with them lying down.

Several useful correlations among the tissue thicknesses and skull bone measurements were identified, but many more bone measurements can be appended to the input memory matrix to try and identify more. The initial development of IDAS has led to the opportunity to efficiently discover other features that could be used as facial tissue thickness. A more complete data set with ethnic and body mass diversity will allow for more accurate tissue measurements. Each of these concerns must be examined in future work.

Implications for Policy and Practice

The findings from this pilot study have shown a proof of principal for using empirical modeling to predict facial soft tissue thickness. This technology has the promise, with further research, to produce more accurate forensic facial reproductions. More accurate facial reproductions will hopefully have a positive effect on the identification rate of unknown skeletal remains.

Implications for Further Research

A project phase 2 should research more into additional bone measurements that can be included as predictors is vital to improving the performance of predicting facial tissue thickness with either HAKR or inferential modeling. The data collection with the current database of skulls uses the current version of IDAS which requires manual selection of measured points. Completely automating the process is a goal of future research. Also, increasing the number of Black male subjects, along with finding a database of subjects with more diverse BMIs must be addressed. Sources for collecting a more complete data set of CT images of the cranium have been identified. A proposal titled "Automated Facial Reconstruction Using Empirical Modeling" was submitted for the current NIJ solicitation, Research and Development on Forensic Crime Scene and Medicolegal Death Investigations. The objectives of the proposal are explained below. In order to improve on this technology and discover better methods to perform facial

reproductions with higher identification rates there are four objectives for the proposed research:

1. Apply the methods to a more complete data set. The original data set consisted of 100 males who were predominantly older and overweight.
2. Develop an automated feature extraction system that can be used to more exhaustively search for good predictors of skin thickness.
3. Optimize the kernel based model which may also involve separate models using demographic information.
4. Automated surface rendering using skin thickness Atlases.

V. References

- Atkeson, C. G., Moore, A. W., & Schaal, S. (1997b). Locally Weighted Learning for Control. *Artificial Intelligence Review* , 75-113.
- Bass, W. M. (1995). *Human Osteology*. Columbia: Missouri Archaeological Society.
- Besl, P. J. (1992). A Method for Registration of 3D Shapes. *IEEE Transactions on Pattern Analysis and Machine Intelligence* .
- Hines, J., & Garvey, D. (2006). *Empirical Methods for Process and Equipment Monitoring*.
- Kee-Doeg, K., Ruprecht, A., & Wang, G. (2005). Accuracy of facial soft tissue thickness measurements in personal computer-based multiplanar reconstructed computed tomographic images. *Forensic Science International* , 28-34.
- Lebedinskaya, G. (1993). Principles of facial reconstruction. *Forensic Analysis of the Skull* , 183-198.
- Mahfouz, M. (2007). Patella sex determination by 3D statistical shape models and nonlinear classifiers. *Forensic Science International* , 161-170.
- Moore, M. (2008), "Body Mass Estimation from the Human Skeleton," Ph.D. Dissertation, The University of Tennessee, Knoxville, TN, 2008.
- Panenkova, P. (2007, June 16-30). Face Approximation and Information About Facial Soft Tissue Thickness . Prague, Czech Republic.
- Phillips, V., & Smuts, N. (1996). Facial reconstruction: utilization of computerized tomography to measure facial tissue thickness in a mixed racial population. *Forensic Science International* , 51-59 (83).
- Rasmussen, B., & Hines, J. (2005). On-Line Sensor Calibration Monitoring Uncertainty Estimation. *Nuclear Technology* , 151.
- Rasmussen, B. (2003), "Prediction Interval Estimation Techniques for Empirical Modeling Strategies and Their Application to Signal Validation Tasks," Ph.D. Dissertation, The University of Tennessee, Knoxville, TN, 2003.
- Rhine, J., & Campbell, H. (1980). Thickness of Facial Tissues in American Blacks. *Journal of Forensic Sciences* , 847-858.
- Rhine, J., & Moore, G. (1982). Facial Reproduction: Tables of Facial Tissue Thicknesses of American Caucasoids in Forensic Anthropology. *Maxwell Museum Technical Series #1* .

Stephan, C. (2003). Anthropological Facial 'reconstruction' - recognizing the fallacies, 'unembracing' the errors, and realizing method limits. *Science & Justice* , 193-200.

Taylor, K. T. (2001). *Forensic Art and Illustration*. Boca Raton: CRC Press LLC.

Vargas, J. E., Sucar, L. E. (2005). Predicting the most probable facial features using Bayesian networks, mathematical morphology, and computer graphics. In: *Computer-Graphic Facial Reconstruction*, Clement, J. G. and Marks, M. K. (eds), Elsevier Academic Press, pp. 129-143.

VI. Dissemination

The study progress and results were presented at the NIJ Forensic Anthropology Grantees Focus Group Meeting in Alexandria, Virginia on December 7th, 2009. With the study fully complete, manuscripts will be submitted to a forensic science journal and/or conference.

Appendix A

DOJ Live Cranium Data Preparation Procedure

Location of data: [\\CMR-PORTAL\CT-MRI-Datasets\CT\Live Bone\DOJ Project](#)

EXPORTING THE DICOMS IN MIMICS

- Open Mimics and select FILE and IMPORT IMAGES
- Select all of the dicoms from the folder and hit NEXT
- Once the dicoms have loaded, select CONVERT
- A Change Orientation box will open once the dicoms have finished converting
 - Click on the top X and select TOP and then click OK
- Once the dicoms open in the full screen mode you will select EXPORT and then DICOMS
- Select the Exported Dicoms folder as the location to save the outputted dicoms
- Update the “Dicoms exported in Mimics” column on cmr-portal with YES

EDITING THE EXPORTED DICOMS IN AMIRA 4.0

- Load the dicoms in the Exported Dicoms folder in Amira 4.0
- Crop the dicoms
 - Select BOUNDING BOX and ORTHOSLICE
 - Scroll through the slices in the xy plane (axial) and determine which slices you want to crop
 - Select the CROP tool and input your cropped slice numbers
 - The axial plane refers to the x-direction
- Create a Segmentations folder in the main folder and save your cropped dicoms as #_Dicom_Crop.am (use the number e.g. M55 and not the name)
- From your cropped dicoms, RIGHT click and select COMPUTE and RESAMPLE
 - From the Filter menu, select CUBIC – WIDTH 6
 - Click on VOXEL SIZE and change the z-value from 0.3 to 0.06
 - Hit APPLY to continue
- A new box will appear with Resampled at the end of the name, LEFT click and then RIGHT click and select COMPUTE and CASTFIELD
 - From the Output Datatype menu, select UNSIGNED CHAR (8 BIT)
 - Hit APPLY to continue
- Save your edited dicoms as #_Edited_Dicoms.am

SEGMENTING AND CREATING THE 3D MODEL IN AMIRA 3.1

- Load the #_Edited_Dicoms.am file from the Segmentation folder
- Open the LABELFIELD as you normally would

- *Do not* change your data window
- Threshold with a minimum value of 150 and a maximum value of 255
- **Look for any scattering along the regions of the teeth where metal fillings could be
- **Make sure that only the cranium and mandible are selected in your labels
- **Use the three views to try and find the separation between the base of the cranium and vertebrae. It is very difficult to tell which bone is which. It might be beneficial to create your 3D model and select an orthoslice from the dicoms in order to help determine which slice is the division between the two.
- Save your labels as #_Edited_Dicom_Labels.am in the Segmentation folder
- Create the 3D model and select NO SMOOTHING from the Smoothing menu
 - Reduce number of faces to 100,000.

Appendix B

MATLAB Code used to build memory matrices

```
%Load text files from IDAS into training matrices
clear all

wb = waitbar(0, 'Building Facial Measurement Matricies');

filename = {'Supraglabella/WM1.txt', 'Glabella/WM1.txt', 'Nasion/WM1.txt', 'End
of Nasals/WM1.txt', 'Mid-Philtrum/WM1.txt', 'Chin-Lip Fold/WM1.txt', 'Mental
Eminence/WM1.txt', 'Beneath Chin/WM1.txt', 'Frontal Eminence
Left/WM1.txt', 'Supraorbital Left/WM1.txt', 'Suborbital Left/WM1.txt', 'Lateral
Orbit Left/WM1.txt', 'Zygomatic Arch Left/WM1.txt';
    'Supraglabella/WM3.txt', 'Glabella/WM3.txt', 'Nasion/WM3.txt', 'End of
Nasals/WM3.txt', 'Mid-Philtrum/WM3.txt', 'Chin-Lip Fold/WM3.txt', 'Mental
Eminence/WM3.txt', 'Beneath Chin/WM3.txt', 'Frontal Eminence
Left/WM3.txt', 'Supraorbital Left/WM3.txt', 'Suborbital Left/WM3.txt', 'Lateral
Orbit Left/WM3.txt', 'Zygomatic Arch Left/WM3.txt';
    'Supraglabella/WM4.txt', 'Glabella/WM4.txt', 'Nasion/WM4.txt', 'End of
Nasals/WM4.txt', 'Mid-Philtrum/WM4.txt', 'Chin-Lip Fold/WM4.txt', 'Mental
Eminence/WM4.txt', 'Beneath Chin/WM4.txt', 'Frontal Eminence
Left/WM4.txt', 'Supraorbital Left/WM4.txt', 'Suborbital Left/WM4.txt', 'Lateral
Orbit Left/WM4.txt', 'Zygomatic Arch Left/WM4.txt';
    'Supraglabella/WM5.txt', 'Glabella/WM5.txt', 'Nasion/WM5.txt', 'End of
Nasals/WM5.txt', 'Mid-Philtrum/WM5.txt', 'Chin-Lip Fold/WM5.txt', 'Mental
Eminence/WM5.txt', 'Beneath Chin/WM5.txt', 'Frontal Eminence
Left/WM5.txt', 'Supraorbital Left/WM5.txt', 'Suborbital Left/WM5.txt', 'Lateral
Orbit Left/WM5.txt', 'Zygomatic Arch Left/WM5.txt';
    'Supraglabella/WM6.txt', 'Glabella/WM6.txt', 'Nasion/WM6.txt', 'End of
Nasals/WM6.txt', 'Mid-Philtrum/WM6.txt', 'Chin-Lip Fold/WM6.txt', 'Mental
Eminence/WM6.txt', 'Beneath Chin/WM6.txt', 'Frontal Eminence
Left/WM6.txt', 'Supraorbital Left/WM6.txt', 'Suborbital Left/WM6.txt', 'Lateral
Orbit Left/WM6.txt', 'Zygomatic Arch Left/WM6.txt';
    'Supraglabella/WM7.txt', 'Glabella/WM7.txt', 'Nasion/WM7.txt', 'End of
Nasals/WM7.txt', 'Mid-Philtrum/WM7.txt', 'Chin-Lip Fold/WM7.txt', 'Mental
Eminence/WM7.txt', 'Beneath Chin/WM7.txt', 'Frontal Eminence
Left/WM7.txt', 'Supraorbital Left/WM7.txt', 'Suborbital Left/WM7.txt', 'Lateral
Orbit Left/WM7.txt', 'Zygomatic Arch Left/WM7.txt';
    'Supraglabella/WM8.txt', 'Glabella/WM8.txt', 'Nasion/WM8.txt', 'End of
Nasals/WM8.txt', 'Mid-Philtrum/WM8.txt', 'Chin-Lip Fold/WM8.txt', 'Mental
Eminence/WM8.txt', 'Beneath Chin/WM8.txt', 'Frontal Eminence
Left/WM8.txt', 'Supraorbital Left/WM8.txt', 'Suborbital Left/WM8.txt', 'Lateral
Orbit Left/WM8.txt', 'Zygomatic Arch Left/WM8.txt';
    'Supraglabella/WM9.txt', 'Glabella/WM9.txt', 'Nasion/WM9.txt', 'End of
Nasals/WM9.txt', 'Mid-Philtrum/WM9.txt', 'Chin-Lip Fold/WM9.txt', 'Mental
Eminence/WM9.txt', 'Beneath Chin/WM9.txt', 'Frontal Eminence
Left/WM9.txt', 'Supraorbital Left/WM9.txt', 'Suborbital Left/WM9.txt', 'Lateral
Orbit Left/WM9.txt', 'Zygomatic Arch Left/WM9.txt';
    'Supraglabella/WM10.txt', 'Glabella/WM10.txt', 'Nasion/WM10.txt', 'End of
Nasals/WM10.txt', 'Mid-Philtrum/WM10.txt', 'Chin-Lip Fold/WM10.txt', 'Mental
Eminence/WM10.txt', 'Beneath Chin/WM10.txt', 'Frontal Eminence
```

Left/WM10.txt', 'Supraorbital Left/WM10.txt', 'Suborbital
Left/WM10.txt', 'Lateral Orbit Left/WM10.txt', 'Zygomatic Arch Left/WM10.txt';
 'Supraglabella/WM11.txt', 'Glabella/WM11.txt', 'Nasion/WM11.txt', 'End of
Nasals/WM11.txt', 'Mid-Philtrum/WM11.txt', 'Chin-Lip Fold/WM11.txt', 'Mental
Eminence/WM11.txt', 'Beneath Chin/WM11.txt', 'Frontal Eminence
Left/WM11.txt', 'Supraorbital Left/WM11.txt', 'Suborbital
Left/WM11.txt', 'Lateral Orbit Left/WM11.txt', 'Zygomatic Arch Left/WM11.txt';
 'Supraglabella/WM12.txt', 'Glabella/WM12.txt', 'Nasion/WM12.txt', 'End of
Nasals/WM12.txt', 'Mid-Philtrum/WM12.txt', 'Chin-Lip Fold/WM12.txt', 'Mental
Eminence/WM12.txt', 'Beneath Chin/WM12.txt', 'Frontal Eminence
Left/WM12.txt', 'Supraorbital Left/WM12.txt', 'Suborbital
Left/WM12.txt', 'Lateral Orbit Left/WM12.txt', 'Zygomatic Arch Left/WM12.txt';
 'Supraglabella/WM15.txt', 'Glabella/WM15.txt', 'Nasion/WM15.txt', 'End of
Nasals/WM15.txt', 'Mid-Philtrum/WM15.txt', 'Chin-Lip Fold/WM15.txt', 'Mental
Eminence/WM15.txt', 'Beneath Chin/WM15.txt', 'Frontal Eminence
Left/WM15.txt', 'Supraorbital Left/WM15.txt', 'Suborbital
Left/WM15.txt', 'Lateral Orbit Left/WM15.txt', 'Zygomatic Arch Left/WM15.txt';
 'Supraglabella/WM18.txt', 'Glabella/WM18.txt', 'Nasion/WM18.txt', 'End of
Nasals/WM18.txt', 'Mid-Philtrum/WM18.txt', 'Chin-Lip Fold/WM18.txt', 'Mental
Eminence/WM18.txt', 'Beneath Chin/WM18.txt', 'Frontal Eminence
Left/WM18.txt', 'Supraorbital Left/WM18.txt', 'Suborbital
Left/WM18.txt', 'Lateral Orbit Left/WM18.txt', 'Zygomatic Arch Left/WM18.txt';
 'Supraglabella/WM19.txt', 'Glabella/WM19.txt', 'Nasion/WM19.txt', 'End of
Nasals/WM19.txt', 'Mid-Philtrum/WM19.txt', 'Chin-Lip Fold/WM19.txt', 'Mental
Eminence/WM19.txt', 'Beneath Chin/WM19.txt', 'Frontal Eminence
Left/WM19.txt', 'Supraorbital Left/WM19.txt', 'Suborbital
Left/WM19.txt', 'Lateral Orbit Left/WM19.txt', 'Zygomatic Arch Left/WM19.txt';
 'Supraglabella/WM20.txt', 'Glabella/WM20.txt', 'Nasion/WM20.txt', 'End of
Nasals/WM20.txt', 'Mid-Philtrum/WM20.txt', 'Chin-Lip Fold/WM20.txt', 'Mental
Eminence/WM20.txt', 'Beneath Chin/WM20.txt', 'Frontal Eminence
Left/WM20.txt', 'Supraorbital Left/WM20.txt', 'Suborbital
Left/WM20.txt', 'Lateral Orbit Left/WM20.txt', 'Zygomatic Arch Left/WM20.txt';
 'Supraglabella/WM21.txt', 'Glabella/WM21.txt', 'Nasion/WM21.txt', 'End of
Nasals/WM21.txt', 'Mid-Philtrum/WM21.txt', 'Chin-Lip Fold/WM21.txt', 'Mental
Eminence/WM21.txt', 'Beneath Chin/WM21.txt', 'Frontal Eminence
Left/WM21.txt', 'Supraorbital Left/WM21.txt', 'Suborbital
Left/WM21.txt', 'Lateral Orbit Left/WM21.txt', 'Zygomatic Arch Left/WM21.txt';
 'Supraglabella/WM22.txt', 'Glabella/WM22.txt', 'Nasion/WM22.txt', 'End of
Nasals/WM22.txt', 'Mid-Philtrum/WM22.txt', 'Chin-Lip Fold/WM22.txt', 'Mental
Eminence/WM22.txt', 'Beneath Chin/WM22.txt', 'Frontal Eminence
Left/WM22.txt', 'Supraorbital Left/WM22.txt', 'Suborbital
Left/WM22.txt', 'Lateral Orbit Left/WM22.txt', 'Zygomatic Arch Left/WM22.txt';
 'Supraglabella/WM23.txt', 'Glabella/WM23.txt', 'Nasion/WM23.txt', 'End of
Nasals/WM23.txt', 'Mid-Philtrum/WM23.txt', 'Chin-Lip Fold/WM23.txt', 'Mental
Eminence/WM23.txt', 'Beneath Chin/WM23.txt', 'Frontal Eminence
Left/WM23.txt', 'Supraorbital Left/WM23.txt', 'Suborbital
Left/WM23.txt', 'Lateral Orbit Left/WM23.txt', 'Zygomatic Arch Left/WM23.txt';
 'Supraglabella/WM24.txt', 'Glabella/WM24.txt', 'Nasion/WM24.txt', 'End of
Nasals/WM24.txt', 'Mid-Philtrum/WM24.txt', 'Chin-Lip Fold/WM24.txt', 'Mental
Eminence/WM24.txt', 'Beneath Chin/WM24.txt', 'Frontal Eminence
Left/WM24.txt', 'Supraorbital Left/WM24.txt', 'Suborbital
Left/WM24.txt', 'Lateral Orbit Left/WM24.txt', 'Zygomatic Arch Left/WM24.txt';

'Supraglabella/WM25.txt', 'Glabella/WM25.txt', 'Nasion/WM25.txt', 'End of Nasals/WM25.txt', 'Mid-Philtrum/WM25.txt', 'Chin-Lip Fold/WM25.txt', 'Mental Eminence/WM25.txt', 'Beneath Chin/WM25.txt', 'Frontal Eminence Left/WM25.txt', 'Supraorbital Left/WM25.txt', 'Suborbital Left/WM25.txt', 'Lateral Orbit Left/WM25.txt', 'Zygomatic Arch Left/WM25.txt';

'Supraglabella/WM26.txt', 'Glabella/WM26.txt', 'Nasion/WM26.txt', 'End of Nasals/WM26.txt', 'Mid-Philtrum/WM26.txt', 'Chin-Lip Fold/WM26.txt', 'Mental Eminence/WM26.txt', 'Beneath Chin/WM26.txt', 'Frontal Eminence Left/WM26.txt', 'Supraorbital Left/WM26.txt', 'Suborbital Left/WM26.txt', 'Lateral Orbit Left/WM26.txt', 'Zygomatic Arch Left/WM26.txt';

'Supraglabella/WM28.txt', 'Glabella/WM28.txt', 'Nasion/WM28.txt', 'End of Nasals/WM28.txt', 'Mid-Philtrum/WM28.txt', 'Chin-Lip Fold/WM28.txt', 'Mental Eminence/WM28.txt', 'Beneath Chin/WM28.txt', 'Frontal Eminence Left/WM28.txt', 'Supraorbital Left/WM28.txt', 'Suborbital Left/WM28.txt', 'Lateral Orbit Left/WM28.txt', 'Zygomatic Arch Left/WM28.txt';

'Supraglabella/WM29.txt', 'Glabella/WM29.txt', 'Nasion/WM29.txt', 'End of Nasals/WM29.txt', 'Mid-Philtrum/WM29.txt', 'Chin-Lip Fold/WM29.txt', 'Mental Eminence/WM29.txt', 'Beneath Chin/WM29.txt', 'Frontal Eminence Left/WM29.txt', 'Supraorbital Left/WM29.txt', 'Suborbital Left/WM29.txt', 'Lateral Orbit Left/WM29.txt', 'Zygomatic Arch Left/WM29.txt';

'Supraglabella/WM30.txt', 'Glabella/WM30.txt', 'Nasion/WM30.txt', 'End of Nasals/WM30.txt', 'Mid-Philtrum/WM30.txt', 'Chin-Lip Fold/WM30.txt', 'Mental Eminence/WM30.txt', 'Beneath Chin/WM30.txt', 'Frontal Eminence Left/WM30.txt', 'Supraorbital Left/WM30.txt', 'Suborbital Left/WM30.txt', 'Lateral Orbit Left/WM30.txt', 'Zygomatic Arch Left/WM30.txt';

'Supraglabella/WM32.txt', 'Glabella/WM32.txt', 'Nasion/WM32.txt', 'End of Nasals/WM32.txt', 'Mid-Philtrum/WM32.txt', 'Chin-Lip Fold/WM32.txt', 'Mental Eminence/WM32.txt', 'Beneath Chin/WM32.txt', 'Frontal Eminence Left/WM32.txt', 'Supraorbital Left/WM32.txt', 'Suborbital Left/WM32.txt', 'Lateral Orbit Left/WM32.txt', 'Zygomatic Arch Left/WM32.txt';

'Supraglabella/WM33.txt', 'Glabella/WM33.txt', 'Nasion/WM33.txt', 'End of Nasals/WM33.txt', 'Mid-Philtrum/WM33.txt', 'Chin-Lip Fold/WM33.txt', 'Mental Eminence/WM33.txt', 'Beneath Chin/WM33.txt', 'Frontal Eminence Left/WM33.txt', 'Supraorbital Left/WM33.txt', 'Suborbital Left/WM33.txt', 'Lateral Orbit Left/WM33.txt', 'Zygomatic Arch Left/WM33.txt';

'Supraglabella/WM34.txt', 'Glabella/WM34.txt', 'Nasion/WM34.txt', 'End of Nasals/WM34.txt', 'Mid-Philtrum/WM34.txt', 'Chin-Lip Fold/WM34.txt', 'Mental Eminence/WM34.txt', 'Beneath Chin/WM34.txt', 'Frontal Eminence Left/WM34.txt', 'Supraorbital Left/WM34.txt', 'Suborbital Left/WM34.txt', 'Lateral Orbit Left/WM34.txt', 'Zygomatic Arch Left/WM34.txt';

'Supraglabella/WM35.txt', 'Glabella/WM35.txt', 'Nasion/WM35.txt', 'End of Nasals/WM35.txt', 'Mid-Philtrum/WM35.txt', 'Chin-Lip Fold/WM35.txt', 'Mental Eminence/WM35.txt', 'Beneath Chin/WM35.txt', 'Frontal Eminence Left/WM35.txt', 'Supraorbital Left/WM35.txt', 'Suborbital Left/WM35.txt', 'Lateral Orbit Left/WM35.txt', 'Zygomatic Arch Left/WM35.txt';

'Supraglabella/WM37.txt', 'Glabella/WM37.txt', 'Nasion/WM37.txt', 'End of Nasals/WM37.txt', 'Mid-Philtrum/WM37.txt', 'Chin-Lip Fold/WM37.txt', 'Mental Eminence/WM37.txt', 'Beneath Chin/WM37.txt', 'Frontal Eminence Left/WM37.txt', 'Supraorbital Left/WM37.txt', 'Suborbital Left/WM37.txt', 'Lateral Orbit Left/WM37.txt', 'Zygomatic Arch Left/WM37.txt';

'Supraglabella/WM38.txt', 'Glabella/WM38.txt', 'Nasion/WM38.txt', 'End of Nasals/WM38.txt', 'Mid-Philtrum/WM38.txt', 'Chin-Lip Fold/WM38.txt', 'Mental Eminence/WM38.txt', 'Beneath Chin/WM38.txt', 'Frontal Eminence

Left/WM38.txt', 'Supraorbital Left/WM38.txt', 'Suborbital
Left/WM38.txt', 'Lateral Orbit Left/WM38.txt', 'Zygomatic Arch Left/WM38.txt';
 'Supraglabella/WM45.txt', 'Glabella/WM45.txt', 'Nasion/WM45.txt', 'End of
Nasals/WM45.txt', 'Mid-Philtrum/WM45.txt', 'Chin-Lip Fold/WM45.txt', 'Mental
Eminence/WM45.txt', 'Beneath Chin/WM45.txt', 'Frontal Eminence
Left/WM45.txt', 'Supraorbital Left/WM45.txt', 'Suborbital
Left/WM45.txt', 'Lateral Orbit Left/WM45.txt', 'Zygomatic Arch Left/WM45.txt';
 'Supraglabella/M49.txt', 'Glabella/M49.txt', 'Nasion/M49.txt', 'End of
Nasals/M49.txt', 'Mid-Philtrum/M49.txt', 'Chin-Lip Fold/M49.txt', 'Mental
Eminence/M49.txt', 'Beneath Chin/M49.txt', 'Frontal Eminence
Left/M49.txt', 'Supraorbital Left/M49.txt', 'Suborbital Left/M49.txt', 'Lateral
Orbit Left/M49.txt', 'Zygomatic Arch Left/M49.txt';
 'Supraglabella/M51.txt', 'Glabella/M51.txt', 'Nasion/M51.txt', 'End of
Nasals/M51.txt', 'Mid-Philtrum/M51.txt', 'Chin-Lip Fold/M51.txt', 'Mental
Eminence/M51.txt', 'Beneath Chin/M51.txt', 'Frontal Eminence
Left/M51.txt', 'Supraorbital Left/M51.txt', 'Suborbital Left/M51.txt', 'Lateral
Orbit Left/M51.txt', 'Zygomatic Arch Left/M51.txt';
 'Supraglabella/M52.txt', 'Glabella/M52.txt', 'Nasion/M52.txt', 'End of
Nasals/M52.txt', 'Mid-Philtrum/M52.txt', 'Chin-Lip Fold/M52.txt', 'Mental
Eminence/M52.txt', 'Beneath Chin/M52.txt', 'Frontal Eminence
Left/M52.txt', 'Supraorbital Left/M52.txt', 'Suborbital Left/M52.txt', 'Lateral
Orbit Left/M52.txt', 'Zygomatic Arch Left/M52.txt';
 'Supraglabella/M53.txt', 'Glabella/M53.txt', 'Nasion/M53.txt', 'End of
Nasals/M53.txt', 'Mid-Philtrum/M53.txt', 'Chin-Lip Fold/M53.txt', 'Mental
Eminence/M53.txt', 'Beneath Chin/M53.txt', 'Frontal Eminence
Left/M53.txt', 'Supraorbital Left/M53.txt', 'Suborbital Left/M53.txt', 'Lateral
Orbit Left/M53.txt', 'Zygomatic Arch Left/M53.txt';
 'Supraglabella/M54.txt', 'Glabella/M54.txt', 'Nasion/M54.txt', 'End of
Nasals/M54.txt', 'Mid-Philtrum/M54.txt', 'Chin-Lip Fold/M54.txt', 'Mental
Eminence/M54.txt', 'Beneath Chin/M54.txt', 'Frontal Eminence
Left/M54.txt', 'Supraorbital Left/M54.txt', 'Suborbital Left/M54.txt', 'Lateral
Orbit Left/M54.txt', 'Zygomatic Arch Left/M54.txt';
 'Supraglabella/M55.txt', 'Glabella/M55.txt', 'Nasion/M55.txt', 'End of
Nasals/M55.txt', 'Mid-Philtrum/M55.txt', 'Chin-Lip Fold/M55.txt', 'Mental
Eminence/M55.txt', 'Beneath Chin/M55.txt', 'Frontal Eminence
Left/M55.txt', 'Supraorbital Left/M55.txt', 'Suborbital Left/M55.txt', 'Lateral
Orbit Left/M55.txt', 'Zygomatic Arch Left/M55.txt';
 'Supraglabella/M56.txt', 'Glabella/M56.txt', 'Nasion/M56.txt', 'End of
Nasals/M56.txt', 'Mid-Philtrum/M56.txt', 'Chin-Lip Fold/M56.txt', 'Mental
Eminence/M56.txt', 'Beneath Chin/M56.txt', 'Frontal Eminence
Left/M56.txt', 'Supraorbital Left/M56.txt', 'Suborbital Left/M56.txt', 'Lateral
Orbit Left/M56.txt', 'Zygomatic Arch Left/M56.txt';
 'Supraglabella/M57.txt', 'Glabella/M57.txt', 'Nasion/M57.txt', 'End of
Nasals/M57.txt', 'Mid-Philtrum/M57.txt', 'Chin-Lip Fold/M57.txt', 'Mental
Eminence/M57.txt', 'Beneath Chin/M57.txt', 'Frontal Eminence
Left/M57.txt', 'Supraorbital Left/M57.txt', 'Suborbital Left/M57.txt', 'Lateral
Orbit Left/M57.txt', 'Zygomatic Arch Left/M57.txt';
 'Supraglabella/M58.txt', 'Glabella/M58.txt', 'Nasion/M58.txt', 'End of
Nasals/M58.txt', 'Mid-Philtrum/M58.txt', 'Chin-Lip Fold/M58.txt', 'Mental
Eminence/M58.txt', 'Beneath Chin/M58.txt', 'Frontal Eminence
Left/M58.txt', 'Supraorbital Left/M58.txt', 'Suborbital Left/M58.txt', 'Lateral
Orbit Left/M58.txt', 'Zygomatic Arch Left/M58.txt';

'Supraglabella/M59.txt', 'Glabella/M59.txt', 'Nasion/M59.txt', 'End of Nasals/M59.txt', 'Mid-Philtrum/M59.txt', 'Chin-Lip Fold/M59.txt', 'Mental Eminence/M59.txt', 'Beneath Chin/M59.txt', 'Frontal Eminence Left/M59.txt', 'Supraorbital Left/M59.txt', 'Suborbital Left/M59.txt', 'Lateral Orbit Left/M59.txt', 'Zygomatic Arch Left/M59.txt';

'Supraglabella/M60.txt', 'Glabella/M60.txt', 'Nasion/M60.txt', 'End of Nasals/M60.txt', 'Mid-Philtrum/M60.txt', 'Chin-Lip Fold/M60.txt', 'Mental Eminence/M60.txt', 'Beneath Chin/M60.txt', 'Frontal Eminence Left/M60.txt', 'Supraorbital Left/M60.txt', 'Suborbital Left/M60.txt', 'Lateral Orbit Left/M60.txt', 'Zygomatic Arch Left/M60.txt';

'Supraglabella/M61.txt', 'Glabella/M61.txt', 'Nasion/M61.txt', 'End of Nasals/M61.txt', 'Mid-Philtrum/M61.txt', 'Chin-Lip Fold/M61.txt', 'Mental Eminence/M61.txt', 'Beneath Chin/M61.txt', 'Frontal Eminence Left/M61.txt', 'Supraorbital Left/M61.txt', 'Suborbital Left/M61.txt', 'Lateral Orbit Left/M61.txt', 'Zygomatic Arch Left/M61.txt';

'Supraglabella/M62.txt', 'Glabella/M62.txt', 'Nasion/M62.txt', 'End of Nasals/M62.txt', 'Mid-Philtrum/M62.txt', 'Chin-Lip Fold/M62.txt', 'Mental Eminence/M62.txt', 'Beneath Chin/M62.txt', 'Frontal Eminence Left/M62.txt', 'Supraorbital Left/M62.txt', 'Suborbital Left/M62.txt', 'Lateral Orbit Left/M62.txt', 'Zygomatic Arch Left/M62.txt';

'Supraglabella/M63.txt', 'Glabella/M63.txt', 'Nasion/M63.txt', 'End of Nasals/M63.txt', 'Mid-Philtrum/M63.txt', 'Chin-Lip Fold/M63.txt', 'Mental Eminence/M63.txt', 'Beneath Chin/M63.txt', 'Frontal Eminence Left/M63.txt', 'Supraorbital Left/M63.txt', 'Suborbital Left/M63.txt', 'Lateral Orbit Left/M63.txt', 'Zygomatic Arch Left/M63.txt';

'Supraglabella/M64.txt', 'Glabella/M64.txt', 'Nasion/M64.txt', 'End of Nasals/M64.txt', 'Mid-Philtrum/M64.txt', 'Chin-Lip Fold/M64.txt', 'Mental Eminence/M64.txt', 'Beneath Chin/M64.txt', 'Frontal Eminence Left/M64.txt', 'Supraorbital Left/M64.txt', 'Suborbital Left/M64.txt', 'Lateral Orbit Left/M64.txt', 'Zygomatic Arch Left/M64.txt';

'Supraglabella/M65.txt', 'Glabella/M65.txt', 'Nasion/M65.txt', 'End of Nasals/M65.txt', 'Mid-Philtrum/M65.txt', 'Chin-Lip Fold/M65.txt', 'Mental Eminence/M65.txt', 'Beneath Chin/M65.txt', 'Frontal Eminence Left/M65.txt', 'Supraorbital Left/M65.txt', 'Suborbital Left/M65.txt', 'Lateral Orbit Left/M65.txt', 'Zygomatic Arch Left/M65.txt';

'Supraglabella/M66.txt', 'Glabella/M66.txt', 'Nasion/M66.txt', 'End of Nasals/M66.txt', 'Mid-Philtrum/M66.txt', 'Chin-Lip Fold/M66.txt', 'Mental Eminence/M66.txt', 'Beneath Chin/M66.txt', 'Frontal Eminence Left/M66.txt', 'Supraorbital Left/M66.txt', 'Suborbital Left/M66.txt', 'Lateral Orbit Left/M66.txt', 'Zygomatic Arch Left/M66.txt';

'Supraglabella/M67.txt', 'Glabella/M67.txt', 'Nasion/M67.txt', 'End of Nasals/M67.txt', 'Mid-Philtrum/M67.txt', 'Chin-Lip Fold/M67.txt', 'Mental Eminence/M67.txt', 'Beneath Chin/M67.txt', 'Frontal Eminence Left/M67.txt', 'Supraorbital Left/M67.txt', 'Suborbital Left/M67.txt', 'Lateral Orbit Left/M67.txt', 'Zygomatic Arch Left/M67.txt';

'Supraglabella/M68.txt', 'Glabella/M68.txt', 'Nasion/M68.txt', 'End of Nasals/M68.txt', 'Mid-Philtrum/M68.txt', 'Chin-Lip Fold/M68.txt', 'Mental Eminence/M68.txt', 'Beneath Chin/M68.txt', 'Frontal Eminence Left/M68.txt', 'Supraorbital Left/M68.txt', 'Suborbital Left/M68.txt', 'Lateral Orbit Left/M68.txt', 'Zygomatic Arch Left/M68.txt';

'Supraglabella/M69.txt', 'Glabella/M69.txt', 'Nasion/M69.txt', 'End of Nasals/M69.txt', 'Mid-Philtrum/M69.txt', 'Chin-Lip Fold/M69.txt', 'Mental Eminence/M69.txt', 'Beneath Chin/M69.txt', 'Frontal Eminence

Left/M69.txt', 'Supraorbital Left/M69.txt', 'Suborbital Left/M69.txt', 'Lateral Orbit Left/M69.txt', 'Zygomatic Arch Left/M69.txt';
'Supraglabella/M70.txt', 'Glabella/M70.txt', 'Nasion/M70.txt', 'End of Nasals/M70.txt', 'Mid-Philtrum/M70.txt', 'Chin-Lip Fold/M70.txt', 'Mental Eminence/M70.txt', 'Beneath Chin/M70.txt', 'Frontal Eminence Left/M70.txt', 'Supraorbital Left/M70.txt', 'Suborbital Left/M70.txt', 'Lateral Orbit Left/M70.txt', 'Zygomatic Arch Left/M70.txt';
'Supraglabella/M71.txt', 'Glabella/M71.txt', 'Nasion/M71.txt', 'End of Nasals/M71.txt', 'Mid-Philtrum/M71.txt', 'Chin-Lip Fold/M71.txt', 'Mental Eminence/M71.txt', 'Beneath Chin/M71.txt', 'Frontal Eminence Left/M71.txt', 'Supraorbital Left/M71.txt', 'Suborbital Left/M71.txt', 'Lateral Orbit Left/M71.txt', 'Zygomatic Arch Left/M71.txt';
'Supraglabella/M72.txt', 'Glabella/M72.txt', 'Nasion/M72.txt', 'End of Nasals/M72.txt', 'Mid-Philtrum/M72.txt', 'Chin-Lip Fold/M72.txt', 'Mental Eminence/M72.txt', 'Beneath Chin/M72.txt', 'Frontal Eminence Left/M72.txt', 'Supraorbital Left/M72.txt', 'Suborbital Left/M72.txt', 'Lateral Orbit Left/M72.txt', 'Zygomatic Arch Left/M72.txt';
'Supraglabella/M73.txt', 'Glabella/M73.txt', 'Nasion/M73.txt', 'End of Nasals/M73.txt', 'Mid-Philtrum/M73.txt', 'Chin-Lip Fold/M73.txt', 'Mental Eminence/M73.txt', 'Beneath Chin/M73.txt', 'Frontal Eminence Left/M73.txt', 'Supraorbital Left/M73.txt', 'Suborbital Left/M73.txt', 'Lateral Orbit Left/M73.txt', 'Zygomatic Arch Left/M73.txt';
'Supraglabella/M74.txt', 'Glabella/M74.txt', 'Nasion/M74.txt', 'End of Nasals/M74.txt', 'Mid-Philtrum/M74.txt', 'Chin-Lip Fold/M74.txt', 'Mental Eminence/M74.txt', 'Beneath Chin/M74.txt', 'Frontal Eminence Left/M74.txt', 'Supraorbital Left/M74.txt', 'Suborbital Left/M74.txt', 'Lateral Orbit Left/M74.txt', 'Zygomatic Arch Left/M74.txt';
'Supraglabella/M75.txt', 'Glabella/M75.txt', 'Nasion/M75.txt', 'End of Nasals/M75.txt', 'Mid-Philtrum/M75.txt', 'Chin-Lip Fold/M75.txt', 'Mental Eminence/M75.txt', 'Beneath Chin/M75.txt', 'Frontal Eminence Left/M75.txt', 'Supraorbital Left/M75.txt', 'Suborbital Left/M75.txt', 'Lateral Orbit Left/M75.txt', 'Zygomatic Arch Left/M75.txt';
'Supraglabella/M76.txt', 'Glabella/M76.txt', 'Nasion/M76.txt', 'End of Nasals/M76.txt', 'Mid-Philtrum/M76.txt', 'Chin-Lip Fold/M76.txt', 'Mental Eminence/M76.txt', 'Beneath Chin/M76.txt', 'Frontal Eminence Left/M76.txt', 'Supraorbital Left/M76.txt', 'Suborbital Left/M76.txt', 'Lateral Orbit Left/M76.txt', 'Zygomatic Arch Left/M76.txt';
'Supraglabella/M77.txt', 'Glabella/M77.txt', 'Nasion/M77.txt', 'End of Nasals/M77.txt', 'Mid-Philtrum/M77.txt', 'Chin-Lip Fold/M77.txt', 'Mental Eminence/M77.txt', 'Beneath Chin/M77.txt', 'Frontal Eminence Left/M77.txt', 'Supraorbital Left/M77.txt', 'Suborbital Left/M77.txt', 'Lateral Orbit Left/M77.txt', 'Zygomatic Arch Left/M77.txt';
'Supraglabella/M78.txt', 'Glabella/M78.txt', 'Nasion/M78.txt', 'End of Nasals/M78.txt', 'Mid-Philtrum/M78.txt', 'Chin-Lip Fold/M78.txt', 'Mental Eminence/M78.txt', 'Beneath Chin/M78.txt', 'Frontal Eminence Left/M78.txt', 'Supraorbital Left/M78.txt', 'Suborbital Left/M78.txt', 'Lateral Orbit Left/M78.txt', 'Zygomatic Arch Left/M78.txt';
'Supraglabella/M79.txt', 'Glabella/M79.txt', 'Nasion/M79.txt', 'End of Nasals/M79.txt', 'Mid-Philtrum/M79.txt', 'Chin-Lip Fold/M79.txt', 'Mental Eminence/M79.txt', 'Beneath Chin/M79.txt', 'Frontal Eminence Left/M79.txt', 'Supraorbital Left/M79.txt', 'Suborbital Left/M79.txt', 'Lateral Orbit Left/M79.txt', 'Zygomatic Arch Left/M79.txt';

'Supraglabella/M80.txt', 'Glabella/M80.txt', 'Nasion/M80.txt', 'End of Nasals/M80.txt', 'Mid-Philtrum/M80.txt', 'Chin-Lip Fold/M80.txt', 'Mental Eminence/M80.txt', 'Beneath Chin/M80.txt', 'Frontal Eminence Left/M80.txt', 'Supraorbital Left/M80.txt', 'Suborbital Left/M80.txt', 'Lateral Orbit Left/M80.txt', 'Zygomatic Arch Left/M80.txt';

'Supraglabella/M81.txt', 'Glabella/M81.txt', 'Nasion/M81.txt', 'End of Nasals/M81.txt', 'Mid-Philtrum/M81.txt', 'Chin-Lip Fold/M81.txt', 'Mental Eminence/M81.txt', 'Beneath Chin/M81.txt', 'Frontal Eminence Left/M81.txt', 'Supraorbital Left/M81.txt', 'Suborbital Left/M81.txt', 'Lateral Orbit Left/M81.txt', 'Zygomatic Arch Left/M81.txt';

'Supraglabella/M82.txt', 'Glabella/M82.txt', 'Nasion/M82.txt', 'End of Nasals/M82.txt', 'Mid-Philtrum/M82.txt', 'Chin-Lip Fold/M82.txt', 'Mental Eminence/M82.txt', 'Beneath Chin/M82.txt', 'Frontal Eminence Left/M82.txt', 'Supraorbital Left/M82.txt', 'Suborbital Left/M82.txt', 'Lateral Orbit Left/M82.txt', 'Zygomatic Arch Left/M82.txt';

'Supraglabella/M83.txt', 'Glabella/M83.txt', 'Nasion/M83.txt', 'End of Nasals/M83.txt', 'Mid-Philtrum/M83.txt', 'Chin-Lip Fold/M83.txt', 'Mental Eminence/M83.txt', 'Beneath Chin/M83.txt', 'Frontal Eminence Left/M83.txt', 'Supraorbital Left/M83.txt', 'Suborbital Left/M83.txt', 'Lateral Orbit Left/M83.txt', 'Zygomatic Arch Left/M83.txt';

'Supraglabella/M84.txt', 'Glabella/M84.txt', 'Nasion/M84.txt', 'End of Nasals/M84.txt', 'Mid-Philtrum/M84.txt', 'Chin-Lip Fold/M84.txt', 'Mental Eminence/M84.txt', 'Beneath Chin/M84.txt', 'Frontal Eminence Left/M84.txt', 'Supraorbital Left/M84.txt', 'Suborbital Left/M84.txt', 'Lateral Orbit Left/M84.txt', 'Zygomatic Arch Left/M84.txt';

'Supraglabella/M85.txt', 'Glabella/M85.txt', 'Nasion/M85.txt', 'End of Nasals/M85.txt', 'Mid-Philtrum/M85.txt', 'Chin-Lip Fold/M85.txt', 'Mental Eminence/M85.txt', 'Beneath Chin/M85.txt', 'Frontal Eminence Left/M85.txt', 'Supraorbital Left/M85.txt', 'Suborbital Left/M85.txt', 'Lateral Orbit Left/M85.txt', 'Zygomatic Arch Left/M85.txt';

'Supraglabella/M86.txt', 'Glabella/M86.txt', 'Nasion/M86.txt', 'End of Nasals/M86.txt', 'Mid-Philtrum/M86.txt', 'Chin-Lip Fold/M86.txt', 'Mental Eminence/M86.txt', 'Beneath Chin/M86.txt', 'Frontal Eminence Left/M86.txt', 'Supraorbital Left/M86.txt', 'Suborbital Left/M86.txt', 'Lateral Orbit Left/M86.txt', 'Zygomatic Arch Left/M86.txt';

'Supraglabella/M87.txt', 'Glabella/M87.txt', 'Nasion/M87.txt', 'End of Nasals/M87.txt', 'Mid-Philtrum/M87.txt', 'Chin-Lip Fold/M87.txt', 'Mental Eminence/M87.txt', 'Beneath Chin/M87.txt', 'Frontal Eminence Left/M87.txt', 'Supraorbital Left/M87.txt', 'Suborbital Left/M87.txt', 'Lateral Orbit Left/M87.txt', 'Zygomatic Arch Left/M87.txt';

'Supraglabella/M88.txt', 'Glabella/M88.txt', 'Nasion/M88.txt', 'End of Nasals/M88.txt', 'Mid-Philtrum/M88.txt', 'Chin-Lip Fold/M88.txt', 'Mental Eminence/M88.txt', 'Beneath Chin/M88.txt', 'Frontal Eminence Left/M88.txt', 'Supraorbital Left/M88.txt', 'Suborbital Left/M88.txt', 'Lateral Orbit Left/M88.txt', 'Zygomatic Arch Left/M88.txt';

'Supraglabella/M89.txt', 'Glabella/M89.txt', 'Nasion/M89.txt', 'End of Nasals/M89.txt', 'Mid-Philtrum/M89.txt', 'Chin-Lip Fold/M89.txt', 'Mental Eminence/M89.txt', 'Beneath Chin/M89.txt', 'Frontal Eminence Left/M89.txt', 'Supraorbital Left/M89.txt', 'Suborbital Left/M89.txt', 'Lateral Orbit Left/M89.txt', 'Zygomatic Arch Left/M89.txt';

'Supraglabella/M90.txt', 'Glabella/M90.txt', 'Nasion/M90.txt', 'End of Nasals/M90.txt', 'Mid-Philtrum/M90.txt', 'Chin-Lip Fold/M90.txt', 'Mental Eminence/M90.txt', 'Beneath Chin/M90.txt', 'Frontal Eminence

Left/M90.txt', 'Supraorbital Left/M90.txt', 'Suborbital Left/M90.txt', 'Lateral Orbit Left/M90.txt', 'Zygomatic Arch Left/M90.txt';
'Supraglabella/M91.txt', 'Glabella/M91.txt', 'Nasion/M91.txt', 'End of Nasals/M91.txt', 'Mid-Philtrum/M91.txt', 'Chin-Lip Fold/M91.txt', 'Mental Eminence/M91.txt', 'Beneath Chin/M91.txt', 'Frontal Eminence Left/M91.txt', 'Supraorbital Left/M91.txt', 'Suborbital Left/M91.txt', 'Lateral Orbit Left/M91.txt', 'Zygomatic Arch Left/M91.txt';
'Supraglabella/M92.txt', 'Glabella/M92.txt', 'Nasion/M92.txt', 'End of Nasals/M92.txt', 'Mid-Philtrum/M92.txt', 'Chin-Lip Fold/M92.txt', 'Mental Eminence/M92.txt', 'Beneath Chin/M92.txt', 'Frontal Eminence Left/M92.txt', 'Supraorbital Left/M92.txt', 'Suborbital Left/M92.txt', 'Lateral Orbit Left/M92.txt', 'Zygomatic Arch Left/M92.txt';
'Supraglabella/M93.txt', 'Glabella/M93.txt', 'Nasion/M93.txt', 'End of Nasals/M93.txt', 'Mid-Philtrum/M93.txt', 'Chin-Lip Fold/M93.txt', 'Mental Eminence/M93.txt', 'Beneath Chin/M93.txt', 'Frontal Eminence Left/M93.txt', 'Supraorbital Left/M93.txt', 'Suborbital Left/M93.txt', 'Lateral Orbit Left/M93.txt', 'Zygomatic Arch Left/M93.txt';
'Supraglabella/M94.txt', 'Glabella/M94.txt', 'Nasion/M94.txt', 'End of Nasals/M94.txt', 'Mid-Philtrum/M94.txt', 'Chin-Lip Fold/M94.txt', 'Mental Eminence/M94.txt', 'Beneath Chin/M94.txt', 'Frontal Eminence Left/M94.txt', 'Supraorbital Left/M94.txt', 'Suborbital Left/M94.txt', 'Lateral Orbit Left/M94.txt', 'Zygomatic Arch Left/M94.txt';
'Supraglabella/M95.txt', 'Glabella/M95.txt', 'Nasion/M95.txt', 'End of Nasals/M95.txt', 'Mid-Philtrum/M95.txt', 'Chin-Lip Fold/M95.txt', 'Mental Eminence/M95.txt', 'Beneath Chin/M95.txt', 'Frontal Eminence Left/M95.txt', 'Supraorbital Left/M95.txt', 'Suborbital Left/M95.txt', 'Lateral Orbit Left/M95.txt', 'Zygomatic Arch Left/M95.txt';
'Supraglabella/M96.txt', 'Glabella/M96.txt', 'Nasion/M96.txt', 'End of Nasals/M96.txt', 'Mid-Philtrum/M96.txt', 'Chin-Lip Fold/M96.txt', 'Mental Eminence/M96.txt', 'Beneath Chin/M96.txt', 'Frontal Eminence Left/M96.txt', 'Supraorbital Left/M96.txt', 'Suborbital Left/M96.txt', 'Lateral Orbit Left/M96.txt', 'Zygomatic Arch Left/M96.txt';
'Supraglabella/M97.txt', 'Glabella/M97.txt', 'Nasion/M97.txt', 'End of Nasals/M97.txt', 'Mid-Philtrum/M97.txt', 'Chin-Lip Fold/M97.txt', 'Mental Eminence/M97.txt', 'Beneath Chin/M97.txt', 'Frontal Eminence Left/M97.txt', 'Supraorbital Left/M97.txt', 'Suborbital Left/M97.txt', 'Lateral Orbit Left/M97.txt', 'Zygomatic Arch Left/M97.txt';
'Supraglabella/M98.txt', 'Glabella/M98.txt', 'Nasion/M98.txt', 'End of Nasals/M98.txt', 'Mid-Philtrum/M98.txt', 'Chin-Lip Fold/M98.txt', 'Mental Eminence/M98.txt', 'Beneath Chin/M98.txt', 'Frontal Eminence Left/M98.txt', 'Supraorbital Left/M98.txt', 'Suborbital Left/M98.txt', 'Lateral Orbit Left/M98.txt', 'Zygomatic Arch Left/M98.txt';
'Supraglabella/M99.txt', 'Glabella/M99.txt', 'Nasion/M99.txt', 'End of Nasals/M99.txt', 'Mid-Philtrum/M99.txt', 'Chin-Lip Fold/M99.txt', 'Mental Eminence/M99.txt', 'Beneath Chin/M99.txt', 'Frontal Eminence Left/M99.txt', 'Supraorbital Left/M99.txt', 'Suborbital Left/M99.txt', 'Lateral Orbit Left/M99.txt', 'Zygomatic Arch Left/M99.txt';
'Supraglabella/M100.txt', 'Glabella/M100.txt', 'Nasion/M100.txt', 'End of Nasals/M100.txt', 'Mid-Philtrum/M100.txt', 'Chin-Lip Fold/M100.txt', 'Mental Eminence/M100.txt', 'Beneath Chin/M100.txt', 'Frontal Eminence Left/M100.txt', 'Supraorbital Left/M100.txt', 'Suborbital Left/M100.txt', 'Lateral Orbit Left/M100.txt', 'Zygomatic Arch Left/M100.txt';

'Supraglabella/M101.txt', 'Glabella/M101.txt', 'Nasion/M101.txt', 'End of Nasals/M101.txt', 'Mid-Philtrum/M101.txt', 'Chin-Lip Fold/M101.txt', 'Mental Eminence/M101.txt', 'Beneath Chin/M101.txt', 'Frontal Eminence Left/M101.txt', 'Supraorbital Left/M101.txt', 'Suborbital Left/M101.txt', 'Lateral Orbit Left/M101.txt', 'Zygomatic Arch Left/M101.txt';

'Supraglabella/M102.txt', 'Glabella/M102.txt', 'Nasion/M102.txt', 'End of Nasals/M102.txt', 'Mid-Philtrum/M102.txt', 'Chin-Lip Fold/M102.txt', 'Mental Eminence/M102.txt', 'Beneath Chin/M102.txt', 'Frontal Eminence Left/M102.txt', 'Supraorbital Left/M102.txt', 'Suborbital Left/M102.txt', 'Lateral Orbit Left/M102.txt', 'Zygomatic Arch Left/M102.txt';

'Supraglabella/M103.txt', 'Glabella/M103.txt', 'Nasion/M103.txt', 'End of Nasals/M103.txt', 'Mid-Philtrum/M103.txt', 'Chin-Lip Fold/M103.txt', 'Mental Eminence/M103.txt', 'Beneath Chin/M103.txt', 'Frontal Eminence Left/M103.txt', 'Supraorbital Left/M103.txt', 'Suborbital Left/M103.txt', 'Lateral Orbit Left/M103.txt', 'Zygomatic Arch Left/M103.txt';

'Supraglabella/M104.txt', 'Glabella/M104.txt', 'Nasion/M104.txt', 'End of Nasals/M104.txt', 'Mid-Philtrum/M104.txt', 'Chin-Lip Fold/M104.txt', 'Mental Eminence/M104.txt', 'Beneath Chin/M104.txt', 'Frontal Eminence Left/M104.txt', 'Supraorbital Left/M104.txt', 'Suborbital Left/M104.txt', 'Lateral Orbit Left/M104.txt', 'Zygomatic Arch Left/M104.txt';

'Supraglabella/M105.txt', 'Glabella/M105.txt', 'Nasion/M105.txt', 'End of Nasals/M105.txt', 'Mid-Philtrum/M105.txt', 'Chin-Lip Fold/M105.txt', 'Mental Eminence/M105.txt', 'Beneath Chin/M105.txt', 'Frontal Eminence Left/M105.txt', 'Supraorbital Left/M105.txt', 'Suborbital Left/M105.txt', 'Lateral Orbit Left/M105.txt', 'Zygomatic Arch Left/M105.txt';

'Supraglabella/M106.txt', 'Glabella/M106.txt', 'Nasion/M106.txt', 'End of Nasals/M106.txt', 'Mid-Philtrum/M106.txt', 'Chin-Lip Fold/M106.txt', 'Mental Eminence/M106.txt', 'Beneath Chin/M106.txt', 'Frontal Eminence Left/M106.txt', 'Supraorbital Left/M106.txt', 'Suborbital Left/M106.txt', 'Lateral Orbit Left/M106.txt', 'Zygomatic Arch Left/M106.txt';

'Supraglabella/M108.txt', 'Glabella/M108.txt', 'Nasion/M108.txt', 'End of Nasals/M108.txt', 'Mid-Philtrum/M108.txt', 'Chin-Lip Fold/M108.txt', 'Mental Eminence/M108.txt', 'Beneath Chin/M108.txt', 'Frontal Eminence Left/M108.txt', 'Supraorbital Left/M108.txt', 'Suborbital Left/M108.txt', 'Lateral Orbit Left/M108.txt', 'Zygomatic Arch Left/M108.txt';

'Supraglabella/M109.txt', 'Glabella/M109.txt', 'Nasion/M109.txt', 'End of Nasals/M109.txt', 'Mid-Philtrum/M109.txt', 'Chin-Lip Fold/M109.txt', 'Mental Eminence/M109.txt', 'Beneath Chin/M109.txt', 'Frontal Eminence Left/M109.txt', 'Supraorbital Left/M109.txt', 'Suborbital Left/M109.txt', 'Lateral Orbit Left/M109.txt', 'Zygomatic Arch Left/M109.txt';

'Supraglabella/M110.txt', 'Glabella/M110.txt', 'Nasion/M110.txt', 'End of Nasals/M110.txt', 'Mid-Philtrum/M110.txt', 'Chin-Lip Fold/M110.txt', 'Mental Eminence/M110.txt', 'Beneath Chin/M110.txt', 'Frontal Eminence Left/M110.txt', 'Supraorbital Left/M110.txt', 'Suborbital Left/M110.txt', 'Lateral Orbit Left/M110.txt', 'Zygomatic Arch Left/M110.txt';

'Supraglabella/M111.txt', 'Glabella/M111.txt', 'Nasion/M111.txt', 'End of Nasals/M111.txt', 'Mid-Philtrum/M111.txt', 'Chin-Lip Fold/M111.txt', 'Mental Eminence/M111.txt', 'Beneath Chin/M111.txt', 'Frontal Eminence Left/M111.txt', 'Supraorbital Left/M111.txt', 'Suborbital Left/M111.txt', 'Lateral Orbit Left/M111.txt', 'Zygomatic Arch Left/M111.txt';

'Supraglabella/M112.txt', 'Glabella/M112.txt', 'Nasion/M112.txt', 'End of Nasals/M112.txt', 'Mid-Philtrum/M112.txt', 'Chin-Lip Fold/M112.txt', 'Mental Eminence/M112.txt', 'Beneath Chin/M112.txt', 'Frontal Eminence

```
Left/M112.txt', 'Supraorbital Left/M112.txt', 'Suborbital
Left/M112.txt', 'Lateral Orbit Left/M112.txt', 'Zygomatic Arch Left/M112.txt';
  'Supraglabella/M113.txt', 'Glabella/M113.txt', 'Nasion/M113.txt', 'End of
Nasals/M113.txt', 'Mid-Philtrum/M113.txt', 'Chin-Lip Fold/M113.txt', 'Mental
Eminence/M113.txt', 'Beneath Chin/M113.txt', 'Frontal Eminence
Left/M113.txt', 'Supraorbital Left/M113.txt', 'Suborbital
Left/M113.txt', 'Lateral Orbit Left/M113.txt', 'Zygomatic Arch Left/M113.txt';
  'Supraglabella/M115.txt', 'Glabella/M115.txt', 'Nasion/M115.txt', 'End of
Nasals/M115.txt', 'Mid-Philtrum/M115.txt', 'Chin-Lip Fold/M115.txt', 'Mental
Eminence/M115.txt', 'Beneath Chin/M115.txt', 'Frontal Eminence
Left/M115.txt', 'Supraorbital Left/M115.txt', 'Suborbital
Left/M115.txt', 'Lateral Orbit Left/M115.txt', 'Zygomatic Arch Left/M115.txt';
  'Supraglabella/M117.txt', 'Glabella/M117.txt', 'Nasion/M117.txt', 'End of
Nasals/M117.txt', 'Mid-Philtrum/M117.txt', 'Chin-Lip Fold/M117.txt', 'Mental
Eminence/M117.txt', 'Beneath Chin/M117.txt', 'Frontal Eminence
Left/M117.txt', 'Supraorbital Left/M117.txt', 'Suborbital
Left/M117.txt', 'Lateral Orbit Left/M117.txt', 'Zygomatic Arch Left/M117.txt';
  'Supraglabella/M118.txt', 'Glabella/M118.txt', 'Nasion/M118.txt', 'End of
Nasals/M118.txt', 'Mid-Philtrum/M118.txt', 'Chin-Lip Fold/M118.txt', 'Mental
Eminence/M118.txt', 'Beneath Chin/M118.txt', 'Frontal Eminence
Left/M118.txt', 'Supraorbital Left/M118.txt', 'Suborbital
Left/M118.txt', 'Lateral Orbit Left/M118.txt', 'Zygomatic Arch Left/M118.txt';
  'Supraglabella/M119.txt', 'Glabella/M119.txt', 'Nasion/M119.txt', 'End of
Nasals/M119.txt', 'Mid-Philtrum/M119.txt', 'Chin-Lip Fold/M119.txt', 'Mental
Eminence/M119.txt', 'Beneath Chin/M119.txt', 'Frontal Eminence
Left/M119.txt', 'Supraorbital Left/M119.txt', 'Suborbital
Left/M119.txt', 'Lateral Orbit Left/M119.txt', 'Zygomatic Arch Left/M119.txt';
  'Supraglabella/M120.txt', 'Glabella/M120.txt', 'Nasion/M120.txt', 'End of
Nasals/M120.txt', 'Mid-Philtrum/M120.txt', 'Chin-Lip Fold/M120.txt', 'Mental
Eminence/M120.txt', 'Beneath Chin/M120.txt', 'Frontal Eminence
Left/M120.txt', 'Supraorbital Left/M120.txt', 'Suborbital
Left/M120.txt', 'Lateral Orbit Left/M120.txt', 'Zygomatic Arch Left/M120.txt';
  'Supraglabella/M121.txt', 'Glabella/M121.txt', 'Nasion/M121.txt', 'End of
Nasals/M121.txt', 'Mid-Philtrum/M121.txt', 'Chin-Lip Fold/M121.txt', 'Mental
Eminence/M121.txt', 'Beneath Chin/M121.txt', 'Frontal Eminence
Left/M121.txt', 'Supraorbital Left/M121.txt', 'Suborbital
Left/M121.txt', 'Lateral Orbit Left/M121.txt', 'Zygomatic Arch
Left/M121.txt'};};
```

```
filename2 = {'Bone measurements/WM1.txt'; 'Bone measurements/WM3.txt'; 'Bone
measurements/WM4.txt';
  'Bone measurements/WM5.txt'; 'Bone measurements/WM6.txt'; 'Bone
measurements/WM7.txt';
  'Bone measurements/WM8.txt'; 'Bone measurements/WM9.txt'; 'Bone
measurements/WM10.txt';
  'Bone measurements/WM11.txt'; 'Bone measurements/WM12.txt'; 'Bone
measurements/WM15.txt';
  'Bone measurements/WM18.txt'; 'Bone measurements/WM19.txt'; 'Bone
measurements/WM20.txt';
  'Bone measurements/WM21.txt'; 'Bone measurements/WM22.txt'; 'Bone
measurements/WM23.txt';
  'Bone measurements/WM24.txt'; 'Bone measurements/WM25.txt'; 'Bone
measurements/WM26.txt';
```

```
'Bone measurements/WM28.txt'; 'Bone measurements/WM29.txt'; 'Bone
measurements/WM30.txt';
'Bone measurements/WM32.txt'; 'Bone measurements/WM33.txt'; 'Bone
measurements/WM34.txt'; 'Bone measurements/WM35.txt';
'Bone measurements/WM37.txt'; 'Bone measurements/WM38.txt'; 'Bone
measurements/WM45.txt';
'Bone measurements/M49.txt'; 'Bone measurements/M51.txt'; 'Bone
measurements/M52.txt';
'Bone measurements/M53.txt'; 'Bone measurements/M54.txt'; 'Bone
measurements/M55.txt';
'Bone measurements/M56.txt'; 'Bone measurements/M57.txt'; 'Bone
measurements/M58.txt';
'Bone measurements/M59.txt'; 'Bone measurements/M60.txt'; 'Bone
measurements/M61.txt'; 'Bone measurements/M62.txt';
'Bone measurements/M63.txt'; 'Bone measurements/M64.txt'; 'Bone
measurements/M65.txt'; 'Bone measurements/M66.txt';
'Bone measurements/M67.txt'; 'Bone measurements/M68.txt'; 'Bone
measurements/M69.txt'; 'Bone measurements/M70.txt';
'Bone measurements/M71.txt'; 'Bone measurements/M72.txt'; 'Bone
measurements/M73.txt'; 'Bone measurements/M74.txt';
'Bone measurements/M75.txt'; 'Bone measurements/M76.txt'; 'Bone
measurements/M77.txt'; 'Bone measurements/M78.txt';
'Bone measurements/M79.txt'; 'Bone measurements/M80.txt'; 'Bone
measurements/M81.txt'; 'Bone measurements/M82.txt';
'Bone measurements/M83.txt'; 'Bone measurements/M84.txt'; 'Bone
measurements/M85.txt'; 'Bone measurements/M86.txt';
'Bone measurements/M87.txt'; 'Bone measurements/M88.txt'; 'Bone
measurements/M89.txt';
'Bone measurements/M90.txt'; 'Bone measurements/M91.txt'; 'Bone
measurements/M92.txt';
'Bone measurements/M93.txt'; 'Bone measurements/M94.txt'; 'Bone
measurements/M95.txt'; 'Bone measurements/M96.txt';
'Bone measurements/M97.txt'; 'Bone measurements/M98.txt'; 'Bone
measurements/M99.txt'; 'Bone measurements/M100.txt';
'Bone measurements/M101.txt'; 'Bone measurements/M102.txt'; 'Bone
measurements/M103.txt'; 'Bone measurements/M104.txt';
'Bone measurements/M105.txt'; 'Bone measurements/M106.txt'; 'Bone
measurements/M108.txt'; 'Bone measurements/M109.txt';
'Bone measurements/M110.txt'; 'Bone measurements/M111.txt'; 'Bone
measurements/M112.txt'; 'Bone measurements/M113.txt';
'Bone measurements/M115.txt'; 'Bone measurements/M117.txt'; 'Bone
measurements/M118.txt'; 'Bone measurements/M119.txt';
'Bone measurements/M120.txt'; 'Bone measurements/M121.txt';};
```

```
load pat_info
```

```
yt = zeros(size(filename,1),size(filename,2));
xt = zeros(size(filename,1),size(filename,2));
no_measure1=zeros(size(filename,1),size(filename,2));
no_measure2=zeros(size(filename,1),size(filename,2));
for m = 1:size(filename,2)
```

```
mx = mat2str(['Building Facial Measurement Matricies ('
mat2str(round(100*m/size(yt,2)) '%)']);
waitbar(m/size(yt,2),wb,mx);
for f = 1:size(filename,1)
    try
x = importdata(filename{f,m},'\t');
    end
i = find(~isnan(x.data));
x.data = x.data(i);
tissue = x.data;
bone_thick = x.textdata;
j = 1:2:size(bone_thick,1);
bone_thick(j) = [];
bones = zeros(size(bone_thick));
for n = 1:size(bone_thick,1)
    bones(n) = str2double(bone_thick{n});
end
%trimmean the measurements to produce a single value each craniometric
location
tissue_mean = trimmean(tissue,10);

if f ~= 1
if tissue_mean == yt(f-1,m)
    no_measure1(f,m)=no_measure1(f,m)+100000;
    tissue_mean = mean(yt(1:f-1,m));
end
end

yt(f,m) = tissue_mean*10;
%yt(f,m) = tissue_mode;
bone_mean = trimmean(bones,10);
%bone_mode = mode(bones);

if f ~= 1
if bone_mean == xt(f-1,m)
    no_measure2(f,m)=no_measure2(f,m)+100000;
    bone_mean = mean(xt(1:f-1,m));
end
end

xt(f,m) = bone_mean;
%xt(f,m) = bone_mode;
end
end

%load ethnicity determination bone measurement data
for f = 1:size(filename2,1)
    try
xb = importdata(filename2{f,:},'\t');
    end
basion_to_prothion(f) = xb.data(1);
basion_to_nasion(f) = xb.data(2);
```

```
orbit_height(f) = xb.data(3);
nasal_width(f) = xb.data(4);
biauricular_width(f) = xb.data(5);
end
xt = [xt, [basion_to_prothion', basion_to_nasion', orbit_height', ...
         nasal_width', biauricular_width']];

%attach demographic info to xt matrix
p=[1, 3:12, 15, 17, 18, 19:36, 38:99, 101, 103:107];
pat_data = I(p, :);
xt = [xt, pat_data];

%save xt and yt
save('yt.mat', 'yt')
save('xt.mat', 'xt')

close(wb);

%display correlation coefficients
cc = [yt xt];
corr = abs(corrcoef(cc));
pred_corr = corr(1:size(yt,2), size(yt,2)+1:end);
figure;
imagesc(pred_corr); colorbar
ylabel('Tissue Thickness Craniometric Location');
xlabel('Bone Measurement Predictor');
```

Bandwidth optimization used for Inferential Model

```
%Bandwidth Optimization
clear all
load xt
load yt
wb = waitbar(0, 'Running Bandwidth Optimization for Inferential KR Model'
);

%set bandwidth
h=.1:.1:5;

for b=1:length(h)
for l=1:size(xt,1)

    %waitbar
    m = mat2str(['Running Bandwidth Optimization for Inferential KR Model('
mat2str(round(100*b/length(h)) '%) ']);
    waitbar(b/length(h), wb, m);

%set the LOOCV memory matrices
loocv_x = xt;
loocv_y = yt;
```

```
%query vector using demographics
q = loocv_x(1,:);

%query vector not using demographics
%q = q.*[ones(1,18),0,0,0,0];

%remove query from memory matrix
loocv_x(1,:) = [];
loocv_y(1,:) = [];

%send query and memory matrices to model
[yhat(1,:) predu(1,:) pvar(1,:)] = Face_Pred_Inf(q,h(b),loocv_x,loocv_y);

end

%Compute root mean squared error for entire LOOCV
RMSE_Inf(b) = mean(sqrt(mean((yhat - yt).^2)));
mpredu(b,:) = mean(predu);
mpvar(b,:) = mean(pvar);
end

%close waitbar
close (wb);

%plot the bandwidth optimization
plot(h,RMSE_Inf)
xlabel('Bandwidth (h)')
ylabel('Root Mean Squared Error (RMSE)')
[min ind] = min(RMSE_Inf);
opt_h_Inf = h(ind)
save ('opt_h_Inf','opt_h_Inf')
```

Bandwidth Optimization for HAKR model

```
%HAKR Bandwidth Optimization
clear all
load xt
load yt

wb = waitbar(0,'Running Bandwidth Optimization for HAKR Model');

%set bandwidth
h=.1:.1:5;

for b=1:length(h)
for l=1:size(xt,1)
```

```
m = mat2str(['Running Bandwidth Optimization for HAKR Model('
mat2str(round(100*b/length(h)) '%)']);
waitbar(b/length(h),wb,m);

loocv_x = xt;
loocv_y = yt;

%query vector using demographics
q = loocv_x(1,:);

%query vector not using demographics
%q = q.*[ones(1,18),0,0,0,0];

%remove query from memory matrix
loocv_x(1,:) = [];
loocv_y(1,:) = [];

[yhat(1,:) r(1,:) predu(1,:)] = Face_Pred_HAKR(q,h(b),loocv_x,loocv_y);

end

RMSE_HAKR(b) = mean(sqrt(mean((yhat - yt).^2)));

end
close (wb);

plot(h, RMSE_HAKR)
xlabel('Bandwidth (h)')
ylabel('Root Mean Squared Error (RMSE)')
[min ind] = min(RMSE_HAKR);
opt_h_HAKR = h(ind)
save('opt_h_HAKR','opt_h_HAKR')
```

LOOCV for Inferential Model

```
%LOOCV for Inferential Model
clear all
load xt
load yt

wb = waitbar(0,'Running LOOCV for Inferential KR Model');
load 'Rhine&Moore thicknesses.mat'

%set bandwidth
load opt_h_Inf
h = opt_h_Inf;

for l=1:size(xt,1)

    %waitbar
```

```
m = mat2str(['Running LOOCV for Inferential KR Model('
mat2str(round(100*1/size(yt,1)) '%)']);
waitbar(1/size(yt,1),wb,m);

%set the LOOCV memory matrices
loocv_x = xt;
loocv_y = yt;

%query vector using demographics
q = loocv_x(1,:);

%query vector not using demographics
%q = q.*[ones(1,18),0,0,0,0];

%remove query from memory matrix
loocv_x(1,:) = [];
loocv_y(1,:) = [];

%send query and memory matrices to model
[yhat(1,:) r(1,:) predu(1,:) PI(1,:) w pvar(1,:) pbias nvar] =
Face_Pred_Inf(q,h,loocv_x,loocv_y);

end

%Compute root mean squared error for entire LOOCV
RMSE1_Inf = mean(sqrt(mean((yhat - yt).^2)))
error = mean((yt-yhat).^2,2);
evrc = corrcoef(error,mean(r,2));

%Compute the RMSE for the actual versus the average actual and then versus
%the tabled values
for p=1:size(yt,1)
RMSE2(p) = sqrt(mean((mean(yt) - yt(p,:)).^2));
RMSE3(p) = sqrt(mean((current_tissue_thickness(:,3)' - yt(p,:)).^2));
end
%mean RMSE for avg actual and actual
RMSE2 = mean(RMSE2)
%mean RMSE of tables
RMSE3 = mean(RMSE3)

%compute mean reliability metric for the LOOCV
m_r = mean(mean(r))

%compute the mean prediction uncertainty for all variables in the LOOCV
pu = (mean(mean(predu))/mean(mean(yhat)))*100

%compute coverage of PI
coverage = uicov(yhat,PI,yt);

%close waitbar
```

```
close (wb);

% %compute correlation between predictors and responses
% cc = [yt xt];
% corr = abs(corrcoef(cc));
% pred_corr = corr(1:size(yt,2),size(yt,2)+1:end);
% figure;
% imagesc(pred_corr);colorbar
% ylabel('Tissue Thickness Craniometric Location');
% xlabel('Bone Measurement Predictor');

%plot actual vs. predicted
% figure;
% plot(yt(5,:), 'rx');hold on; plot(yhat(5,:), 'bo')
% errorbar(yhat(5,:),PI(5,:), 'bo')
% legend('Actual Tissue Thicknesses', 'Predicted Tissue
Thicknesses', 'Location', 'Best')
% xlabel('Anatomical Location of Tissue Thickness')
% ylabel('Facial Soft Tissue Thickness (mm)')
% title('Inferential KR Model Predictions for Query Input')
```

Inferential Prediction Model

```
function [yhat r predu PI w pvar pbias] = Face_Pred_Inf(q,h,xt,yt)

%remove variables that are zero
os = find(q);
xt = xt(:,os);
o = find(q);
q = q(:,o);

%standardize the data
[xts xm xstd] = zscore1(xt);
[yts ym ystd] = zscore1(yt);
[qs] = zscore1(q, xm(1:size(q,2)), xstd(1:size(q,2)));

%compute the noise variance of the output memory matrix
nvar = enovar(yt, 'medianfilter', 5);

%Build Inferential KR model
for k = 1:size(yt,2)
%use correlation coefficients to choose best predictors for each model
p_inf{:,k} = CC(xt(:,1:size(qs,2)),yt(:,k),0.3);

%Set query for each inferential model with best predictors
x = xts(:,p_inf{:,k});
y = yts(:,k);

%Expand the query observation to have the same dimension as the
%training vectors
xq = ones(size(x,1),1)*qs(:,p_inf{:,k});
```

```
%Calculate the Euclidean distances
d = sqrt(sum((x'-xq').^2,1));

%Calculate the weights
%w = (1/sqrt(2*3.14*h^2))*exp(-(d.^2)/(2*h^2))';
w(:,k) = exp(-(d.^2)/(h^2))';

%Weighted prediction
s = sum(w(:,k));
pred = (w(:,k)'*y)/s;

%reliability
[r(k) ind(k)] = max(w(:,k));

%normalize the weights
wts=w(:,k)./s;

%Load prediction bias
load 'bias2.mat'
pbias = Bias2;

%Calculte the analytic variance
pvar(:,k) = wts'*wts*nvar(:,k);

%Unscale the predictions
prediction(:,k) = unscore(pred,ym(:,k),ystd(:,k));

end

%Compute prediction uncertainty and interval
predu = sqrt(nvar+pvar+pbias);
PI = 2*sqrt(nvar+pvar+pbias);

%predictions
yhat = prediction;

end

LOOCV for HAKR Modeling
%LOOCV for HAKR model
clear all
load xt
load yt

wb = waitbar(0,'Running LOOCV for Inferential KR Model');
```

```
load 'Rhine&Moore thicknesses.mat'

%set bandwidth
load opt_h_HAKR
h = opt_h_HAKR;

for l=1:size(xt,1)

    m = mat2str(['Running LOOCV for Inferential KR Model('
mat2str(round(100*l/size(yt,1))) '%) ']);
    waitbar(l/size(yt,1),wb,m);

    loocv_x = xt;
    loocv_y = yt;

    %query vector using demographics
    q = loocv_x(l,:);

    %query vector not using demographics
    %q = q.*[ones(1,18),0,0,0,0];

    %remove query from memory matrix
    loocv_x(l,:) = [];
    loocv_y(l,:) = [];

    [yhat(l,:) r(l,:) predu(l,:) PI(l,:) w] =
    Face_Pred_HAKR(q,h,loocv_x,loocv_y);

    %compute squared error for the LOOCV predictions
    SE(l,:) = (yhat(l,:)- yt(l,:)).^2;

end

RMSE1_HAKR = mean(sqrt(mean((yhat - yt).^2)))
% error = yhat-yt;
% evrc = corrcoef(error(:,1),r);

close (wb);

% %compute bias
% MSE = mean(SE);
% Var = var(yhat);
% Bias2_HAKR = MSE-Var;
% save('bias2_HAKR.mat','Bias2_HAKR')

for p=1:size(yt,1)
RMSE2(p) = sqrt(mean((mean(yt) - yt(p,:)).^2));
RMSE3(p) = sqrt(mean((current_tissue_thickness(:,3)' - yt(p,:)).^2));
end
```

```
%mean RMSE for avg actual and actual
RMSE2 = mean(RMSE2)
%mean RMSE of tables
RMSE3 = mean(RMSE3)

m_r = mean(r)

%compute the mean prediction uncertainty in % of mean prediction values
%for the LOOCV
pu = (mean(mean(predu))/mean(mean(yhat)))*100
%
% %compute correlation between predictors and responses
% cc = [yt xt];
% corr = abs(corrcoef(cc));
% pred_corr = corr(1:size(yt,2),size(yt,2)+1:end);
% figure;
% imagesc(pred_corr);colorbar
% ylabel('Tissue Thickness Craniometric Location');
% xlabel('Bone Measurement Predictor');

%plot actual vs. predicted
figure;
plot(yt(5,:), 'rx');hold on; plot(yhat(5,:), 'bo')
errorbar(yhat(5,:), PI(5,:), 'bo')
legend('Actual Tissue Thicknesses', 'Predicted Tissue
Thicknesses', 'Location', 'Best')
xlabel('Anatomial Location of Tissue Thickness')
ylabel('Facial Soft Tissue Thickness (mm)')
title('Hetero-Associative KR Model Predictions for Query Input')
```

HAKR Model used in LOOCV

```
function [yhat r predu PI w] = Face_Pred_HAKR(q,h,xt,yt)
```

```
%remove variables that are zero
os = find(q);
xt = xt(:,os);
o = find(q);
q = q(:,o);

%standardize the data
[xts xm xstd] = zscore1(xt);
[yts ym ystd] = zscore1(yt);
[qs] = zscore1(q, xm(1:size(q,2)), xstd(1:size(q,2)));

%compute the noise variance of the output memory matrix
nvar = enovar(yt, 'medianfilter', 5);

%Calculate the predictions for each query observation

%Expand the query observation to have the same dimension as the
```

```
%training vectors
xq = ones(size(xts,1),1)*qs;

%Calculate the Euclidean distances
d = sqrt(sum((xts'-xq').^2,1));

%Calculate the weights
%w = (1/sqrt(2*3.14*h^2))*exp(-(d.^2)/(2*h^2))';
w = exp(-(d.^2)/(h^2))';

%Weighted prediction
s = sum(w);
pred = (w'*yts)/s;

%reliability
[r ind] = max(w);

wts=w./s;

% Load prediction bias
load 'bias2_HAKR.mat'
pbias = Bias2_HAKR;

% Calculte the analytic variance
pvar = wts'*wts*nvar;

prediction = unscore(pred,ym,ystd);

%Compute prediction uncertainty and interval
predu = sqrt(nvar+pvar+pbias);
PI = 2*sqrt(nvar+pvar+pbias);

yhat = prediction;

end
```

Inferential Model function used for 5 unknown skulls

```
function [yhat, r, predu, PI, pvar, pbias, w, ind, diff_norm, diff_obe,
diff_avg, p_inf scaling_ratio1 scaling_ratio2 scaling_ratio3] = face(q)
load xt
load yt
load opt_h_Inf
h = opt_h_Inf;

%remove variables that are zero
zeros = find(q);
xt = xt(:,zeros);
q = q(:,zeros);
```

```
%standardize the data
[xts xm xstd] = zscore1(xt);
[yts ym ystd] = zscore1(yt);
[qs] = zscore1(q, xm, xstd);

%Estimate the noise variance of the output memory matrix
%Assume variance as the resolution of the CT imageset squared
nvar = ones(1,13)*.36;

cc = [yt xt];
corr = abs(corrcoef(cc));
pred_corr = corr(1:size(yt,2), size(yt,2)+1:end);

%Build Inferential KR model
for k = 1:size(yt,2)
    %use correlation coefficients to choose best predictors for each model
    p_inf{:,k} = CC(xt,yt(:,k),0.3);

    %Set query for each inferential model with best predictors
    x = xts(:,p_inf{:,k});
    y = yts(:,k);

    %Expand the query observation to have the same dimension as the
    %training vectors
    xq = ones(size(x,1),1)*qs(:,p_inf{:,k});

    %Calculate the Euclidean distances
    d(:,k) = sqrt(sum((x'-xq').^2,1));

    %Calculate the weights
    w(:,k) = exp(-(d(:,k).^2)/(h^2))';

    %Weighted prediction
    s = sum(w(:,k));
    pred = (w(:,k)'*y)/s;

    %reliability
    [r(k) ind(k)] = max(w(:,k));

    %normalize the weights
    wts=w(:,k)./s;

    %Load prediction bias
    load 'bias2.mat'
    pbias = Bias2;

    %Calculte the analytic variance
    pvar(:,k) = wts'*wts*nvar(:,k);

%Unscale the predictions
```

```
yhat(:,k) = unscore(pred,ym(:,k),ystd(:,k));

end

load 'Rhine&Moore thicknesses.mat'
diff_norm = current_tissue_thickness(:,2) '-yhat;
diff_obc = current_tissue_thickness(:,3) '-yhat;
diff_avg = mean(yt)-yhat;
scaling_ratio1 = mean(yhat./current_tissue_thickness(:,2)');
scaling_ratio2 = mean(yhat./current_tissue_thickness(:,3)');
scaling_ratio3 =
mean(current_tissue_thickness(:,3)./current_tissue_thickness(:,2));

%Compute prediction uncertainty in % and 95% PI
predu = (sqrt(nvar+pvar+pbias)./yhat).*100;
PI = 2*sqrt(nvar+pvar+pbias);

%bar graph of prediction uncertainties
figure;
bar(predu)
xlabel('Anatomial Location of Tissue Thickness')
ylabel('Prediction Uncertainty (% of prediction value)')
title('Facial Tissue Thickness Prediction Uncertainties')

%bar graph of reliabilities
figure;
bar(r)
xlabel('Anatomial Location of Tissue Thickness')
ylabel('Predication Reliability')
title('Facial Tissue Thickness Prediction Reliabilities')

%plot predicted with 95% PI
figure;
errorbar(yhat,PI,'bo')
legend('Predicted Tissue Thicknesses','Location','Best')
xlabel('Anatomial Location of Tissue Thickness')
ylabel('Facial Soft Tissue Thickness (mm)')
title('Inferential KR Model Predictions for Query Input')
end
```

Appendix C

Model's Predicted Facial Tissue Thicknesses for 3 Unknown Skulls

	Subject A (mm)	Subject C (mm)	Subject B (mm)
Supraglabella	5.85	8.92	6.45
Glabella	7.29	7.96	7.43
Nasion	8.93	10.74	9.19
End of Nasals	4.50	5.30	4.97
Mid-Philtrum	16.59	16.99	17.07
Chin-Lip Fold	14.75	18.54	14.17
Mental Eminence	12.29	15.64	12.01
Beneath Chin Frontal Eminence	11.87	15.59	12.10
Supraorbital	6.18	8.45	6.48
Suborbital	8.90	11.20	8.91
Lateral Orbit	8.93	14.65	8.92
Zygomatic Arch	10.21	15.80	9.38
	10.74	20.65	13.26
		Scaling ratio = 1.87	Scaling ratio = 1.44

Appendix D

Full Correlation Matrix of Collected Data

	A	B	C	D	E	F	G	H	I	J	K	L	M	N	O	P	Q	R	S	T	V	U	W	X	Y	Z	AA	BB	CC	DD	EE	FF	GG	HH	II
A	1	0.62	0.51	0.55	0.24	0.57	0.49	0.38	0.87	0.69	0.57	0.65	0.69	0.03	-0.11	-0.04	0.08	-0.11	-0.16	0.08	0.32	0.10	0.11	-0.20	0.13	-0.15	0.32	0.26	-0.20	0.00	-0.09	-0.29	0.65	0.19	0.58
B	0.62	1	0.72	0.43	0.15	0.52	0.53	0.25	0.51	0.60	0.50	0.45	0.58	0.08	0.09	0.07	0.05	0.06	-0.16	-0.06	0.20	0.13	0.09	-0.03	0.05	0.01	0.19	0.10	-0.16	-0.11	-0.15	-0.21	0.44	0.09	0.42
C	0.51	0.72	1	0.58	0.12	0.51	0.41	0.22	0.46	0.53	0.40	0.41	0.49	0.09	-0.02	0.04	0.00	0.08	-0.10	-0.03	0.12	0.14	0.12	-0.11	0.05	0.18	0.27	0.02	-0.23	-0.16	-0.12	-0.25	0.36	0.15	0.38
D	0.55	0.43	0.58	1	0.11	0.42	0.42	0.24	0.56	0.56	0.49	0.50	0.44	0.17	-0.08	-0.21	-0.06	-0.19	-0.04	0.06	0.26	0.26	0.15	-0.26	0.18	-0.16	0.27	0.15	-0.18	-0.05	0.03	-0.15	0.37	0.08	0.36
E	0.24	0.15	0.12	0.11	1	0.25	0.33	0.33	0.24	0.31	0.42	0.41	0.31	0.03	-0.02	-0.08	-0.14	-0.22	0.08	-0.07	0.12	0.01	0.02	0.08	0.12	-0.05	-0.12	0.02	-0.03	-0.06	0.12	-0.28	0.33	-0.04	0.27
F	0.57	0.52	0.51	0.42	0.25	1	0.72	0.39	0.58	0.57	0.55	0.57	0.60	0.21	0.02	-0.06	-0.04	0.05	-0.20	0.06	0.31	0.19	0.24	-0.13	0.14	-0.09	0.32	0.07	-0.24	-0.07	0.00	-0.21	0.57	0.23	0.60
G	0.49	0.53	0.41	0.42	0.33	0.72	1	0.51	0.49	0.55	0.55	0.61	0.62	0.19	0.00	-0.12	-0.21	-0.14	-0.18	-0.04	0.30	0.26	0.20	-0.10	0.09	-0.13	0.17	0.11	-0.14	0.01	-0.01	-0.13	0.55	0.11	0.58
H	0.38	0.25	0.22	0.24	0.33	0.39	0.51	1	0.38	0.31	0.31	0.43	0.54	0.06	-0.05	-0.04	-0.15	-0.16	-0.01	-0.02	0.17	0.18	-0.02	-0.12	0.06	-0.17	0.08	0.04	-0.29	-0.09	-0.03	-0.28	0.49	0.03	0.44
I	0.87	0.51	0.46	0.56	0.24	0.58	0.49	0.38	1	0.69	0.55	0.64	0.64	0.15	-0.05	-0.08	0.02	-0.19	-0.13	0.14	0.41	0.22	0.24	-0.24	0.24	-0.19	0.34	0.28	-0.19	-0.03	-0.16	-0.26	0.64	0.17	0.57
J	0.69	0.60	0.53	0.56	0.31	0.57	0.55	0.31	0.69	1	0.66	0.64	0.71	0.14	0.04	0.02	-0.01	-0.08	-0.09	0.13	0.38	0.27	0.19	-0.18	0.23	-0.10	0.25	0.12	-0.22	-0.01	-0.19	-0.27	0.64	0.11	0.59
K	0.57	0.50	0.40	0.49	0.42	0.55	0.55	0.31	0.55	0.66	1	0.80	0.65	0.09	-0.11	-0.04	0.11	-0.10	-0.07	0.05	0.30	0.17	0.14	0.04	0.13	-0.08	0.04	0.02	-0.14	-0.06	0.06	-0.08	0.59	0.03	0.56
L	0.65	0.45	0.41	0.50	0.41	0.57	0.61	0.43	0.64	0.64	0.80	1	0.71	0.00	-0.22	-0.13	0.05	-0.17	-0.15	0.04	0.36	0.16	0.14	-0.05	0.00	-0.16	0.21	0.13	-0.26	-0.12	-0.02	-0.20	0.67	0.12	0.64
M	0.69	0.58	0.49	0.44	0.31	0.60	0.62	0.54	0.64	0.71	0.65	0.71	1	0.09	-0.02	-0.04	-0.02	-0.25	-0.04	-0.08	0.26	0.20	-0.01	-0.12	0.20	-0.16	0.26	0.09	-0.18	-0.10	-0.08	-0.40	0.72	0.21	0.73
N	0.03	0.08	0.09	0.17	0.03	0.21	0.19	0.06	0.15	0.14	0.09	0.00	0.09	1	0.21	-0.21	-0.35	-0.32	0.22	0.42	0.49	0.79	0.46	-0.24	0.66	-0.29	0.13	0.08	0.10	0.16	0.17	-0.06	0.13	0.02	0.14
O	-0.11	0.09	-0.02	-0.08	-0.02	0.02	0.00	-0.05	-0.05	0.04	-0.11	-0.22	-0.02	0.21	1	0.27	-0.10	-0.16	0.09	-0.10	0.12	0.13	0.21	0.12	0.49	-0.09	-0.20	-0.09	0.01	-0.04	-0.06	0.05	-0.21	-0.25	-0.24
P	-0.04	0.07	0.04	-0.21	-0.08	-0.08	-0.12	-0.04	-0.08	0.02	-0.04	-0.13	-0.04	-0.21	0.27	1	0.43	0.28	0.07	0.04	-0.15	-0.21	0.03	0.24	-0.17	0.21	0.01	0.04	-0.14	-0.10	-0.01	-0.02	-0.08	-0.15	-0.14
Q	0.08	0.05	0.00	-0.06	-0.14	-0.04	-0.21	-0.15	0.02	-0.01	0.11	0.05	-0.02	-0.35	-0.10	0.43	1	0.18	-0.01	0.22	-0.01	-0.25	-0.03	0.11	-0.26	0.08	-0.04	-0.04	-0.10	-0.16	-0.10	0.15	-0.05	0.13	-0.08
R	-0.11	0.06	0.08	-0.19	-0.22	0.05	-0.14	-0.16	-0.19	-0.08	-0.10	-0.17	-0.25	-0.32	-0.16	0.28	0.18	1	-0.04	0.04	-0.24	-0.35	0.03	0.12	-0.43	0.47	-0.03	-0.08	-0.07	-0.09	-0.04	0.07	-0.21	-0.01	-0.18
S	-0.16	-0.16	-0.10	-0.04	0.08	-0.20	-0.18	-0.01	-0.13	-0.09	-0.07	-0.15	-0.04	0.22	0.09	0.07	-0.01	-0.04	1	0.20	-0.01	0.21	0.05	0.17	0.29	-0.03	0.00	0.09	0.08	0.29	-0.16	-0.02	0.02	0.00	0.00
T	0.08	-0.06	-0.03	0.06	-0.07	0.06	-0.04	-0.02	0.14	0.13	0.05	0.04	-0.08	0.42	-0.10	0.04	0.22	0.04	0.20	1	0.59	0.33	0.54	-0.18	0.24	-0.04	0.17	0.23	-0.05	0.10	0.10	0.10	0.09	0.12	0.02
V	0.32	0.20	0.12	0.26	0.12	0.31	0.30	0.17	0.41	0.38	0.30	0.36	0.26	0.49	0.12	-0.15	-0.01	-0.24	-0.01	0.59	1	0.56	0.48	-0.28	0.45	-0.38	0.20	0.19	0.08	0.10	-0.08	-0.06	0.33	0.11	0.25
U	0.10	0.13	0.14	0.26	0.01	0.19	0.26	0.18	0.22	0.27	0.17	0.16	0.20	0.79	0.13	-0.21	-0.25	-0.35	0.21	0.33	0.56	1	0.32	-0.29	0.57	-0.35	0.19	0.08	0.10	0.18	-0.04	-0.13	0.23	0.11	0.20
W	0.11	0.09	0.12	0.15	0.02	0.24	0.20	-0.02	0.24	0.19	0.14	0.14	-0.01	0.46	0.21	0.03	-0.03	0.03	0.05	0.54	0.48	0.32	1	0.00	0.42	-0.04	0.18	0.25	0.06	0.09	0.15	0.00	0.13	0.13	0.11
X	-0.20	-0.03	-0.11	-0.26	0.08	-0.13	-0.10	-0.12	-0.24	-0.18	0.04	-0.05	-0.12	-0.24	0.12	0.24	0.11	0.12	0.17	-0.18	-0.28	-0.29	0.00	1	-0.11	0.32	-0.13	0.00	0.12	-0.13	-0.02	0.09	-0.14	-0.01	-0.11
Y	0.13	0.05	0.05	0.18	0.12	0.14	0.09	0.06	0.24	0.23	0.13	0.00	0.20	0.66	0.49	-0.17	-0.26	-0.43	0.29	0.24	0.45	0.57	0.42	-0.11	1	-0.36	0.03	0.10	0.07	0.20	0.17	-0.08	0.16	0.12	0.16
Z	-0.15	0.01	0.18	-0.16	-0.05	-0.09	-0.13	-0.17	-0.19	-0.10	-0.08	-0.16	-0.16	-0.29	-0.09	0.21	0.08	0.47	-0.03	-0.04	-0.38	-0.35	-0.04	0.32	-0.36	1	-0.09	-0.13	0.00	-0.21	0.00	0.11	-0.12	-0.06	-0.14
AA	0.32	0.19	0.27	0.27	-0.12	0.32	0.17	0.08	0.34	0.25	0.04	0.21	0.26	0.13	-0.20	0.01	-0.04	-0.03	0.00	0.17	0.20	0.19	0.18	-0.13	0.03	-0.09	1	0.72	-0.15	0.05	-0.09	-0.29	0.39	0.31	0.29
BB	0.26	0.10	0.02	0.15	0.02	0.07	0.11	0.04	0.28	0.12	0.02	0.13	0.09	0.08	-0.09	0.04	-0.04	-0.08	0.09	0.23	0.19	0.08	0.25	0.00	0.10	-0.13	0.72	1	-0.08	0.08	0.06	-0.18	0.25	0.17	0.10
CC	-0.20	-0.16	-0.23	-0.18	-0.03	-0.24	-0.14	-0.29	-0.19	-0.22	-0.14	-0.26	-0.18	0.10	0.01	-0.14	-0.10	-0.07	0.09	-0.05	0.08	0.10	0.06	0.12	0.07	0.00	-0.15	-0.08	1	0.13	-0.01	0.13	-0.05	0.07	-0.12
DD	0.00	-0.11	-0.16	-0.05	-0.06	-0.07	0.01	-0.09	-0.03	-0.01	-0.06	-0.12	-0.10	0.16	-0.04	-0.10	-0.16	-0.09	0.08	0.10	0.10	0.18	0.09	-0.13	0.20	-0.21	0.05	0.08	0.13	1	-0.08	0.10	0.01	0.13	0.05
EE	-0.09	-0.15	-0.12	0.03	0.12	0.00	-0.01	-0.03	-0.16	-0.19	0.06	-0.02	-0.08	0.17	-0.06	-0.01	-0.10	-0.04	0.29	0.10	-0.08	-0.04	0.15	-0.02	0.17	0.00	-0.09	0.06	-0.01	-0.08	1	0.17	0.03	0.00	0.04
FF	-0.29	-0.21	-0.25	-0.15	-0.28	-0.21	-0.13	-0.28	-0.26	-0.27	-0.08	-0.20	-0.40	-0.06	0.05	-0.02	0.15	0.07	-0.16	0.10	-0.06	-0.13	0.00	0.09	-0.08	0.11	-0.29	-0.18	0.13	0.10	0.17	1	-0.34	-0.21	-0.35
GG	0.65	0.44	0.36	0.37	0.33	0.57	0.55	0.49	0.64	0.64	0.59	0.67	0.72	0.13	-0.21	-0.08	-0.05	-0.21	-0.02	0.09	0.33	0.23	0.13	-0.14	0.16	-0.12	0.39	0.25	-0.05	0.01	0.03	-0.34	1	0.36	0.89
HH	0.19	0.09	0.15	0.08	-0.04	0.23	0.11	0.03	0.17	0.11	0.03	0.12	0.21	0.02	-0.25	-0.15	0.13	-0.01	0.02	0.12	0.11	0.11	0.13	-0.01	0.12	-0.06	0.31	0.17	0.07	0.13	0.00	-0.21	0.36	1	0.51
II	0.58	0.42	0.38	0.36	0.27	0.60	0.58	0.44	0.57	0.59	0.56	0.64	0.73	0.14	-0.24	-0.14	-0.08	-0.18	0.00	0.02	0.25	0.20	0.11	-0.11	0.16	-0.14	0.29	0.10	-0.12	0.05	0.04	-0.35	0.89	0.51	1

Variable Distinctions:

A: Supraglabella tissue thickness

B: Glabella tissue thickness

C: Nasion tissue thickness

D: End of Nasals tissue thickness

E: Mid-Philtrum tissue thickness

F: Chin-Lip Fold tissue thickness

G: Mental Eminence tissue thickness

H: Beneath Chin tissue thickness
I: Frontal Eminence tissue thickness
J: Supraorbital tissue thickness
K: Suborbital tissue thickness
L: Lateral Orbit tissue thickness
M: Zygomatic Arch tissue thickness
N: Supraglabella bone thickness
O: Glabella bone thickness
P: Nasion bone thickness
Q: End of Nasals bone thickness
R: Mid-Philtrum bone thickness
S: Chin-Lip Fold bone thickness
T: Mental Eminence bone thickness
U: Beneath Chin bone thickness
V: Frontal Eminence bone thickness
W: Supraorbital bone thickness
X: Suborbital bone thickness
Y: Lateral Orbit bone thickness
Z: Zygomatic Arch bone thickness
AA: Basion-Prosthion distance
BB: Basion-Nasion distance
CC: Orbital Width
DD: Nasal Width
EE: Biauricular Breadth

FF: Age

GG: Weight

HH: Height

II: Body Mass Index (BMI)